

Photocopy and Use Authorization

In presenting this thesis in partial fulfillment of the requirements for an advanced degree at Idaho State University, I agree that the Library shall make it freely available for inspection. I further state the permission for extensive copying of my thesis for scholarly purposes may be granted by the Dean of Graduate Studies, Dean of my academic division, or by the University Librarian. It is understood that any copying or publication of this thesis for financial gain shall not be allowed without my written permission.

Signature _____

Harishchandra Aryal

Date _____

Improvement in Transient Testing Reactor (TREAT): Application of Cloud Chamber,
Simulation and Analytical Approach using Filtered Back Projection (FBP)

By

Harishchandra Aryal

A dissertation

Submitted in partial fulfillment

of the requirements for the degree of

Doctor of Philosophy in Nuclear Science and Engineering

Idaho State University

December 2020

To the Graduate Faculty:

The members of the committee appointed to examine the dissertation of
Harishchandra Aryal find it satisfactory and recommend that it be accepted.

Dr. George Imel,

Major Advisor

Dr. Chad Pope

Committee Member

Dr. Marco P. Schoen

Graduate Faculty Representative

Dr. Dustin McNulty

Committee Member

Dr. Jim Wolper

Committee Member

ACKNOWLEDGEMENTS

Before beginning, it is my utmost honor to acknowledge the people who in one way or another contributed in completion of this dissertation. I would not have been able to get it done without the support from my committee members, close friends and family.

A special thanks to my major advisor Dr. George Imel for his continual support throughout my dissertation. His knowledge, patience and encouragement were crucial to the completion. I would like to thank all my committee members. I would like to express my deepest appreciation to all other professors who contributed.

I thank my friendly and cheerful fellow students of the research group especially to Dr. Edward Lum, Dr. Ben Baker, and Dr. Tony Riley for providing valuable insights throughout the work. I am grateful to all my friends mostly my wife, Savyata Subedi for her unfailing support. She has been my constant motivation throughout and she was always there when I needed and I am sure she will be in future. I am fortunate to have such an amazing soulmate full of positivity and encouragement. I can proudly say, you can make anything possible and you should be proud of it.

Words seem inadequate to describe the support my family has provided to come to this point. A billion thank you to my mom for helping me out when I needed. You probably assisted more than you think you did. I am always indebted to my dad for the care, patience and encouragement that had been shown towards me in completing this thesis. I could not forget my sister, Dr. Muna Aryal and brother-in-law, Dr. Binod Rizal for their corroborations. The time they spent and knowledge they shared were truly precious.

Table of Contents

List of Figures	v
List of Tables	vii
Abstract	viii
Chapter 1: Introduction	1
A: Background	1
B: Statement of the Problem	1
Original Path: Cloud Chamber.....	2
Alternate path: Back Projection	3
1.1. Background on Cloud Chamber.....	5
1.2. Literature Review on Cloud Chamber	7
1.3. Cloud Chamber Results	9
Chapter 2: Filtered Back Projection (FBP).....	14
2.1. Literature Review on FBP	14
2.2. TREAT Related References.....	16
Chapter 3: Theory	17
3.1: Theory of Back Projection.....	17
3.2. Object and Image	17
3.3. Fourier Transform.....	18
3.4. Back Projection.....	19
3.5. Filtering.....	21
Chapter 4: Applications of FBP to Different Sources	23
4.1. FBP for a Step Function:.....	23
4.2. FBP for a Cosine Source:.....	27
4.3. FBP for a Hodoscope Plane Flux obtained from TREAT	29
Chapter 5: TREAT L7 Data.....	41
5.1. TREAT Reactor	41
5.2. Hodoscope Raw Data.....	43
5.3. ANL Analysis of Fuel Distribution.....	49
Chapter 6. Hodoscope Data and FBP	57
Chapter 7. Conclusions and Recommendations.....	64
REFERENCES	67
Appendix:.....	70
Appendix A: Cloud Chamber	70
Appendix B: TREAT MCNP.....	73
Appendix C: Filtered Back Projections Calculations	78
Appendix D: ANL Hodogram Data.....	99

List of Figures

Figure 1: Back Projection	4
Figure 2: Mechanism of Cloud Trail Formation (Dennis, 2015).....	5
Figure 3: Critical Super-saturation vs. Alcohol (%)	10
Figure 4: Cloud Trail Image	11
Figure 5: Cloud Trail Image	12
Figure 6: Back Projection (Roth, 2007).....	19
Figure 7: Back Projection	20
Figure 8: Unit Step Function.....	23
Figure 9: Projection of Unit Step Function.....	24
Figure 10: Filtered Back Projection of Unit Step Function	25
Figure 11: Un-Filtered Back Projection of Unit Step Function.....	26
Figure 12: Cosine Source Distribution	27
Figure 13: Projection of Cosine Source Distribution.....	28
Figure 14: Filtered Back Projection of Cosine Source Distribution	29
Figure 15: Plot of TREAT Core X-Y Cross-Section with Slot	31
Figure 17: Flux Plot of TREAT Core X-Z Cross-Section with Slot.....	33
Figure 18: Average Flux Plot at hodoscope Plane.....	34
Figure 19: Reconstruction of TREAT core with No Filter	35
Figure 20: Reconstruction of TREAT core with Ramp Filter	36
Figure 21: Different Filters (Maria, 2011).....	37
Figure 22: Reconstruction of TREAT core with Hann Filter, $w=0.1$	38
Figure 23: Reconstruction of TREAT core with Hann Filter, $w=0.3$	39
Figure 24: Reconstruction of TREAT core with Hann Filter, $w=1$	39
Figure 25: Sketch of TREAT with Hodoscope (Jensen, 2016)	42
Figure 26: Sketch of TREAT with Hodoscope (Plan and Elevation Views) (Jensen, 2016)	42
Figure 27: Neutron Detector Set up.....	44
Figure 28: Three Pin Geometry (Wu, 1982).....	48
Figure 29: Initial Test Fuel Position in Hodoscope View Field (Wu, 1982).....	49
Figure 30: Mass Distribution of L7 after $t=2.242s$	50
Figure 31: Mass distribution L7, 2.242 s after transients [per Column].....	51
Figure 32: Mass distribution L7 after 14.445 s followed by transients	51
Figure 33: Mass Distribution in 2, 4 and 14 Seconds	52
Figure 34: Mass Distribution Percentile Plot.....	53
Figure 35: Residual Plots	54
Figure 36: Original Mass Plot.....	54
Figure 37: Fourier Transformed Mass Plot.....	55
Figure 38: Back Projected Mass Plot.....	55
Figure 39: All 3 Plots at $t=14.445$ second.....	56
Figure 40: Pixelated Hodogram Plot (Jensen, 2016)	57
Figure 41: Reconstructed Pixelated Hodogram Plot [No Filter]	58
Figure 42: Reconstructed Pixelated Hodogram Plot [Ramp Filter].....	59
Figure 43: Reconstructed Pixelated Hodogram Plot [Hann Filter].....	60
Figure 44: Reconstructed Pixelated Hodogram Plot [Hann Filter] $w=0.1$	61

Figure 45: Reconstructed Pixelated Hodogram Plot [Hann Filter] $w=0.3$ 62
Figure 46: Reconstructed Pixelated Hodogram Plot [Hann Filter] $w=1$ 63

List of Tables

Table 1: Critical Super-saturation of Various Liquids.....	8
Table 2: Critical Super-saturation with Percentage Alcohol.....	9
Table 3: Hodogram Data at t=2.242 seconds.....	45
Table 4: Hodogram Data at t=4.879 seconds.....	46
Table 5: Hodogram Data at t=14.445 seconds.....	47
Table 6: Multiple Regression Results.....	53

Improvement in Transient Testing Reactor (TREAT): Application of Cloud Chamber,
Simulation and Analytical Approach using Filtered Back Projection (FBP)

Dissertation Abstract—Idaho State University (2020)

This dissertation presents an innovative method of supporting real time imaging of fuel pins and other structures during transient testing. The major fuel-motion detection device that is studied in this dissertation is the Hodoscope that requires collimators. This dissertation provides 1) feasibility of portable cloud chamber without a collimator to track the origin of neutrons, 2) MCNP model and simulation of TREAT core with central fuel element replaced by slotted fuel element that provides an open path between test samples and hodoscope detector, and 3) an analytical approach of obtaining source information from the flux (image) using Back Projection in Mathematica. Another avenue of this dissertation is to support imaging of the test specimen during transient and quantify the mass based on hodogram data. An analytical approach of Filtered Back Projection (FBP) can be used to understand imaging and with the right choice of filter, we can improve the resolution. Multiple illustrations of the Filtered Back Projection (FBP) technique with the right choice of filters are presented in this dissertation. In addition to numerical computations, analytical analysis helps to build insight and this dissertation provides both the analytical and computational analysis of imaging to improve the resolution.

Key Words: Hodoscope, cloud chamber, transient testing, collimators, MCNP, TREAT, Filtered Back Projection (FBP), Mathematica, hodogram, filters, resolution, numerical computation, analytical approach

Chapter 1: Introduction

A: Background

This research performed at Idaho State University is the part of the collaborative effort among three other universities and Idaho National Laboratory (INL). Other universities are University of Wisconsin-Madison, Ohio State University and Kansas State University. The overall objective was to develop a real time imaging tool to monitor fuel behavior during transient testing in Transient Testing Reactor (TREAT). This team effort was aimed at providing a basic understanding of the science behind fuel slumping behavior. This dissertation presents the feasibility of using a cloud chamber, some simulation, and analytical studies in TREAT as a part of possible improvements. TREAT is an air-cooled reactor fueled with uranium dioxide dispersed in graphite. It was constructed in 1958 and operated from 1959 until 1994. It has been restarted in 2017 and part of this collaborative effort was to support its restart.

B: Statement of the Problem

Safe and reliable operation of nuclear reactors has always been one of the topmost priorities in nuclear industry. Transient testing allows us to understand the time-dependent behavior of the neutron population in response to either a planned change in the reactor conditions or unplanned circumstances. These unforeseen conditions might occur due to sudden reactivity insertions, feedbacks, power excursions, instabilities and accidents. To study such behavior, we need transient testing, which is like car crash testing to estimate the durability and strength of a car design. In nuclear designs, such transient testing is capable of simulating a wide range of accidents due to sudden

reactivity insertions and helps to study feasibility and integrity for the fuel to be used in certain reactor types. This testing involves a high neutron flux environment and a real time imaging technology with advanced instrumentation with appropriate accuracy and resolution to study the fuel slumping behavior. With the aid of transient testing and adequate imaging tools, it is possible to test the safety basis for reactor and fuel designs that serves as a gateway in licensing advanced reactors in future. To that end, it is crucial to fully understand advanced imaging techniques both analytically and via simulations.

This dissertation presents a different method of supporting real time imaging of fuel pins and other structures during transient testing. The major fuel-motion detection device that is studied in this proposal is the hodoscope that requires collimators. This proposal provides 1) feasibility of portable cloud chamber without a collimator to track the origin of neutrons, 2) Monte Carlo N-Particle (MCNP) model and simulation of Transient Reactor Test (TREAT) core with fuel elements replaced by slotted fuel elements that provide an open path between test samples and the hodoscope detectors, 3) an analytical approach of obtaining source information from the flux (image) using Filtered Back Projection (FBP), and 4) an illustration of fuel slumping behavior during a simulated Loss of Flow (LOF) accident using hodogram data from a TREAT test. A comparative study of hodoscope analysis and filtered back projection methods is presented as well.

Original Path: Cloud Chamber

This dissertation is a part of a larger project at Idaho State University (ISU). The project provided some advanced instrumentation studies in support of the Transient Reactor Test (TREAT) facility, which is the principal facility in the US for safety testing of reactor fuel. It was in operation from 1959 to 1994 and has since re-started after a 20-year hiatus.

The TREAT restart effort was completed in February 2018, which was one year ahead of schedule and \$20 million under budget (Wachs, 2019). It is a high flux, air-cooled, thermal, pulsed reactor. A key instrument used in TREAT is the hodoscope. It records the motion of fissionable material in the test capsule as the fuel fails during accident scenarios. It consists of multi-channel front and back collimators. During the experiment, fast neutrons produced in the test capsule are collimated providing a 2-dimensional “map” of fuel location and are time stamped in the hodoscope detection system. Hodoscope system measurements need improvements in order to yield higher resolution images. Thus, the feasibility study of a hodoscope using a cloud chamber without a collimator was performed as the first task.

Alternate path: Back Projection

Images obtained from the hodograms can be improved using an analytical method of back projection. Back projection allows us to unfold the source information from the image. If we have a finite number of projections of an object, by running these projections back through the image, we can obtain the rough approximation of the original source as shown in Figure 5 in the next page. Projections coming from the source region will have constructive interactions in the image plane. However, there will be a noticeable blurring and to reduce such effects, filtering is necessary. The technique of back projection with necessary filtering is called Filtered Back Projection (FBP), which can be found in the following section.

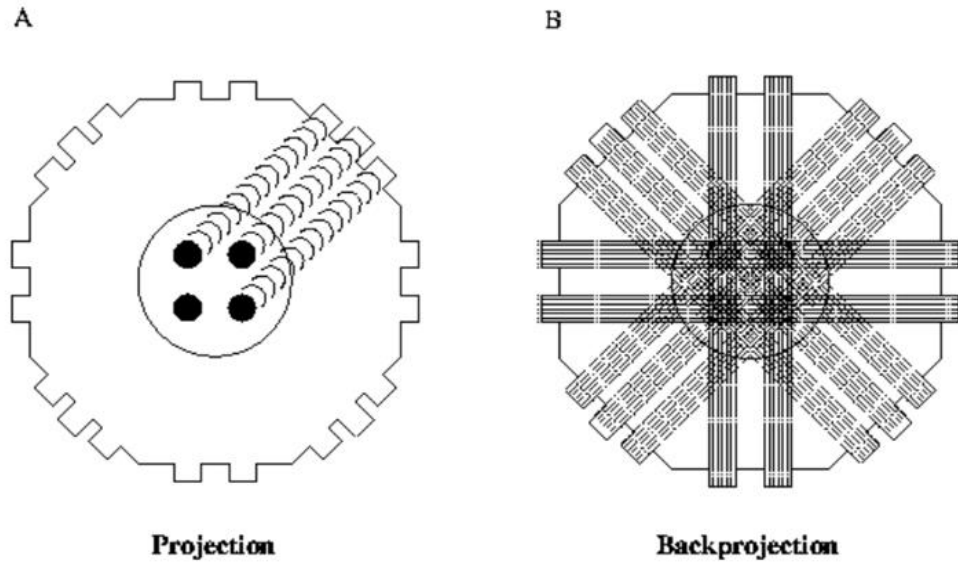


Figure 1: Back Projection

Figure 1A above shows the finite number of projections at 45 degrees intervals of an object containing radioactive source (Anders, 1997). The sides of an octagon represent these projections. Figure 1B shows the back projection which is done by running projections back through the image to obtain the object representation. Dark spots at the center represent the constructive interactions at the source locations. There is a possibility of over representation at the central region. The optimal way to eliminate such overlapping is by using an appropriate filter. The combination of back projection and filtering is the FBP.

1.1. Background on Cloud Chamber

A cloud chamber works by causing a vapor inside to supersaturate. This can be done in several ways depending on the type of fluid used. One of the most typical ways is by creating temperature and pressure gradients. Expansion of the volume inside the chamber causes the drop in pressure and temperature and super saturation may occur. The gas at lower temperature can hold more vapor than it can hold at the saturated state. When ionizing radiation enters the supersaturate molecule (ethyl alcohol) environment, it strips electrons off the molecules. Removal of electrons result in ions and these ions are sometimes called “cloud seeds” since they act as the nucleation sites. The vapor will nucleate on the ions and these ions are only formed in the path of the radiation that allows us to see the visible trails. Figure 2 below shows (a) ionizing radiation striking the alcohol molecule (b) seed nuclei (ionized) attracting other molecules to leave a visible trail.

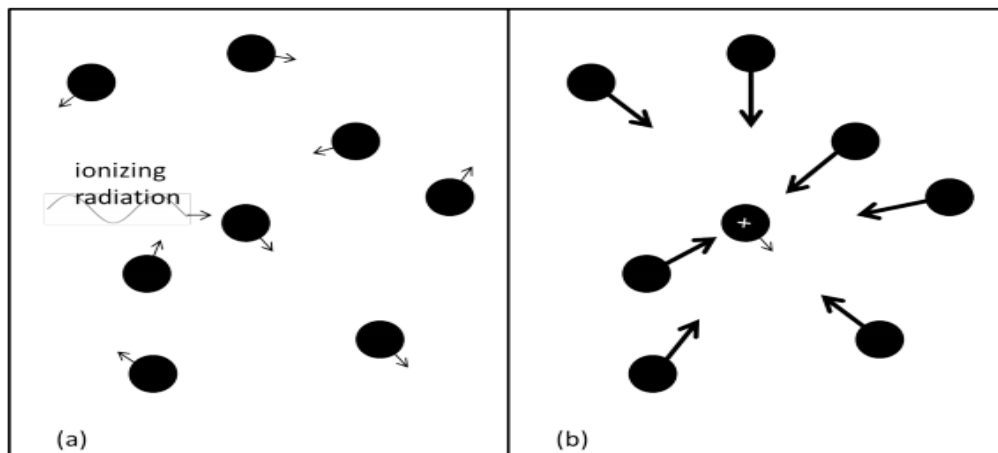


Figure 2: Mechanism of Cloud Trail Formation (Dennis, 2015)

Super saturation depends on the types of mixture used. The amount of super saturation present due to expansion can be calculated by the equation below: (Gupta, 1946)

$$S = \frac{P_1}{P_2} \left(\frac{V_1}{V_2} \right)^\gamma = \frac{P_1}{P_2} \left(\frac{1}{1+\varepsilon} \right)^\gamma \quad [1]$$

where, P_1 and P_2 are the saturation pressures at the initial and final temperatures,

$1 + \varepsilon$ is the expansion ratio and γ is the ratio of specific heats of the gaseous mixture present in the chamber.

In the cloud chamber, a mixture of a vapor and a gas is used, and the specific heat ratio is calculated with the following equation:

$$\frac{1}{\gamma-1} = \frac{1}{\gamma_g-1} * \frac{P_g}{\pi} + \frac{1}{\gamma_v-1} * \frac{P_v}{\pi} \quad [2]$$

where, P_g and P_v are the partial pressures of the gas and vapor respectively, γ_g and γ_v are specific heats of gas and vapor respectively and $\pi = P_g + P_v$ is the total pressure of the mixture.

The optimum liquid combination of ethyl alcohol and water that gives a low expansion ratio, low background fog and good electron tracks in the chamber is theoretically given by Flood's equation given as: (Gupta, 1946)

$$\log S'_c = k \left[\frac{T'}{\theta} \right] \left[\frac{M}{\rho} \right]' \quad [3]$$

where, S_c is the critical super saturation of the mixture, k is the proportionality constant, θ is the absolute temperature, T' is the surface tension, and $\left[\frac{M}{\rho} \right]'$ is the molecular volume of the mixture.

1.2. Literature Review on Cloud Chamber

A report on the “Wilson Cloud Chamber and its Applications in Physics” by N.N. das Gupta and S.K. Ghosh was extensively used to understand the physics of cloud formation for different types of a Wilson Chamber (Gupta, 1946). In addition, this paper presents physical measurements that are carried out using cloud chamber and highlights the factors that influence the quality of the tracks. Other applications of such cloud chambers are to detect alpha, beta, gamma, neutrons, cosmic rays etc. Fundamental equations that describe the temperature and pressure dependence on cloud formation were taken from this paper.

“The Construction and Characterization of a Large Volume Wilson Cloud Chamber Utilizing Orthogonal Cameras for Image Capture” thesis by Cody Womack was used as a good reference to understand the construction and operation of a cloud chamber (Womack, 2016). This thesis provides useful information that a diffusion cloud chamber based on the temperature differential is better suited than the traditional pulsed one and even if the pulsed one were to be used; mechanical piston movement is preferable to the pneumatic type. This is because the mechanical cloud chambers have variable stopping positions to adjust the desired expansion ratio and are relatively fast. Another advantage of mechanical pistons is that they do not require threshold pressure to move the piston, while the pneumatic chambers have some resetting time before the piston can overcome the friction. Other improvements are use of higher resolution cameras with higher framerates, appropriate material selections and desired mixture to yield noticeable cloud trails.

“The Principles of Cloud-Chamber Technique” by J.G. Wilson was used to understand the super-saturation, condensation and growth of drops during cloud formation (Wilson, 1951). Vomer and Flood showed the relation between the critical super-saturation, bulk value of surface tension and molecular mass (Wilson, 1951). Table 1 below shows the theoretical and experimental values for critical super-saturation for several organic liquid candidates. (Wilson, 1951)

Table 1: Critical Super-saturation of Various Liquids

Liquid	Temperature, θ , after expansion °K.	M	σ g./cm. ³	T dyne/cm.	$(p/p_0)_{crit.}$	
					Theor.	Exp.
Water	264	18.0	1.00	77.0	(4.85)	4.85
Methyl alcohol	270	32.0	0.81	24.8	1.84	3.20
Ethyl alcohol	273	46.0	0.81	24.0	2.30	2.34
<i>n</i> -Propyl alcohol	270	60.1	0.82	25.4	3.20	3.05
Isopropyl alcohol	265	60.1	0.81	23.1	2.90	2.80
Butyl alcohol	270	74.1	0.83	26.1	4.50	4.60
Nitromethane	252	61.0	1.20	40.6	6.25	6.05
Ethylacetate	240	88.1	0.94	30.8	11.0	12.3

Flood further extended the relations between critical super-saturation, surface tension and molecular mass for mixed vapors particularly for the mixtures of ethyl alcohol and water (Flood, 1934). His results for the mixtures was of great importance to this dissertation to select an appropriate composition and was used as a reference to validate whether the results we obtain were in accordance to the values we found in the literature. Table 2 below shows Flood’s experimental super-saturation values at different proportions of alcohol and water mixtures at different temperatures. (Wilson, 1951)

Table 2: Critical Super-saturation with Percentage Alcohol

% of alcohol molecules in liquid	Temperature after expansion °K.	Effective M/σ cm. ³ /g.mol.	T dyne/cm.	$(p/p_0)_{crit}$	
				Theor.	Exp.
0	264	18.0	77.0	(4.85)	4.85
3.9	273	19.4	51.3	3.30	2.64
11.5	276	22.1	36.8	2.45	1.97
35.3	280	—	—	1.92	1.75
67.1	277	—	—	1.70	1.62
77.9	275	47.8	25.4	1.97	1.77
100	273	57.1	24.0	2.30	2.34

1.3. Cloud Chamber Results

The optimum liquid combination of ethyl alcohol and water that give low expansion ratio, low background fog and good electron tracks in the chamber was about 67% of alcohol and 33% by volume of water theoretically. Data presented in table 2 were used in conjunction with the equation 3 to obtain the plot. Figure 3 below shows the corresponding plot.

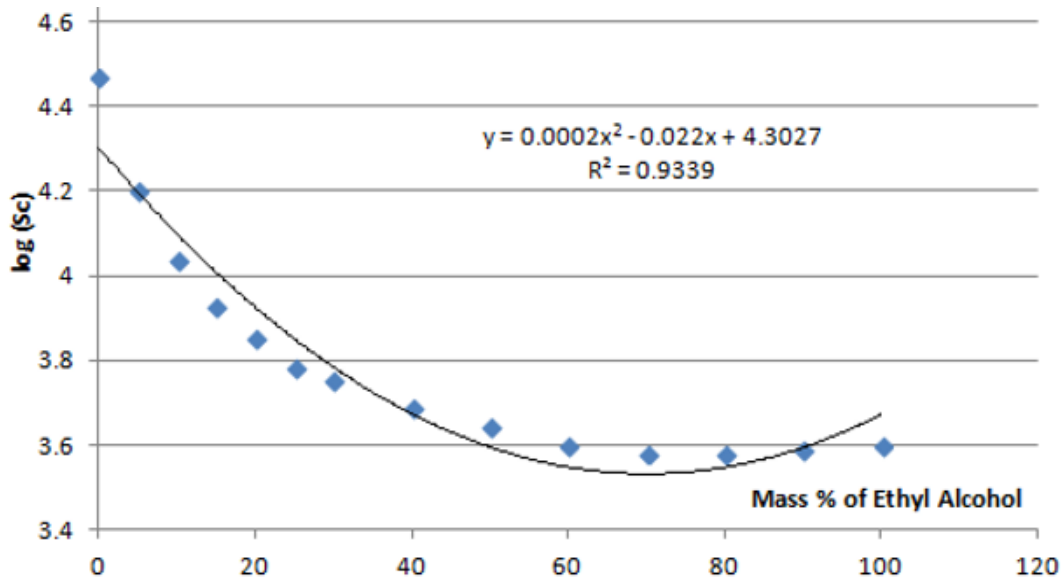


Figure 3: Critical Super-saturation vs. Alcohol (%)

As seen from the plot, the critical super saturation reaches a minimum value with a mixture of about 65-70% alcohol and remaining water. This was in accordance to the results found in the literature.

A cloud chamber was built by the Idaho National Laboratory (INL) to test the feasibility of detecting nuclear fuel in a container. It was subsequently loaned to ISU for our project. Several runs were performed in the cloud chamber to get a better trail.

Figures 4 and 5 below show few of those results.

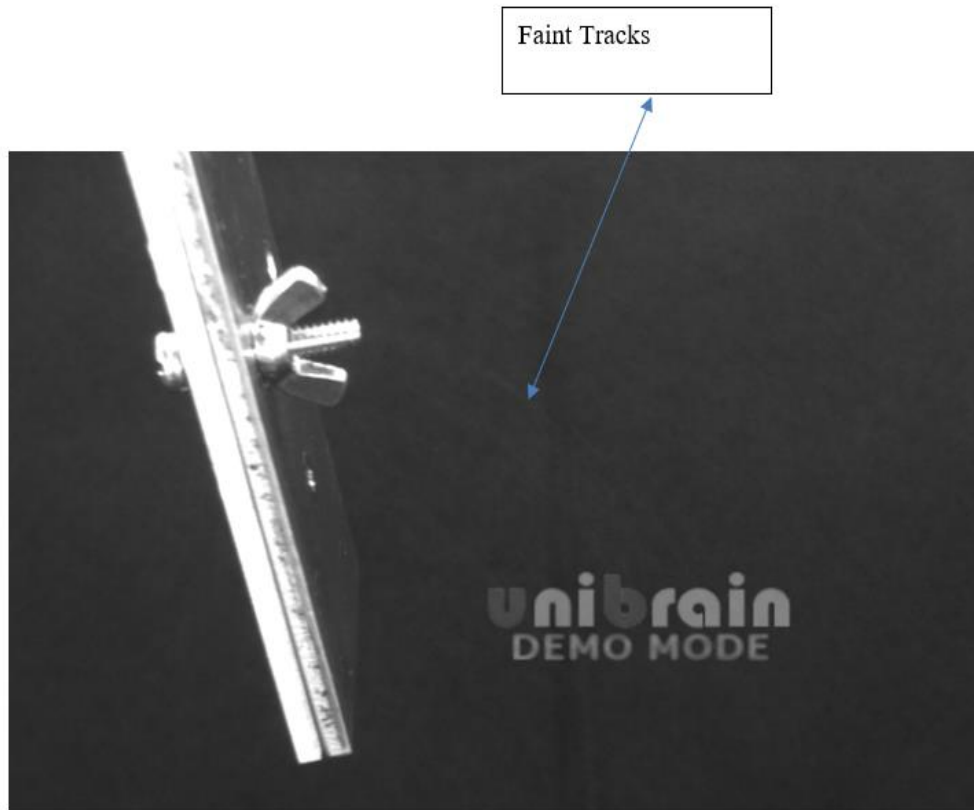


Figure 4: Cloud Trail Image



Figure 5: Cloud Trail Image

In the figures above, the tracks were very faint and last for very small fraction of seconds. The movement of the gas was noticed. At this point, we determined that the cloud chamber is not a viable option even if it might have several advantages (e.g., being able to eliminate the collimator). At this point, our path changed to supporting a collimated hodoscope by using back projection techniques to see if we can enhance the image resolution.

However, we did make several recommendations for further work if desired. A diffusion cloud chamber is recommended to be used instead of a pulsed one. It allows an observer to “see” radiation, because in the wake of the particle a trail of condensation is formed (Welch, 2012). The trails of ionizing radiation are formed when an energetic particle interacts with the gaseous mixture inside the sealed chamber by knocking off the

electrons. These tracks have characteristic shapes such as an alpha particle tracks are thick and straight while that of beta particles are wispy. In the diffusion type, there is a continuous generation of the ions and it needs no resetting. Moreover, the diffusion cloud chamber creates fewer air currents as it is independent of the expansion of gas and it can operate in normal atmospheric pressure. If pulsed chamber were to be used, it would be recommended to implement mechanical method of moving the pistons rather than the pneumatic one. In a mechanical system there is no need of air pressure to be built up and can be easily controlled if it is mechanical. During the operation, there was a minor problem created due to the leakage of the alcohol mixture and it is recommended to use better adhesive material to prevent such hindrance. Also better resolution cameras with upgraded software would provide better resolution images.

Chapter 2: Filtered Back Projection (FBP)

2.1. Literature Review on FBP

Filtered back projection is a technique that helps to unfold the source information from the image. It has two distinct steps: a) Back projection of each event that provides information about the source location. Since these projections are summed up together, there is a significant blurring at the regions where these projections overlap b) Filtering by means of an appropriate filter in the frequency domain of $[w]$, we may reconstruct the image with higher resolution. This technique of back projection with necessary filtering is called Filtered Back Projection (FBP). To understand the physics behind imaging and FBP, the textbook “Intermediate Physics for Medicine and Biology” by Russel K. Hobbie and Bradly J. Roth was used (Roth, 2007). This textbook shows important techniques for analyzing data that ranges from simple curve fitting to continuous Fourier transform. Moreover, it was very useful to obtain the relationship between the image and object. The use of Fourier analysis for image reconstruction from its projections using filtered back projections are discussed in Chapter 12 of this textbook.

The paper titled as “Filtered Back-Projection in 4-Pi Compton Imaging with a Single 3D Position Sensitive CdZnTe Detector” by Dan Xu provides image reconstruction algorithms for Compton scattering cameras that provide higher detection efficiency without the use of a mechanical collimator. This paper investigates a filtered back projection algorithm applied to a single 3-dimensional position sensitive CdZnTe detector. This paper concludes that the filtered back projection algorithm performed in spherical harmonics reduces the computation time and cost and because of its linear property; the FBP reconstruction can be performed event-by-event for real time imaging.

The paper titled “Utilization of an optimum low-pass filter during filtered back projection in the reconstruction of single photon emission computed tomography images of small structures” by Mpumelelo Nyathi was used to understand the types of filters and their application in improving the quality of the filtered back projection (FBP) image by eliminating the noise. This study aimed at selection of an optimum low-pass filter for FBP reconstruction of Single Photon Emission Computed Tomography (SPECT) images of small structures. A low pass filter allows the retention of low frequencies while blocking higher frequencies and when used in conjunction with the ramp filter will yield a better image. The Parzen, the Hanning, and the Butterworth filters are among the commonly used low-pass filters (Nyathi, 2018). The Parzen filter is a smoothing filter, which can eliminate noise at high frequency. However, it degrades the spatial resolution. The Butterworth filter is a low-pass filter that is generally preferred in SPECT image filtering. It has the potential of reducing the noise while preserving image resolution. It is well suited for utilization due to its ability to change the shape through the cut-off frequency and the order parameter (Nyathi, 2018). On the other hand, the ramp filter is a high pass filter that eliminates the star artifact consequences of a simple projection by allowing the passage of high frequencies and restricting the passage of low frequencies. The high pass filter can be applied in trans-axial plane to reduce if not eliminate blurring and has the equations in the frequency domain as: $k = (k_x^2 + k_y^2)^{\frac{1}{2}}$ where k is the ramp filter frequency, and k_x and k_y are values on a rectangular grid of k -space. The use of it can be found in both the theory and results sections.

2.2. TREAT Related References

Loss -of -Flow (L7) data was obtained from “Self-Shielding Corrections for the TREAT Hodoscope Interpretation” by Robert Wu, which was initially provided by A. De Volpi and E. A. Rhodes from Argonne National Laboratory (ANL) (Wu, 1982). This research provides the significance of self-shielding present in the hodoscope data and it might be a major contributor on mass conservation ambiguities. This paper uses a 91-group integral transport method to estimate the effect of self-shielding variations to the hodoscope detector count rate. A process called autoregressive-integrated-moving-average (ARIMA) was used in interpreting the TREAT hodoscope data. Other notable references used for the preparation of this dissertation are “Experimental Results and Improvements in the Fast Neutron Hodoscope” by De Volpi and C.H Freese (DeVolpi, 1978); “High Power Level Transient Reactor Test (TREAT) Facility Sodium Loop Meltdown Experiment on an Unbonded EBR-II Mark I Fuel Pin” by E. Dickerman et al (Dickerman, 1970) ; “Fast Neutron Hodoscope at TREAT: Methods for Quantitative Determination of Fuel Dispersal” by A. De. Volpi et al (DeVolpi, 1980).

Chapter 3: Theory

3.1: Theory of Back Projection

Several image reconstruction techniques have been used such as maximum likelihood algorithms, and algebraic reconstruction techniques (ART). However, these are the indirect methods and are computationally intensive (Xu, 2006). Filtered back projection is preferable when computational time is limited. It is a direct reconstruction method and has powerful applications in imaging. It is necessary to understand the theory behind filtered back projection first. Back projection when combined with necessary filtering constitutes the filtered back projection (FBP).

3.2. Object and Image

The image of an object is formed by the convolution of the object function (source profile) and the point spread function (PSF) of the imaging system. The PSF of the system is the weighted average over the entire energy spectrum that causes blurring effects of diffraction, pinhole geometry and the hodoscope detector. PSF gives the degree of blurring caused by diffraction and this function is useful in extracting the right beam size out of the pinhole image. The equation below represents the relationship between object and image.

$$g(x, y) = \iint_{-\infty}^{\infty} f(x', y')h(x, x'; y, y')dx'dy' \quad [4]$$

where $g(x, y)$ is the two-dimensional image of a two-dimensional object $f(x', y')$, and the function h is the point spread function that tells how information from a point source spreads out over the image plane. If we assume a point source (delta function), the point-

spread function has the same form as the image from a point source like the impulse response in 1D. Equation 5 below represents a simple object-image relationship.

$$g(x, y) = f(x, y) \otimes \otimes h(x, y) \quad [5]$$

Where, the operator $\otimes \otimes$ is the convolution integral and $h(x, y)$ is the point spread function.

3.3. Fourier Transform

Any object or image function can be represented by the Fourier transform in two dimensions as defined by equation below:

$$f(x, y) = \left(\frac{1}{2\pi}\right)^2 \int_{-\infty}^{\infty} dk_x \int_{-\infty}^{\infty} dk_y [C(k_x, k_y) \cos(k_x x, k_y y) + S(k_x, k_y) \sin(k_x x, k_y y)] \quad [6]$$

Where coefficients are given by,

$$C(k_x, k_y) = \int_{-\infty}^{\infty} dx \int_{-\infty}^{\infty} dy f(x, y) (\cos(k_x x, k_y y)),$$

$$S(k_x, k_y) = \int_{-\infty}^{\infty} dx \int_{-\infty}^{\infty} dy f(x, y) (\sin(k_x x, k_y y)) \quad [7]$$

In terms of convolution integrals, the coefficients can be written as: (Roth, 2007)

$$C_g(k_x, k_y) = C_f(k_x, k_y)C_h(k_x, k_y) - S_f(k_x, k_y)S_h(k_x, k_y)$$

$$S_g(k_x, k_y) = C_f(k_x, k_y)S_h(k_x, k_y) + S_f(k_x, k_y)C_h(k_x, k_y) \quad [8]$$

In complex notation, we may define the Fourier transforms as: [Roth, 2007]

$$F(k_x, k_y) = \iint_{-\infty}^{\infty} f(x, y) e^{-i(k_x x + k_y y)} dx dy$$

$$f(x, y) = \left[\frac{1}{2\pi} \right]^2 \iint_{-\infty}^{\infty} F(k_x, k_y) e^{i(k_x x + k_y y)} dk_x dk_y \quad [9]$$

Coefficients given by equation [7] can be simplified by taking $k_y=0$ (the k_x -axis) as follows:

$$C(k_x, 0) = \int_{-\infty}^{\infty} \cos(k_x x) dx \int_{-\infty}^{\infty} f(x, y) dy = \int_{-\infty}^{\infty} \cos(k_x x) F(\theta = 0, x) dx$$

$$S(k_x, 0) = \int_{-\infty}^{\infty} \sin(k_x x) dx \int_{-\infty}^{\infty} f(x, y) dy = \int_{-\infty}^{\infty} \sin(k_x x) F(\theta = 0, x) dx \quad [10]$$

3.4. Back Projection

Every point in the projection contributes to some point in the reconstructed image. Let us consider two points A and B with point A located at the center and has same distance x' while point B will have different values of x' for each projection (Roth, 2007) as shown in figure 6.

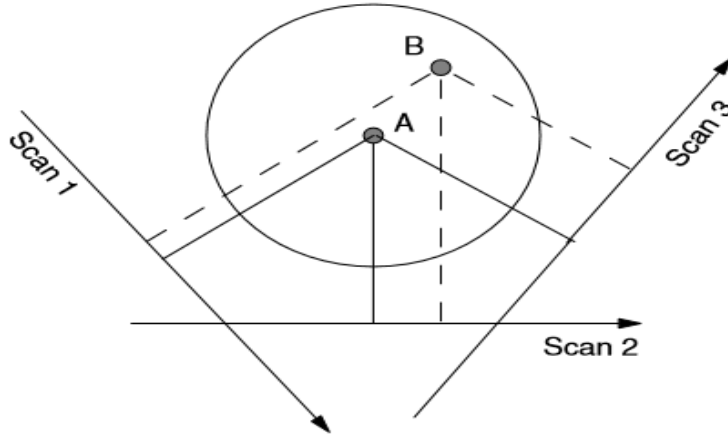


Figure 6: Back Projection (Roth, 2007)

Exact projection distance can be calculated using the transformation equations [11] and inverse transformation equations [12] using vector components of any arbitrary point P in appropriate axes as shown in figure 7.

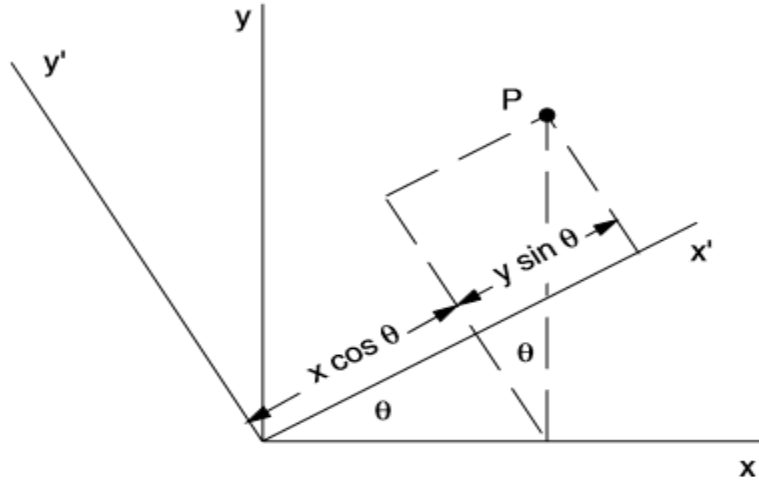


Figure 7: Back Projection

$$x' = x \cos\theta + y \sin\theta,$$

$$y' = -x \sin\theta + y \cos\theta, \quad [11]$$

$$x = x' \cos\theta - y' \sin\theta,$$

$$y = x' \sin\theta + y' \cos\theta \quad [12]$$

The back projection $f_b(x, y)$ at point (x, y) is the sum of $F(\theta, x')$ for every projection where x' is the original projection through that point. Equation [13] is the fundamental basis of back projection that gives the image $f_b(x, y)$ obtained by taking projections of the object $F(\theta, x')$ using convolutions of object with point spread function h .

$$f_b(x, y) = \int_0^\pi F(\theta, x') d\theta \quad [13]$$

where

$$F(\theta, x') = \int f(x, y) dy' = \int f(x' \cos\theta - y' \sin\theta, x' \sin\theta + y' \cos\theta) dy' \quad [14]$$

3.5. Filtering

Filtering is done before making back projection to reduce blurring or noise. In this process, the projection $F(\theta, x')$ is manipulated to produce a new function $G(\theta, x')$ whose back projection is the desired $f(x, y)$. To do this, let us say there is any arbitrary function $g(x, y)$ that we do not know but which, when projected and back projected yields our desired function $f(x, y)$. [Roth, 2007] That is,

$$f(x, y) = g_b(x, y) = \iint_{-\infty}^{\infty} \frac{g(x', y')}{[(x-x')^2 + (y-y')^2]^{\frac{1}{2}}} dx' dy' \quad [15]$$

Rewrite the coefficients as:

$$\begin{aligned} C_f(k_x, k_y) &= C_g(k_x, k_y)C_h(k_x, k_y) - S_g(k_x, k_y)S_h(k_x, k_y) \\ S_f(k_x, k_y) &= C_g(k_x, k_y)S_h(k_x, k_y) + S_g(k_x, k_y)C_h(k_x, k_y) \end{aligned} \quad [16]$$

Solving above simultaneous equations we get:

$$\begin{aligned} S_g &= \frac{C_h S_f - S_h C_f}{C_h^2 + S_h^2} \\ C_g &= \frac{C_h C_f + S_h S_f}{C_h^2 + S_h^2} \end{aligned} \quad [17]$$

$$C_h(k_x, k_y) = 2\pi(k_x^2 + k_y^2)^{-1/2}$$

$$S_h(k_x, k_y) = 0, \quad [18]$$

Using 16, 17 and 18, we get;

$$C_g(k_x, k_y) = \frac{1}{2\pi} (k_x^2 + k_y^2)^{1/2} C_f(k_x, k_y),$$

$$S_g(k_x, k_y) = \frac{1}{2\pi} (k_x^2 + k_y^2)^{1/2} S_f(k_x, k_y). \quad [19]$$

Using projection in the x-axis, ($y=0$, and $k_y=0$), equation 19 is simplified to:

$$\begin{aligned} C_g(k_x, 0) &= C_f(k_x, 0) \frac{|k_x|}{2\pi} \\ S_g(k_x, 0) &= S_f(k_x, 0) \\ C_h &= \frac{|k_x|}{2\pi}, S_h = 0 \end{aligned} \quad [20]$$

It is important to note how coefficients of $g(x, y)$ are related to $f(x, y)$ and note the factor of $\frac{k}{2\pi}$ used in filtering.

Finally, we can relate $G(\theta, x')$ and $F(\theta, x')$ so that we do not need to know $g(x, y)$. Let us consider again the projections on the x-axis:

$$F(0, x) = \frac{1}{2\pi} \int_{-\infty}^{\infty} [C_f(k_x, 0) \cos(k_x x) + S_f(k_x, 0) \sin(k_x x)] dk_x,$$

$$G(0, x) = \frac{1}{2\pi} \int_{-\infty}^{\infty} [C_g(k_x, 0) \cos(k_x x) + S_g(k_x, 0) \sin(k_x x)] dk_x \quad [21]$$

Using equations 20 and 21, we may rewrite a general equation for $G(\theta, x)$ that is independent of the choice of axis;

$$G(0, x) = \frac{1}{2\pi} \int_{-\infty}^{\infty} [C_f(k_x, 0) \cos(k_x x) + S_f(k_x, 0) \sin(k_x x)] \frac{|k_x|}{2\pi} dk_x. \quad [22]$$

Some simple demonstrations of the technique are given in the following chapter.

Chapter 4: Applications of FBP to Different Sources

4.1. FBP for a Step Function:

The technique of FBP is illustrated by using a step function as shown in figure below.

Consider a step function $f(x) = 1, x^2 + y^2 < a^2$ and zero otherwise and the plot of which is shown in figure 8.

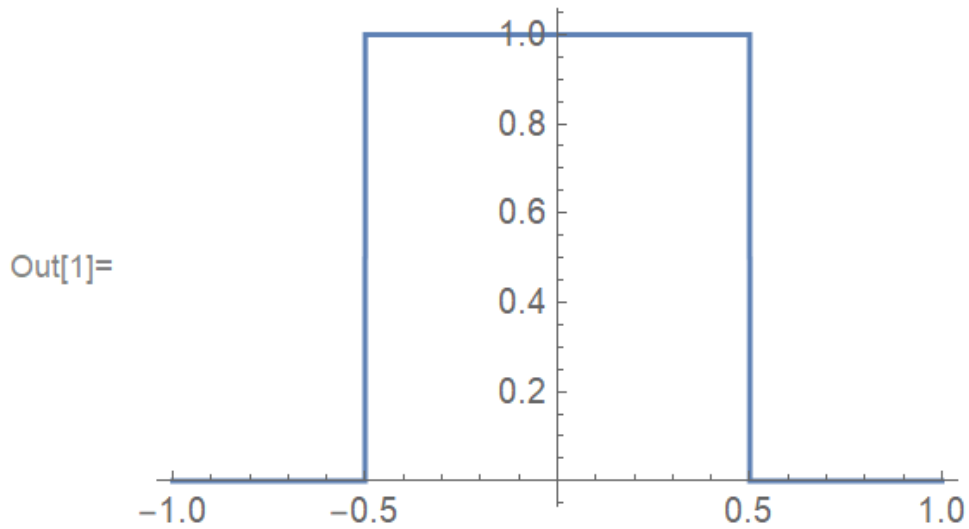


Figure 8: Unit Step Function

The projection of this function is calculated by using equation [14] as:

$F(\theta, x') = 2\sqrt{a^2 - x'^2}$ for $|x'| < a$ and 0 otherwise and the corresponding plot of the projection is given below in figure 9.

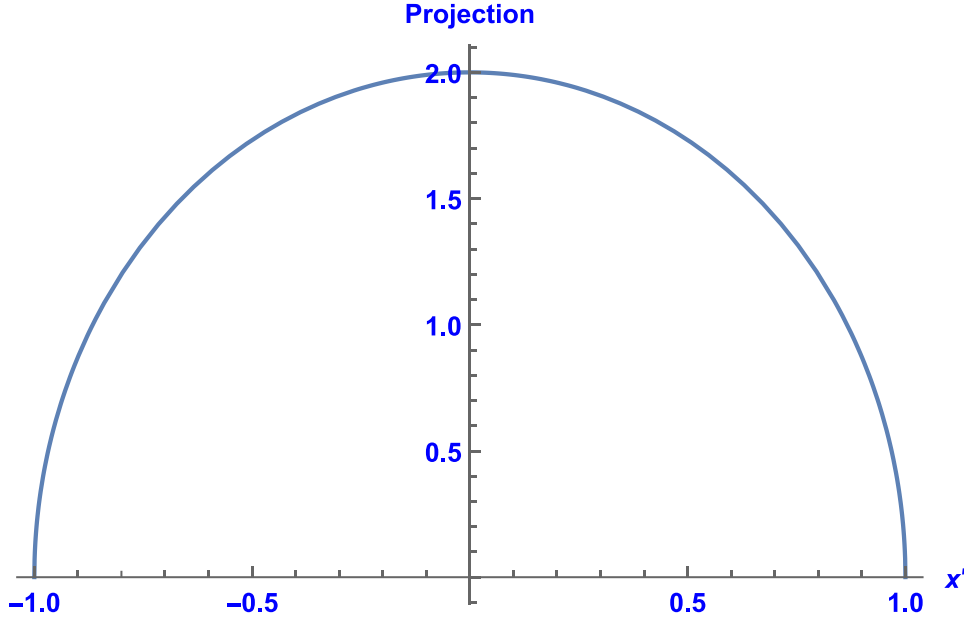


Figure 9: Projection of Unit Step Function

Filtering is done by multiplying the transform by a high-pass filter (ramp filter) and then doing the inverse Fourier transform.

$$C(k_x, 0) = \int_{-\infty}^{\infty} \cos(k_x x) dx \int_{-\infty}^{\infty} f(x, y) dy = \int_{-\infty}^{\infty} \cos(k_x x) F(\theta = 0, x) dx$$

$$C(\theta, k) = \int_{-\infty}^{\infty} \text{Cos}(kx') * 2\sqrt{a^2 - x'^2} dx' = 4 \int_0^a \text{Cos}(kx') * 2\sqrt{a^2 - x'^2} dx'$$

Above integral can be done by using the integral property found in the handbook of mathematical functions [Abramowitz, 1972] presented in the appendix.

$$C(\theta, k) = 4 \int_0^a \text{Cos}(kx') * 2\sqrt{a^2 - x'^2} dx' = 4 * \left[\frac{\pi * a}{2k} * J_1(ka) \right]$$

Where J_1 is the Bessel function of first kind. Now, filtering is done by multiplying the above equation by a factor of $\frac{k}{2\pi}$ which yields:

$$C(\theta, k) = [a * J_1(ka)]$$

It is important to note that the sine term vanishes since the projection is an even function.

After filtering, we need to do the inverse transform by using the equation [21]

$$G(0, x) = \frac{1}{2\pi} \int_{-\infty}^{\infty} [C_g(k_x, 0) \cos(k_x x) + S_g(k_x, 0) \sin(k_x x)] dk_x$$

$$\begin{aligned} G(0, x) &= \frac{1}{2\pi} \int_{-\infty}^{\infty} C(\theta, k) * \text{Cos}(kx) dk = \frac{1}{2\pi} \int_{-\infty}^{\infty} [a * J_1(ka)] * \text{Cos}(kx) dk \\ &= \frac{1}{\pi} \int_0^{\infty} [a * J_1(ka)] * \text{Cos}(kx) dk \\ &= \frac{1}{\pi} \begin{cases} 1 & \text{for } |x| < a \\ \frac{-a}{\sqrt{x^2 - a^2} * [x + \sqrt{x^2 - a^2}]} & \text{for } |x| > a \end{cases} \end{aligned}$$

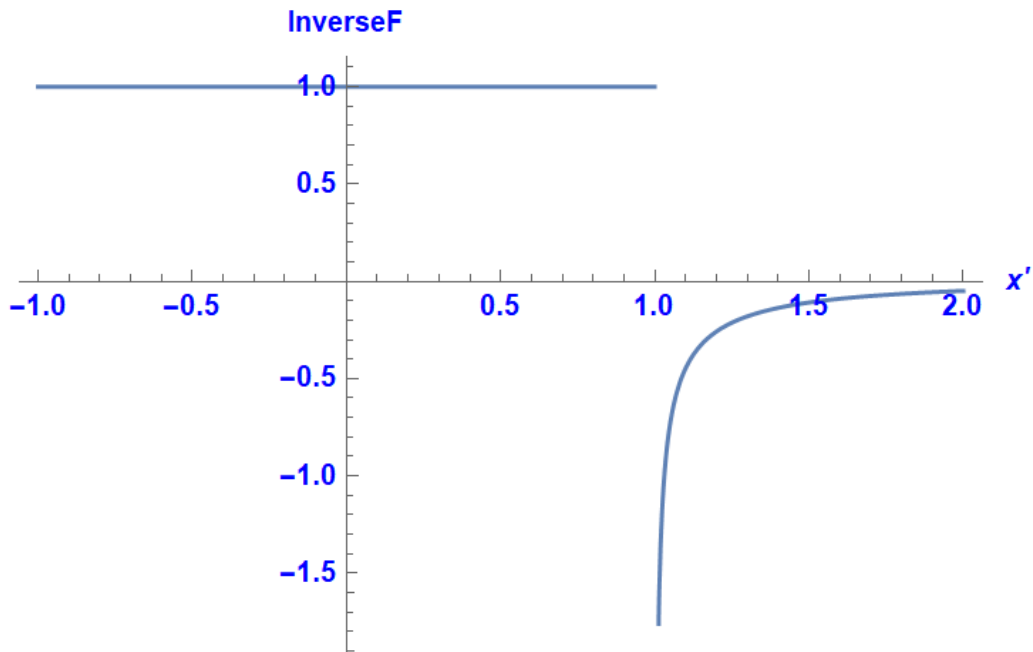


Figure 10: Filtered Back Projection of Unit Step Function

The final step is to use back projection using equation [13] along the y-axis ($x=0$).

$$f_b(x, y) = \int_0^\pi F(\theta, x') d\theta$$

$$f_b(0, y) = \begin{cases} 1 & \text{for } |y| < a \\ 0 & \text{for } |y| > a \end{cases} \quad \text{Same as initial unit function.}$$

Let's solve the same problem without filtering.

Recall $F(\theta, x') = 2\sqrt{a^2 - x'^2}$ for $|x'| < a$ and zero otherwise.

$$f_b(0, y) = \int_0^\pi 2\sqrt{a^2 - (y \sin\theta)^2} d\theta = 4 \int_0^{\pi/2} \sqrt{1^2 - (y \sin\theta/a)^2} d\theta$$

[Which has the form of Elliptical Integral of Second kind $E(\phi, k) =$

$$\int_0^\phi \sqrt{1 - k^2 \sin^2(\theta)} d\theta]$$

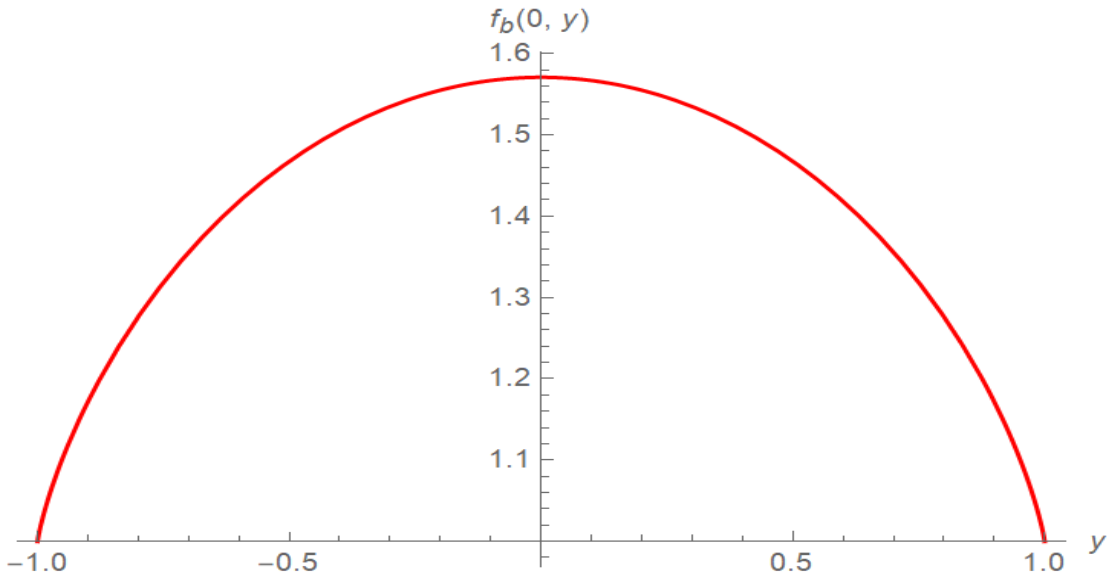


Figure 11: Un-Filtered Back Projection of Unit Step Function

The back projection with filtering yields an accurate representation of the source. It is crucial to note the introductions of the Bessel function of the first kind in back projection

with filtering and an elliptical integral of the second kind when back projected without filtering. The significance of different filters will be explained in later sections.

4.2. FBP for a Cosine Source:

As a part of second illustration, a cosine source distribution was taken. A critical bare reactor in rectangular coordinate system assumes the cosine flux distribution in all three dimensions and possesses a symmetry on either side of a central axis. Consider a flux function,

$f(x) = A * \cos(Bx)$ where A and B are constants , $x^2 + y^2 < a^2$ and zero otherwise and the plot of which is shown in figure 12 below:

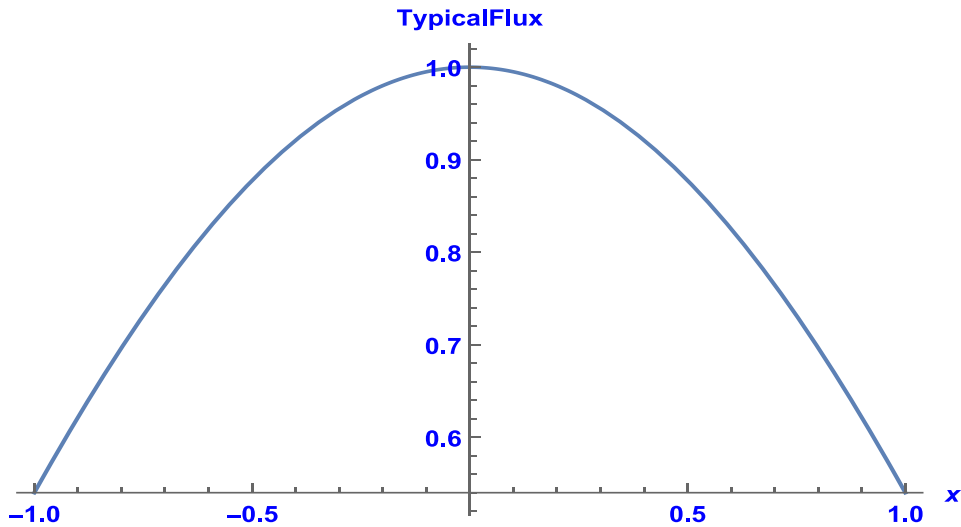


Figure 12: Cosine Source Distribution

The projection of this function is calculated by using equation [14] as:

$F(\theta, x') = \sin(x) * 2\sqrt{a^2 - x^2}$ for $|x'| < a$ and 0 otherwise and the corresponding plot of the projection is given in figure 13.

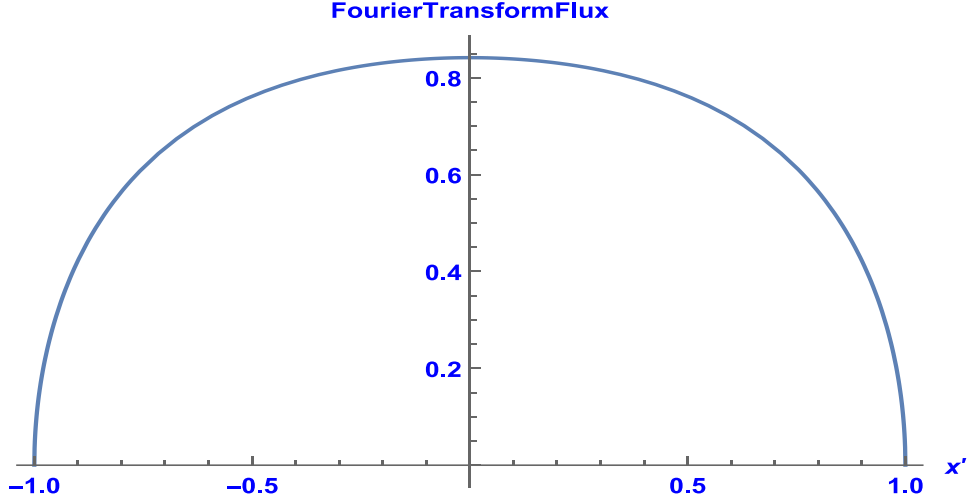


Figure 13: Projection of Cosine Source Distribution

Filtering is done by multiplying the projection with a high-pass filter and then doing the inverse Fourier transform.

$$(k_x, 0) = \int_{-\infty}^{\infty} \cos(k_x x) dx \int_{-\infty}^{\infty} f(x, y) dy = \int_{-\infty}^{\infty} \cos(k_x x) F(\theta = 0, x) dx$$

$$\begin{aligned} C(\theta, k) &= \int_{-\infty}^{\infty} \text{Cos}(kx') * \text{Sin}(x') * 2\sqrt{a^2 - x'^2} dx' \\ &= 4 \int_0^a \text{Cos}(kx') * \text{Sin}(x') * \sqrt{a^2 - x'^2} dx' \end{aligned}$$

The above integration is not trivial; thus, Taylor series expansion of the square root function was used to find the first ten coefficients which were then integrated in Mathematica. Again, the sine terms vanish since the projection is an even function and with necessary filtering and inverse transformation shown below, we obtain the back projected plot.

Equation [21] gives the inverse transform as:

$$G(0, x) = \frac{1}{2\pi} \int_{-\infty}^{\infty} [C_g(k_x, 0) \cos(k_x x) + S_g(k_x, 0) \sin(k_x x)] dk_x$$

$$G(0, x) = \frac{1}{2\pi} \int_{-\infty}^{\infty} C(\theta, k) * \text{Cos}(kx) dk$$

$$= \frac{1}{2\pi} \int_{-\infty}^{\infty} \left[4 \int_0^a \text{Cos}(kx') * \text{Sin}(x') * \sqrt{a^2 - x'^2} dx' \right] * \text{Cos}(kx) dk$$

The final step is to use back projection using equation [13] along the y-axis (x=0) and the corresponding plot can be found in figure 14.

$$f_b(x, y) = \int_0^{\pi} F(\theta, x') d\theta$$

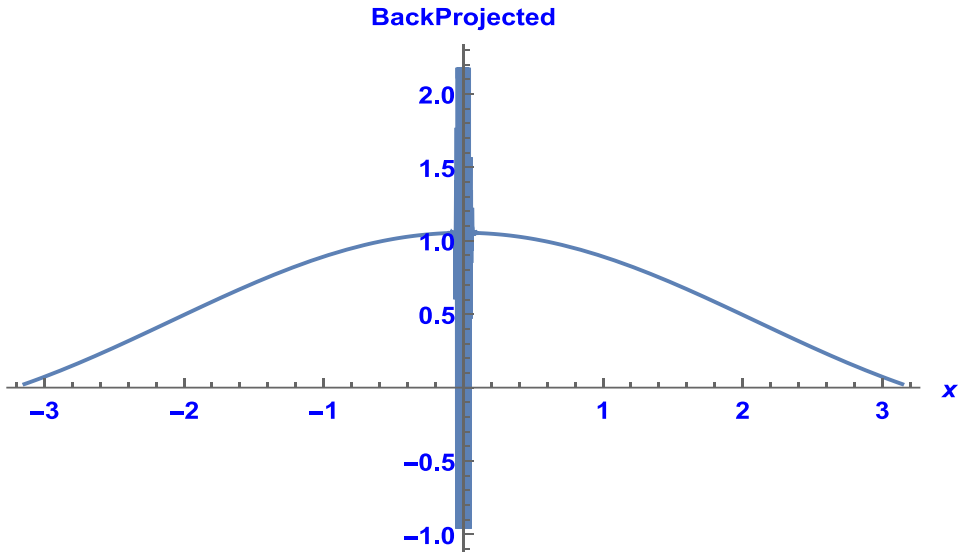


Figure 14: Filtered Back Projection of Cosine Source Distribution

4.3. FBP for a Hodoscope Plane Flux obtained from TREAT

A detailed model of TREAT reactor was built in MCNP with central fuel element replaced by dummy slotted fuel containing the sample (Pope, 2016). In the MCNP model, k-code was run with flux mesh on the xz axis and the point flux tallies on the locations where we need the fluxes. One of the important point to note is that the model obtained was for a critical system and the source driven problem does not work since MCNP need

to track infinite particles. It needs to be modified to be in slightly sub-critical state. One more note, MCNP has no concept of time so we need to define a source and it generates particles and tracks them. Any fluxes we obtain are based on per source particle hence we might notice flux values in decimals.

There are three control rod types. There are four compensation rods located near the center of the core, four pairs of control rods and four pairs of transient rods. Rods are driven from the bottom and are pushed up to add reactivity and dropped down to shut down. Another important point to note is that the transient rods are ejected from the core to produce transient. Figure 15 below shows the corresponding MCNP model with the viewing slot added to provide open path for sample and hodoscope plane.

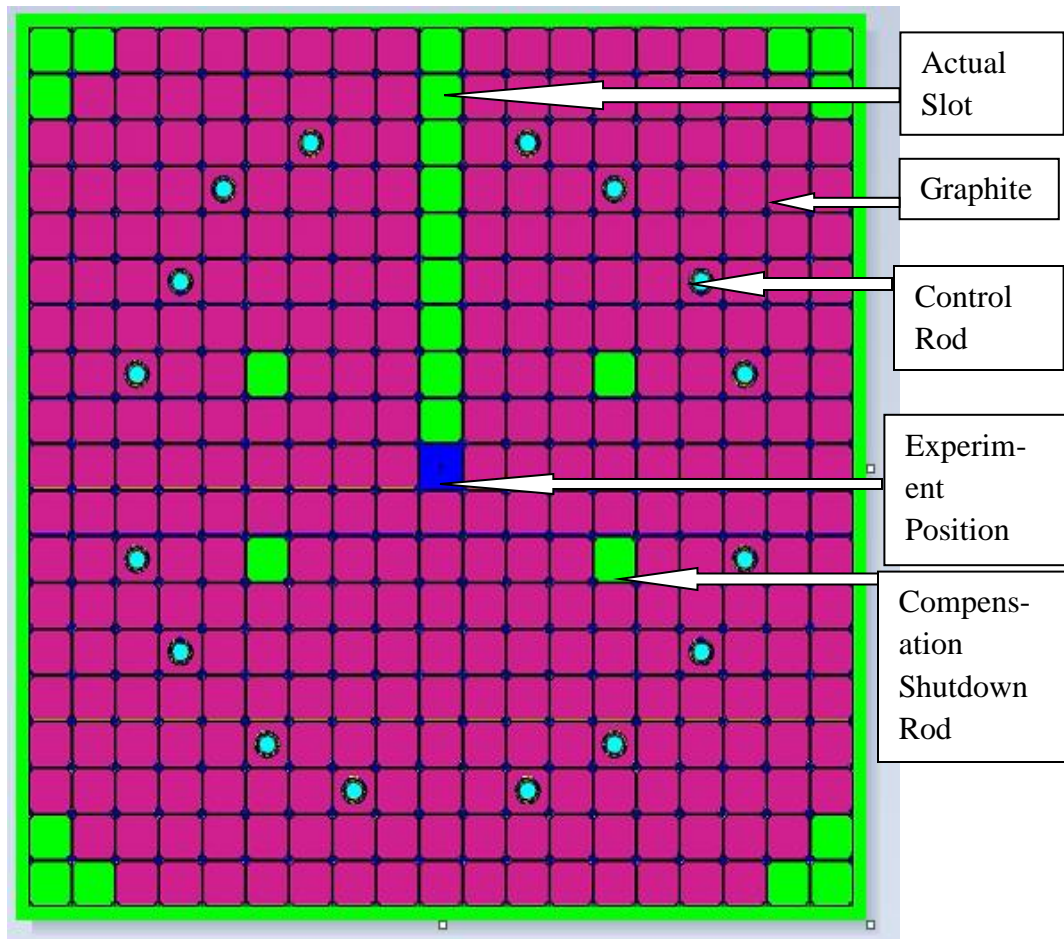


Figure 15: Plot of TREAT Core X-Y Cross-Section with Slot

The MCNP calculations were performed in this model. The MCNP input deck is given in the Appendix B. We ran one million histories and used F4 tallies to obtain the flux plot. F4 tally uses track length estimator and scores the number of particle-track lengths per unit volume. The statistical uncertainties are within the range of 0.015 to 0.02 which fall below 2%.

Figures 16 and 17 below show the x-y and x-z flux plots respectively with the flux measured in the units of # of neutrons/cm² and distances in cm (with million particles) to ensure better quality flux.

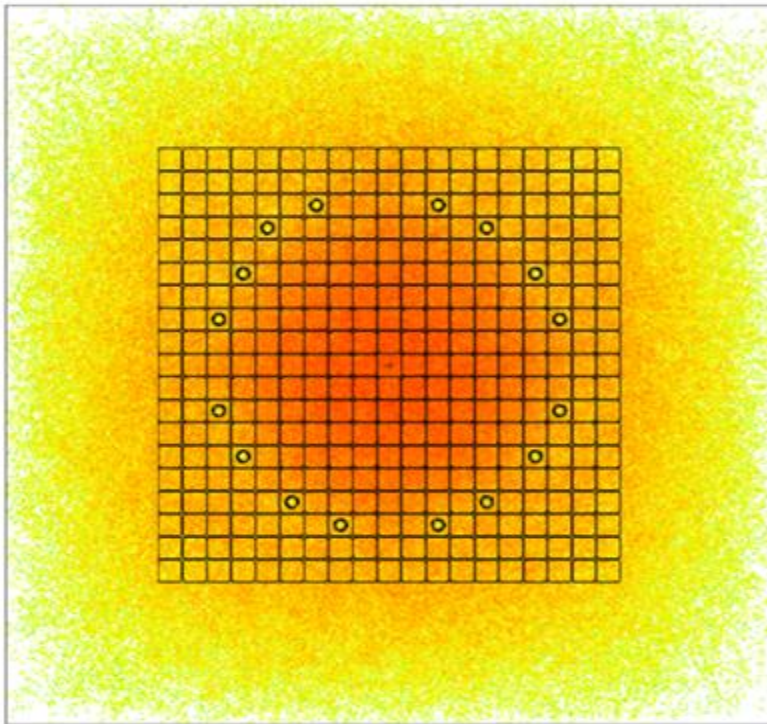


Figure 16: Flux Plot of TREAT Core X-Y Cross-Section with Slot

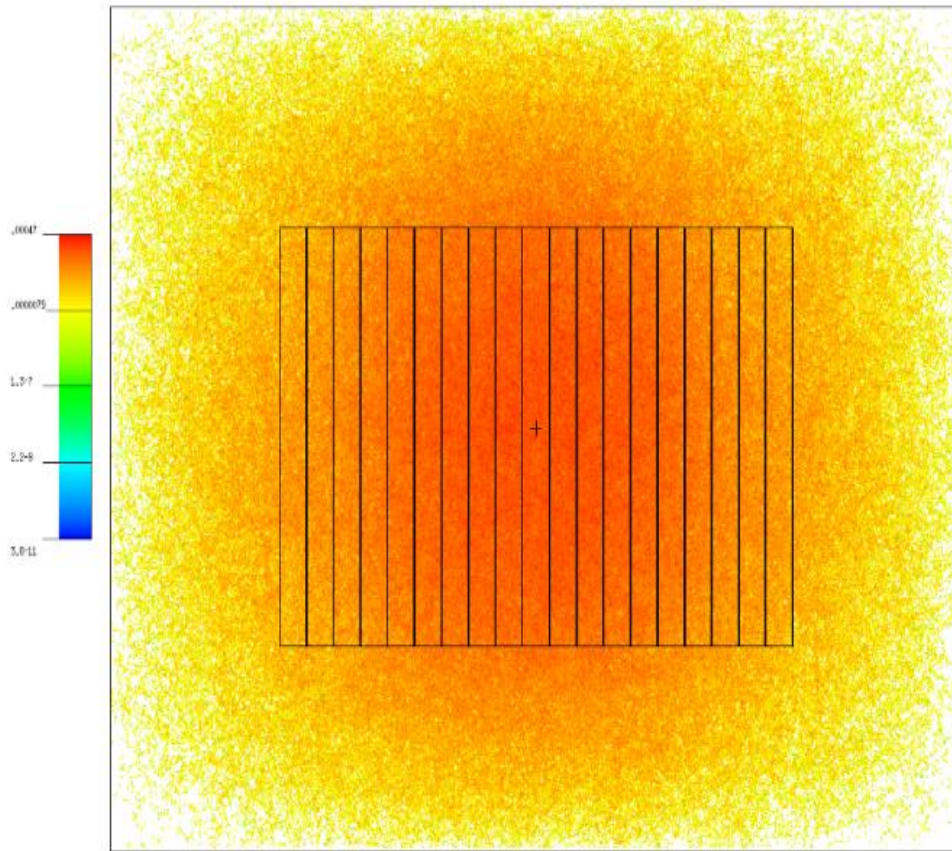


Figure 17: Flux Plot of TREAT Core X-Z Cross-Section with Slot

The point flux tallies, and the mesh tallies were added to determine the flux at different distances from the center to the hodoscope location. It is an eigenvalue calculation but not a fixed source calculation. Flux data at varying distances were imported and plotted first with no fuel in the center. The average and uncollided vertical flux profile at the hodoscope plane ($x=\text{hodoscope distance}$, $y=0$) are plotted in the following figure 18.

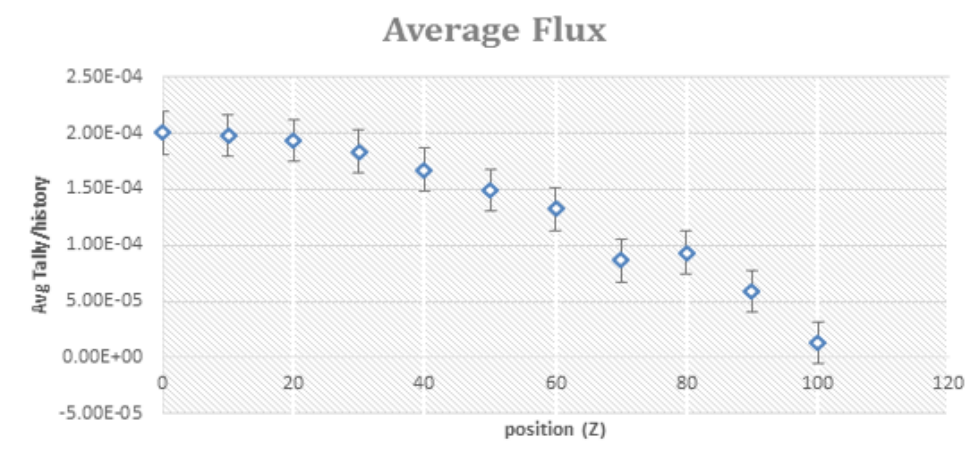


Figure 18: Average Flux Plot at hodoscope Plane

Filtered back projection technique may be applied to the TREAT core imaging with a suitable filter. Figure 19 below shows the reconstruction of the TREAT core with a slotted fuel element for the test capsule without using any filter. TREAT image data that gives figure 15 were extracted in Mathematica to see if we can reconstruct it with a suitable filter. The flux plots presented in figures 16 and 17 were used to make an image. With appropriate radon and inverse radon transformation, following image was reconstructed. Based on the plots, suitable filter will be selected for the future TREAT imaging.

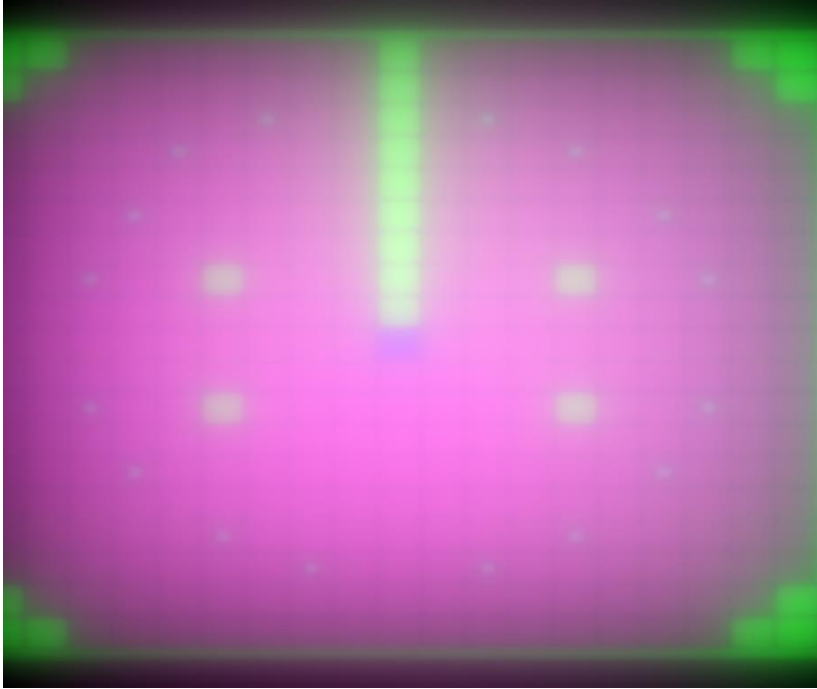


Figure 19: Reconstruction of TREAT core with No Filter

The next step in the process is to include filters to process the image shown in figure 19. Figure 20 below shows the reconstruction of the TREAT core using the FBP technique with a ramp filter. Ramp filter is a high pass filter that filters out the low frequencies and allows the high frequencies. It was found that the ramp filter increased the resolution and quality of the image. However, it still magnifies noise coming from the projection data and it was not the perfect filter. This filter may work reasonably well for images with less complex frequency distribution.

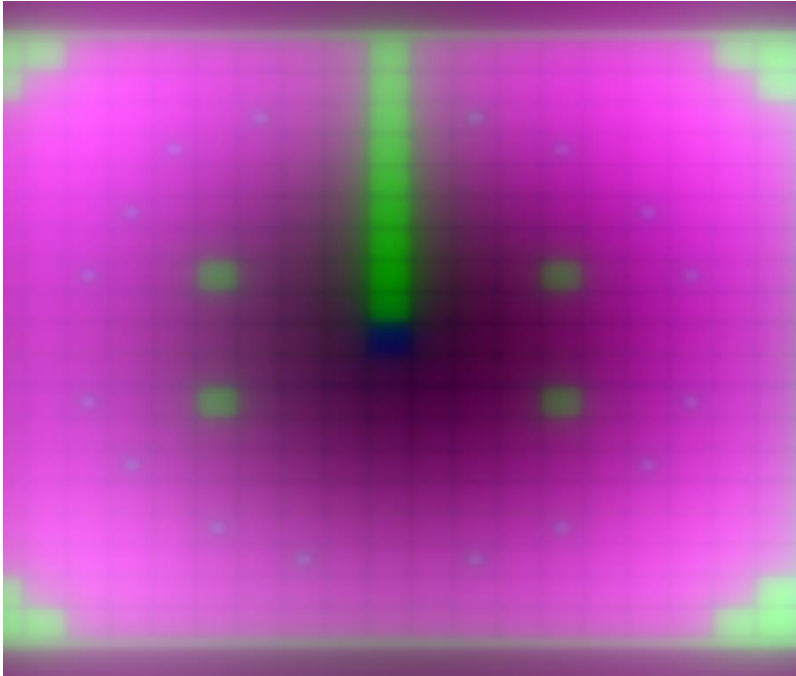


Figure 20: Reconstruction of TREAT core with Ramp Filter

The Hann filter is a low pass filter (smoothing filter) that filters out the high frequencies and allows the low frequencies. It was found that the Hann filter increased the resolution and quality of the image. FBP technique in conjunction with Hann filter reduces the noise that causes blurring to yield better resolution image as expected. However, it does not preserve edges so suitable cut off frequency need to be selected which will be discussed in the following section.

A low pass (e.g., Hann) filter is characterized by the cut off frequency. The cut off frequency or roll-off frequency is defined as the frequency above which the noise is reduced or eliminated. The Hann filter is defined in the frequency domain as: (Maria, 2011)

$$H(f) = \begin{cases} 0.54 + 0.46 \cos\left\{\frac{\pi f}{f_m}\right\}, & 0 \leq |f| \leq f_m \\ 0 & \text{otherwise} \end{cases}$$

where f is the spatial frequencies of the image and f_m is the cut-off frequency. It is very effective in reducing the noise since it reaches zero very quickly as seen from the figure 21.

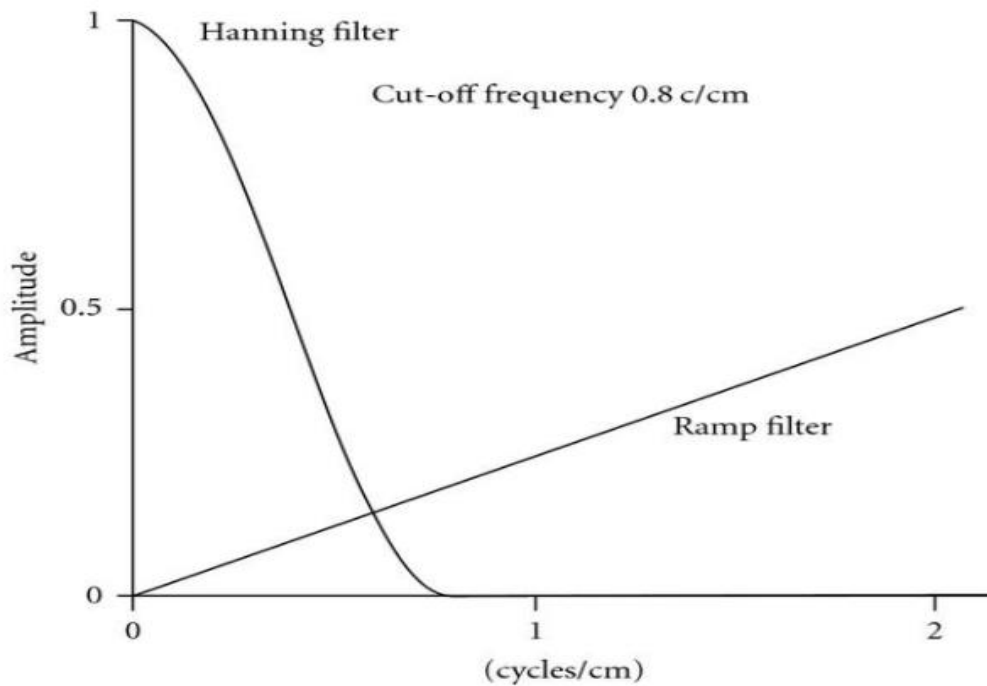


Figure 21: Different Filters (Maria, 2011)

Figures 22, 23 and 24 below shows the reconstruction image of the TREAT core with slotted fuel element using Hann filter with varying cut-off frequencies as 0.1, 0.3 and 1 cycles/cm respectively.

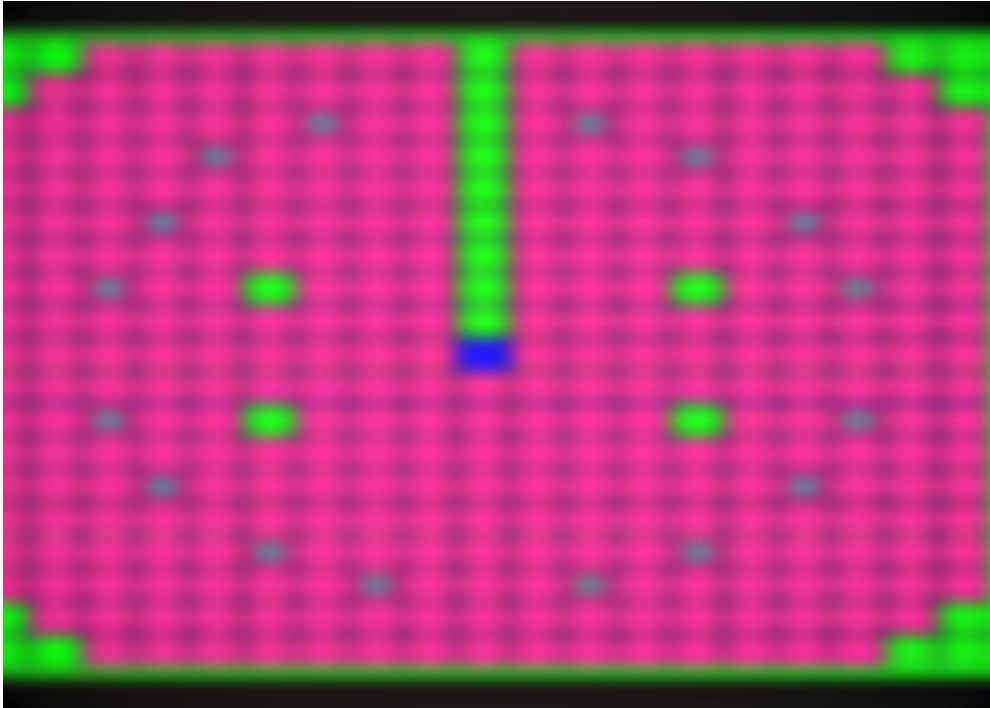


Figure 22: Reconstruction of TREAT core with Hann Filter, $w=0.1$

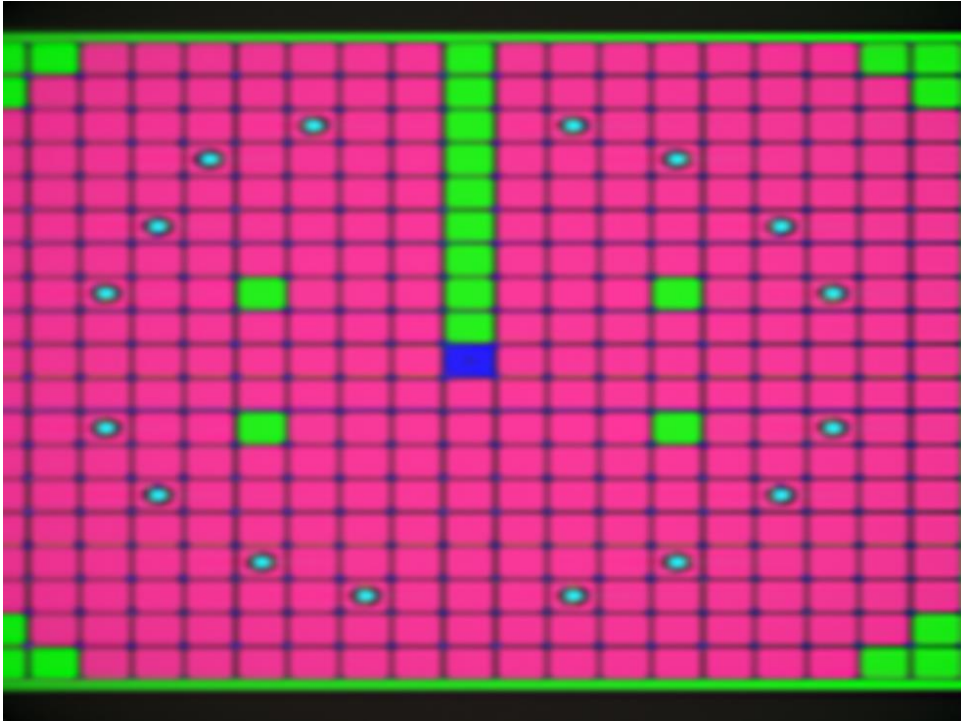


Figure 23: Reconstruction of TREAT core with Hann Filter, $w=0.3$

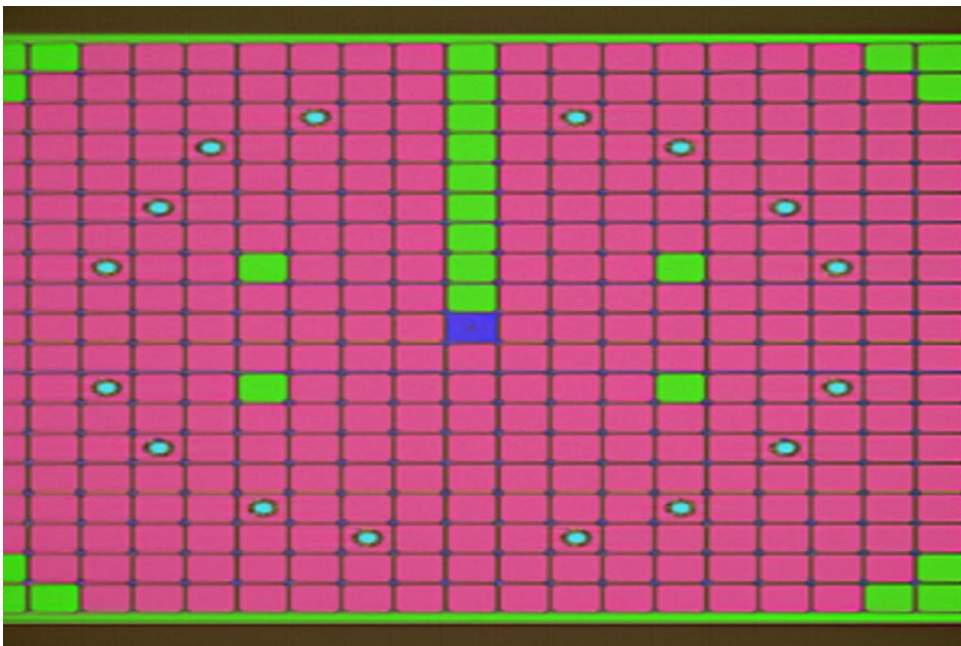


Figure 24: Reconstruction of TREAT core with Hann Filter, $w=1$

It can be observed from the figures above that the value of cut-off frequency determines how the filter will affect both image noise and resolution. In other words, the higher the cut-off frequency, the better is the spatial resolution and therefore much detailed image can be obtained. In conclusion, the Hann filter with a cut-off frequency close to 1 cycle/cm would be recommended for the final image reconstruction.

Chapter 5: TREAT L7 Data

5.1. TREAT Reactor

Transient Reactor Test (TREAT) reactor is the principal facility in the US for safety testing of reactor fuel. It was in operation from 1959 to 1994 and has been restarted in 2017 after a 25-year hiatus. It is a high flux, air-cooled, thermal, pulsed reactor. TREAT was designed by Argonne National Laboratory (ANL) and is located in INL. The reactor core has a 19 by 19 array of fuel and reflector assemblies, which are 10 cm (4 in) square and 2.7 m (8.8 ft) long. The assemblies contain a 1.2-m (4-ft) active fuel region with 0.6-m (2-ft) reflector regions above and below (Jensen, 2016). The fuel used in TREAT is a mixture of highly enriched UO_2 dispersed in graphite. The graphite has sufficient heat capacity to allow the fuel to reach high temperature during a pulse transient that a strong negative temperature coefficient of reactivity will terminate the pulse. Shielding blocks provide necessary biological shielding. The maximum-allowed core energy and peak power are approximately 2.5-GJ and 19 GW, respectively (Jensen, 2016).

A key instrument used in TREAT is the Hodoscope (Jensen, 2016). It can record the motion of fissionable material in the test capsule as the fuel fails during accident scenarios. Figures 25 and 26 below show the schematics of TREAT facility and hodoscope (plan and elevation views) respectively.

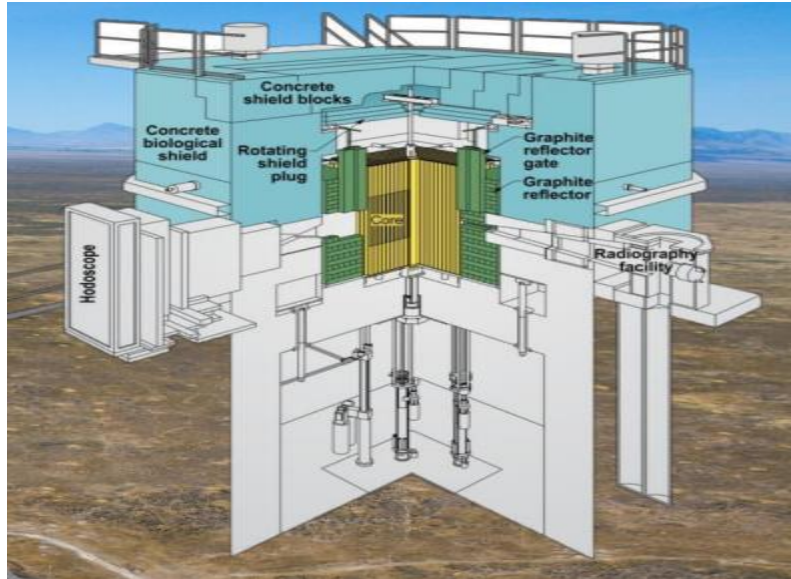


Figure 25: Sketch of TREAT with Hodoscope (Jensen, 2016)

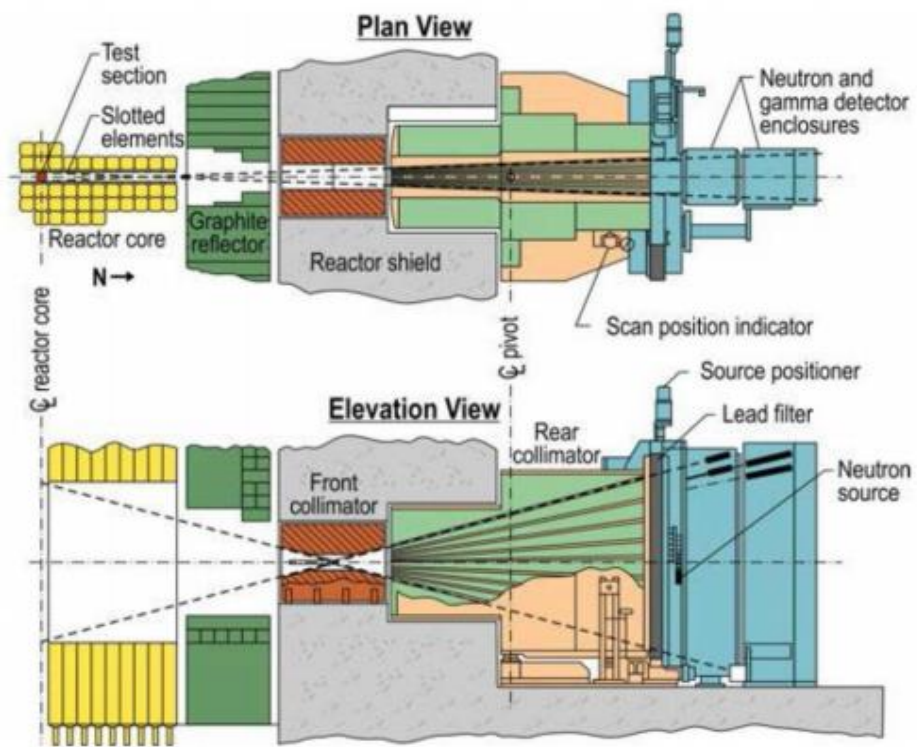


Figure 26: Sketch of TREAT with Hodoscope (Plan and Elevation Views) (Jensen, 2016)

5.2. Hodoscope Raw Data

To illustrate the fuel motion during transients, there have been several tests performed over time. Quantification of the fuel mass from the hodoscope data poses a serious fundamental problem as it would violate the conservation of mass of the fuel. As a part of this dissertation, some of the causes of the violation will be studied. Some of the possible causes are melting of the structure, shelf shielding and flaws in the detector response. Accumulation of mass at different locations with time will be plotted and analyzed and the significant contributor to such unambiguity will be predicted. Before we analyze the data, it is important to know how the TREAT fast neutron hodoscope records the fuel motion.

A hodoscope measures the fast neutrons emitted by fission in the test fuel by having an array of detectors placed after the collimator which looks at the viewing slot (see Figure 27). The test fuel is usually surrounded by steel, sodium and thermal neutron filters that make up the test section (DeVolpi, 1976). The test fuel is placed in the center of the TREAT reactor in a high flux environment which induces fission. Neutrons released after fission are free to travel in all directions and those headed into the collimator can be detected via neutron detectors. It is to be noted that not all the neutrons will register a count in the detector. That depends on detector response, geometric location and neutron energy. For the purpose of detection, an array of 334 Hornyak buttons (ZnS (Ag) scintillation type) fast neutron detectors are used. Such detectors usually operate above 1 MeV energy threshold in order to reduce the gamma sensitivity and noise.

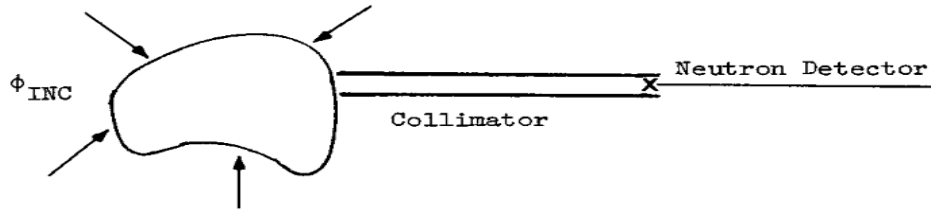


Figure 27: Neutron Detector Set up

The data of TREAT loss-of-flow test, L7 were selected to study the fuel motion behavior (Wu, 1982). L7 is a hypothetical test in liquid metal fast breeder reactor with a rapid burst. Three-time intervals were selected for analysis. The L7 hodogram data for time intervals 2.242s, 4.879s and 14.445 s can be found the tables 3, 4 and 5 respectively. In the hodogram, the numbers under columns 7, 6, 5, 4 and SUM are the fuel masses in each channel in units of grams. ERR75 and ERR65 represent the errors associated with the sum of fuel mass in a row for confidence level of 75% and 65% respectively (Wu, 1982).

Table 3: Hodogram Data at t=2.242 seconds

TIME = 2.24164 SECONDS S/P = .08157

ROW	7	6	5	4	SUM	ERR75	ERR65	RULE	%
1	.3	.0	.0	.0	.3	.7	.4	3	100
2	.0	.0	.0	.0	.0	.7	.4	3	100
3	.3	.1	.4	.1	.9	.7	.4	3	100
4	.1	.2	.0	.0	.3	.7	.4	3	100
5	.3	.0	.0	.0	.3	.7	.4	3	100
6	.4	.0	.1	.0	.5	.7	.4	3	100
7	.2	.0	.1	.4	.8	.7	.4	3	100
8	.5	.9	1.6	.8	3.7	.8	.4	3	100
9	2.2	5.7	4.3	1.3	13.6	1.1	.6	3	100
10	.6	5.4	9.6	1.6	17.2	1.4	.8	3	100
11	.0	6.0	7.7	1.6	15.4	1.4	.8	3	100
12	.8	5.3	6.2	1.3	13.6	1.3	.7	3	100
13	.8	7.0	8.3	.8	17.0	1.5	.9	3	100
14	.3	4.5	6.7	.7	14.3	1.3	.7	3	100
15	.6	5.4	7.2	1.0	14.3	1.3	.7	3	100
16	.5	5.7	10.7	1.2	18.2	1.7	1.0	3	100
17	.8	5.9	7.7	1.1	15.5	1.3	.7	3	100
18	.6	7.6	8.7	.7	17.6	1.5	.9	3	100
19	1.0	5.7	6.7	.7	14.1	1.2	.7	3	100
20	.7	5.1	6.0	1.2	13.0	1.3	.7	3	100
21	.6	6.4	5.9	.5	13.3	1.2	.7	3	100
22	.4	6.5	10.7	1.1	18.6	1.8	1.0	3	100
23	.5	6.6	6.3	.9	14.3	1.4	.8	3	100
24	.9	8.7	9.5	.6	19.7	1.7	1.0	3	100
25	.0	11.6	7.7	1.0	20.3	2.0	1.2	3	100
26	.2	8.9	8.9	.9	18.8	1.6	.9	3	100
27	.8	6.9	8.5	1.0	17.1	1.5	.9	3	100
28	.9	5.9	6.7	1.0	14.6	1.3	.7	3	100
29	.3	5.3	7.2	1.5	14.3	1.3	.7	3	100
30	.7	7.2	6.9	1.6	16.4	1.4	.8	3	100
31	.4	6.9	7.5	1.8	16.6	1.4	.8	3	100
32	.9	6.1	6.6	1.1	14.6	1.4	.8	3	100
33	.3	3.6	4.4	.8	9.2	.9	.5	3	100
34	.9	.4	1.7	.5	3.5	.8	.4	3	100
35	.0	.0	.1	.0	.1	.7	.4	3	100
36	.4	.1	.0	.0	.5	.7	.4	3	100
SUM	19.3	161.7	192.5	28.9	402.2	43.5	24.9	(GRAMS)	

CONFIDENCE LEVEL : 75% 65%

Table 4: Hodogram Data at t=4.879 seconds

TIME = 4.87934 SECONDS		S/P = .07735							
ROW	7	6	5	4	SUM	ERR75	ERR65	RULE	%
1	.0	.0	.0	.3	.3	.7	.4	3	100
2	.0	.1	.0	.8	.9	.7	.4	3	100
3	.0	.0	.0	.0	.0	.7	.4	3	100
4	.0	.0	.0	.0	.0	.7	.4	3	100
5	.0	.4	.4	.0	.9	.7	.4	3	100
6	.9	.3	.1	.2	1.5	.7	.4	3	100
7	.0	.0	.0	.0	.0	.7	.4	3	100
8	.4	1.2	1.0	.2	2.8	.7	.4	3	100
9	1.3	5.8	3.8	.9	11.8	1.0	.6	3	100
10	.9	6.9	9.0	1.6	18.4	1.4	.8	3	100
11	.0	5.8	9.1	1.5	16.3	1.4	.8	3	100
12	1.1	5.9	9.3	1.5	17.8	1.4	.8	3	100
13	1.0	6.1	8.2	1.5	16.8	1.5	.8	3	100
14	.6	5.7	8.5	.8	15.5	1.3	.7	3	100
15	.8	6.4	8.7	1.3	17.2	1.4	.8	3	100
16	.8	6.2	9.0	1.3	17.2	1.4	.8	3	100
17	1.0	5.7	8.4	1.2	16.3	1.3	.7	3	100
18	1.0	6.5	8.5	1.3	17.2	1.4	.8	3	100
19	.6	6.9	7.2	.9	15.7	1.3	.8	3	100
20	.6	5.6	7.1	.9	14.3	1.2	.7	3	100
21	.9	7.0	6.9	1.4	16.2	1.3	.8	3	100
22	.5	7.3	9.0	.9	17.7	1.4	.8	3	100
23	.9	7.7	6.4	.9	15.8	1.3	.8	3	100
24	1.0	7.2	9.0	.6	17.8	1.4	.8	3	100
25	.5	6.8	8.2	1.2	16.6	1.4	.8	3	100
26	.7	7.1	9.4	1.1	18.3	1.5	.9	3	100
27	.8	7.5	8.9	1.2	18.5	1.5	.8	3	100
28	.7	7.3	6.4	1.4	15.5	1.3	.8	3	100
29	.5	6.5	7.4	1.1	15.6	1.4	.8	3	100
30	.4	6.1	7.5	1.2	15.2	1.4	.8	3	100
31	.5	5.6	7.6	1.6	15.2	1.2	.7	3	100
32	.9	6.7	7.2	1.2	15.9	1.4	.8	3	100
33	.2	3.7	3.9	.9	8.0	.8	.5	3	100
34	1.3	1.0	.7	.0	3.1	.7	.4	3	100
35	.0	.0	.0	.0	.0	.7	.4	3	100
36	.0	.0	.0	.0	.0	.7	.4	3	100
SUM	20.9	162.7	196.6	30.8	411.0	41.3	23.6	(GRAMS)	
CONFIDENCE LEVEL :						75%	65%		

Table 5: Hodogram Data at t=14.445 seconds

TIME = 14.44543 SECONDS S/P = .10715

ROW	7	6	5	4	SUM	ERR75	ERR65	RULE	%
1	.0	.3	.3	.0	.6	1.0	.6	3	100
2	.0	.1	2.2	.4	2.8	2.4	1.4	1	84
3	.0	.3	.1	.0	.5	1.0	.6	3	100
4	.0	2.1	.1	.0	2.3	1.1	.6	2	91
5	.0	.1	.2	.0	.4	.8	.5	4	78
6	.2	.0	1.3	.3	1.8	.8	.5	4	83
7	.1	.6	2.9	.5	4.1	.7	.4	5	87
8	1.5	4.8	9.9	5.3	21.5	1.6	.9	5	86
9	3.3	4.8	10.2	7.1	25.4	2.0	1.2	5	86
10	4.8	6.0	10.6	7.9	29.2	2.3	1.3	5	86
11	1.7	5.6	8.1	6.3	21.7	1.6	.9	5	88
12	1.2	4.5	6.3	3.1	15.1	1.2	.7	5	91
13	.7	3.7	4.6	2.1	11.1	.9	.5	5	92
14	.7	4.9	5.3	3.6	14.6	1.5	.8	3	100
15	.5	3.2	7.3	5.4	16.3	1.6	.9	4	92
16	1.0	3.8	13.0	5.6	23.4	2.4	1.4	4	90
17	1.5	4.7	12.1	25.0	43.3	14.0	11.2	4	91
18	1.3	5.1	12.3	5.9	24.6	2.6	1.5	4	91
19	.7	3.1	5.3	1.8	10.9	1.2	.7	4	92
20	.7	4.6	5.3	1.4	12.0	1.2	.7	4	92
21	1.1	2.5	4.9	1.5	10.0	1.0	.6	4	92
22	1.0	2.5	3.7	2.4	9.6	1.0	.6	4	92
23	.8	2.5	3.3	1.0	7.6	1.0	.6	4	92
24	1.3	3.8	3.9	1.9	11.0	1.4	.8	2	91
25	.6	3.0	5.0	1.3	9.8	1.0	.6	4	90
26	.5	3.2	3.9	.8	8.3	1.0	.6	4	90
27	.0	3.3	5.7	1.1	10.1	1.2	.7	4	89
28	.6	4.3	4.2	.8	9.8	1.1	.7	4	88
29	.7	7.1	4.7	.5	13.0	1.6	.9	3	100
30	.4	2.3	3.5	.9	7.1	1.0	.5	4	90
31	.5	5.3	4.7	.7	11.2	1.2	.7	4	92
32	.8	4.2	5.3	1.4	11.6	1.2	.7	4	91
33	.3	3.1	4.6	1.4	9.4	1.1	.6	4	91
34	.1	3.4	14.9	1.6	20.0	2.4	1.4	5	91
35	.1	4.0	6.5	1.8	12.5	1.1	.6	5	90
36	1.2	4.4	10.3	3.3	19.2	3.2	1.8	1	91
SUM	30.0	121.2	206.4	104.1	461.7	63.4	39.4	(GRAMS)	
CONFIDENCE LEVEL :						75%	65%		

Figure 29 below shows the initial position of the test fuel in the hodoscope with 180 channels (36 rows and 4 channels from 3-7). Also shown are the channels with Hornyak detectors. Columns from 1 and 10 do not see the test fuel. The geometry of the three-pin Loss of Fuel L7 hypothetical transient testing used for data interpretation is given in figure 28. The pin inside the loop is deliberately made to fail (large reactivity step /coast down of sodium circulation) to study fuel redistribution.

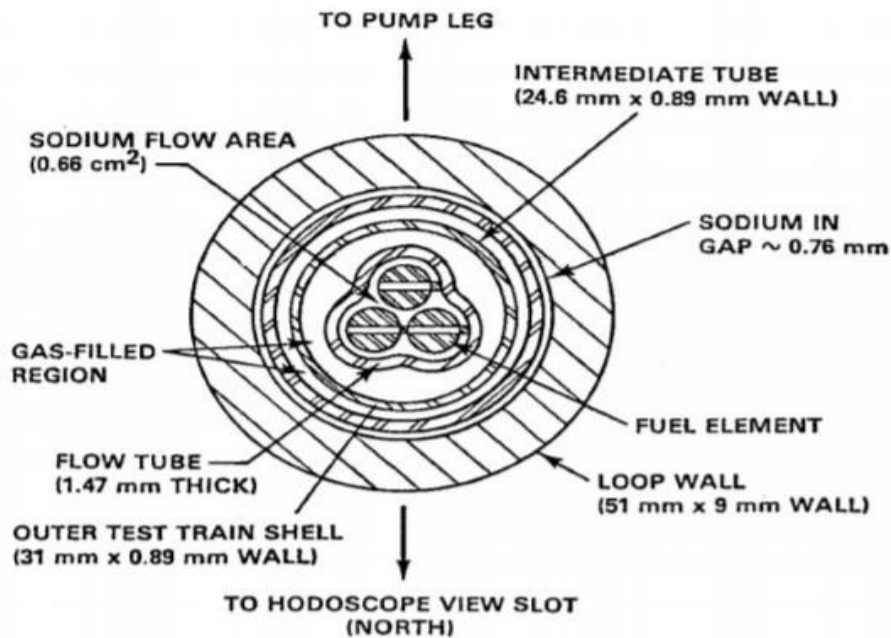


Figure 28: Three Pin Geometry (Wu, 1982)

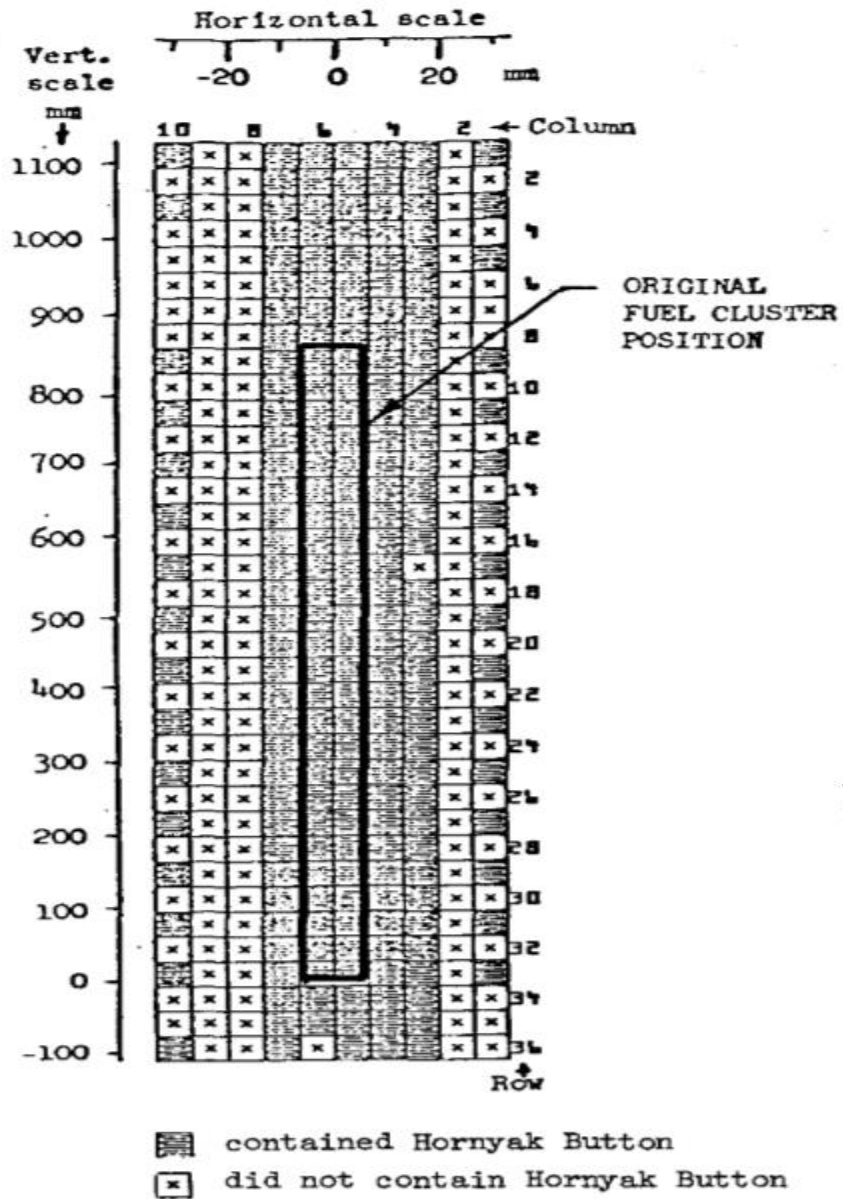


Figure 29: Initial Test Fuel Position in Hodoscope View Field (Wu, 1982)

5.3. ANL Analysis of Fuel Distribution

The hodogram data for L7 were tabulated and exported in a spreadsheet. Several data tables of mass versus hodoscope channels can be found in Appendix D. 3D surface plots were constructed in the spreadsheet to see the two-dimensional distribution of the fuel at

different specified time intervals. There is a significant change in mass in each channel and with the progression in time there is more slumping behavior prominent. Figure 30 represents the surface plot of mass distribution in each channel at time 2.242s after the transient while Figure 31 shows the 2D line graph of mass accumulation in the respective columns. Clearly, columns 5 and 6 show the higher mass accumulation which are centrally located. Figure 32 shows the respective plots with significant mass slumping after 14.445s (well after the transients).

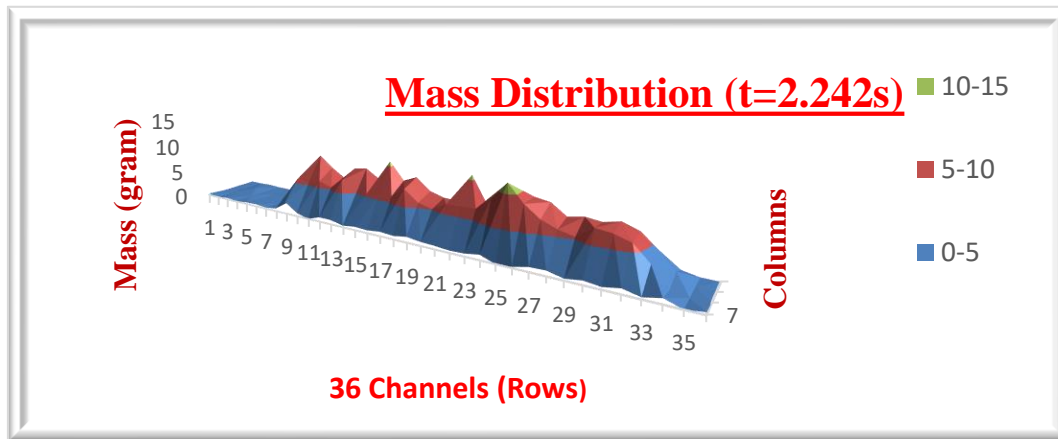


Figure 30: Mass Distribution of L7 after $t=2.242s$

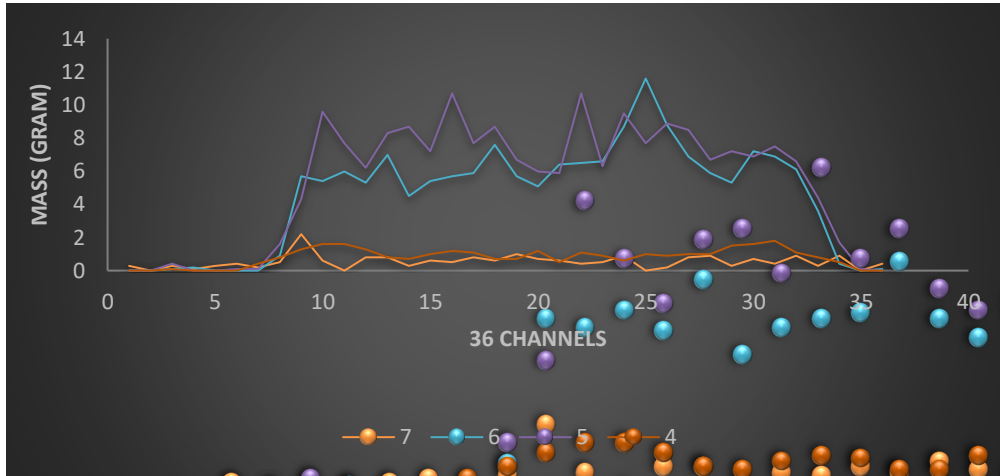


Figure 31: Mass distribution L7, 2.242 s after transients [per Column]

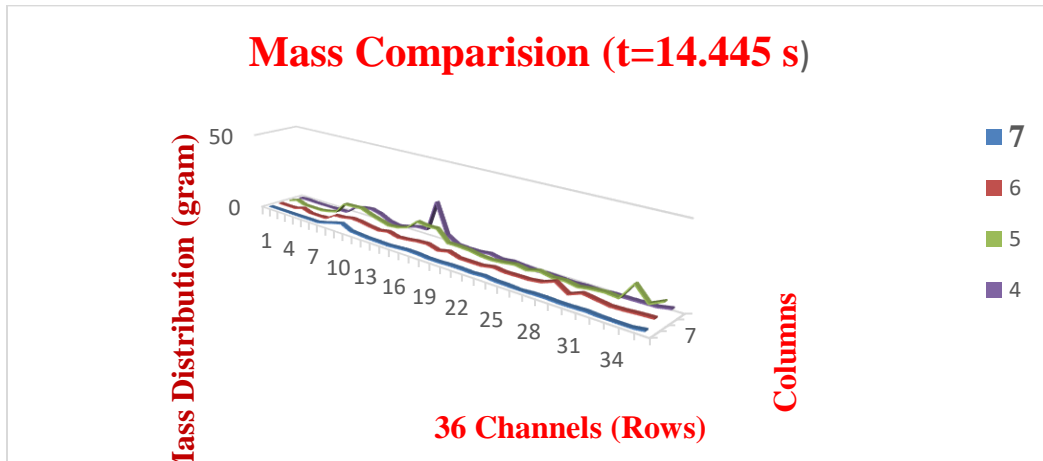


Figure 32: Mass distribution L7 after 14.445 s followed by transients

Determination of the fuel mass and its degree of relocation is important to mass conservation. Slight inconsistency in the mass quantification may exist due to self-shielding variations, error associated with the detector count rate and fuel mass

relationship, and error due to data analysis. However, the model presented predicts the behavior of mass relocation at different intervals followed by the transient.

Figure 33 below shows the plots of mass intensity with channels at three different times after initiation of the transient. This shows the clear redistribution of the fuel during fuel slumping and an appropriate fit to the data helps to quantify the mass. There is a clear slumping and redistribution of the fuel at 14.445 seconds.

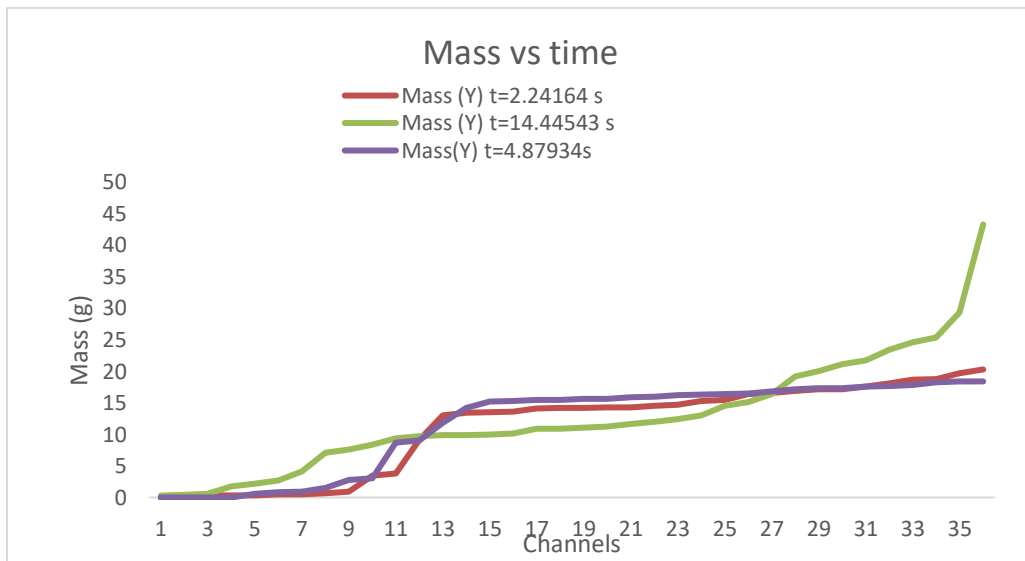


Figure 33: Mass Distribution in 2, 4 and 14 Seconds

Figure 34 below shows the percentile plot of mass probability at 2.242 seconds after transient. An approximate polynomial fit was done, and this equation can be used to predict the mass at any percentile. It was determined that a 4th order would be adequate. Similar plots are obtained for several time after the transient to quantify the mass.

At t=2.242 s

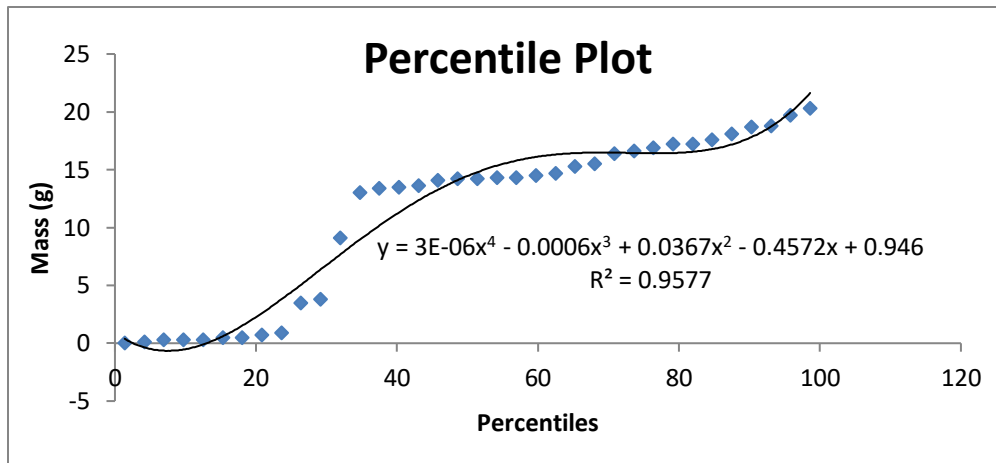


Figure 34: Mass Distribution Percentile Plot

Multiple regression analysis was done to identify the percentage dependence of rows 4, 5, 6 and 7 masses to the total mass. This analysis helps to identify the most significant row data. Table 6 below shows the corresponding result.

Table 6: Multiple Regression Results

ANOVA									
	df	SS	MS	F	Significance F				
Regression	4	1810.36	452.59	9.4E+31	0				
Residual	31	1.5E-28	5E-30						
Total	35	1810.36							
	Coefficient	Standard Err	t Stat	P-value	Lower 95%	Upper 95%	Lower 95.0%	Upper 95.0%	
Intercept	5E-15	7.6E-16	6.677	1.8E-07	3.5471E-15	6.667E-15	3.5471E-15	6.667E-15	
Row 7	1	9.7E-16	1E+15	0	1	1	1	1	1
Row 6	1	2.6E-16	4E+15	0	1	1	1	1	1
Row 5	1	2.5E-16	4E+15	0	1	1	1	1	1
Row 4	1	1.1E-15	9E+14	0	1	1	1	1	1

Residual plots for each row were created and the points are randomly dispersed around the horizontal axis and then a linear regression model can be used. However, while plotting all four rows data, we decided a polynomial fit was better as the data do not seem

linearly related to the total mass intensity. Figures 35 below show the residual plots for individual rows.

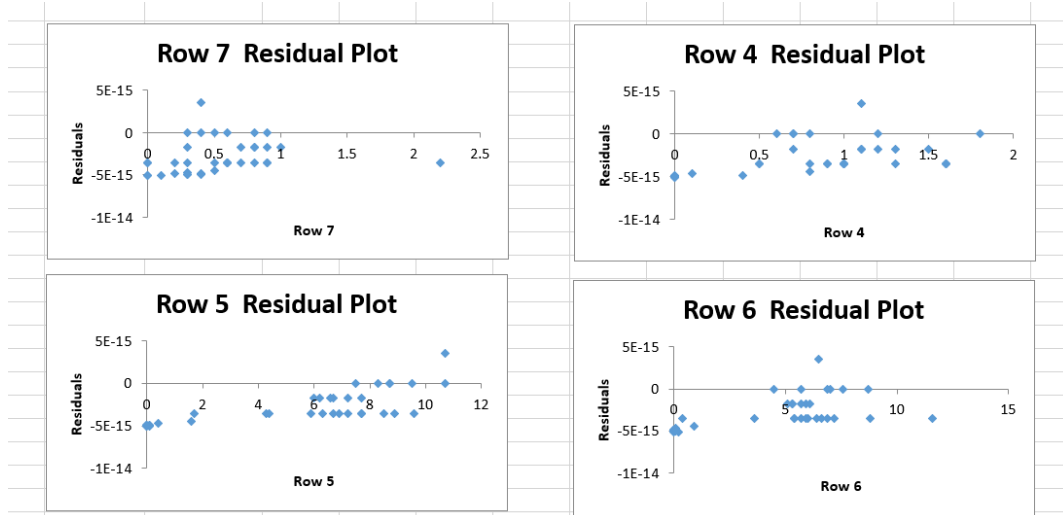


Figure 35: Residual Plots

Figures 36, 37, 38 and 39 below show four plots of the mass distribution versus percentiles at $t=2.242$ s: first the original mass plot, second the Fourier transformed mass plot, third the filtered back projected one and finally all three plots in a single graph.

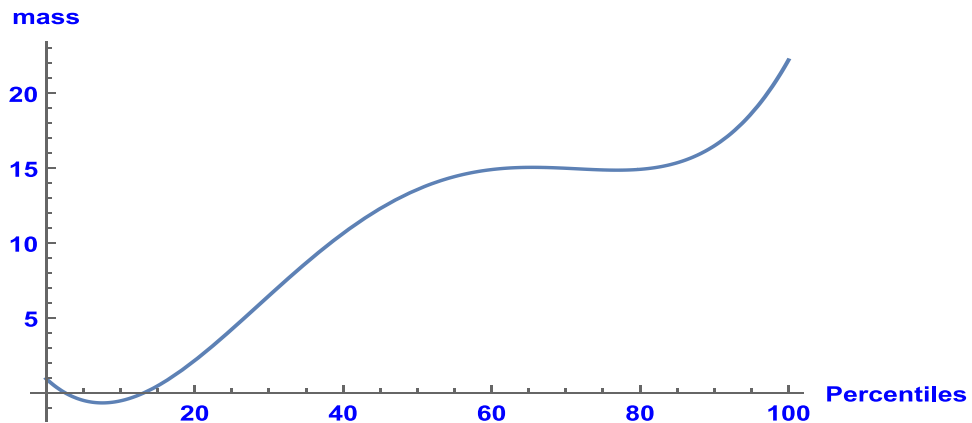


Figure 36: Original Mass Plot

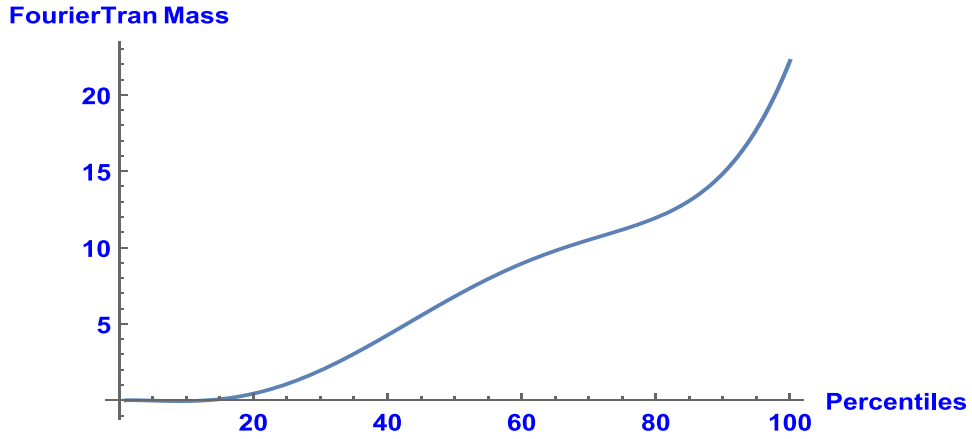


Figure 37: Fourier Transformed Mass Plot

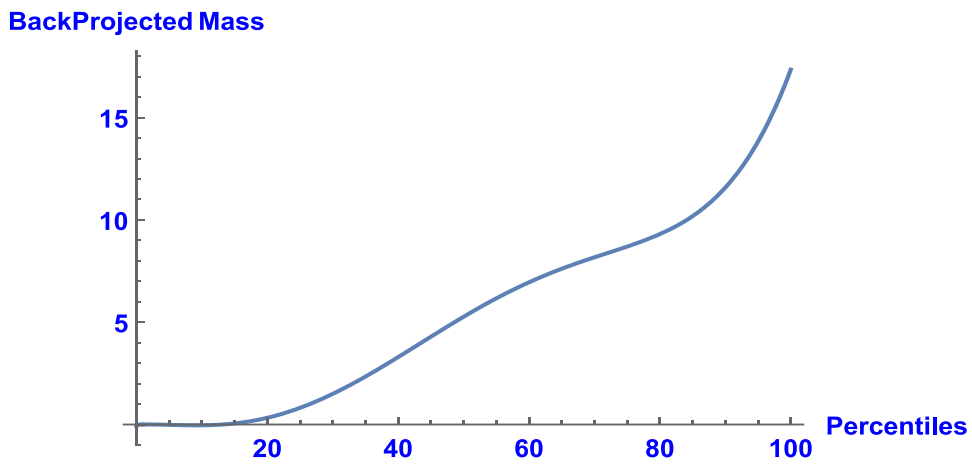


Figure 38: Back Projected Mass Plot

Similar steps were repeated for the second time, $t=14.445$ s after transient and figure 39 below shows all three plots of original mass, Fourier transformed and the filtered back projected.

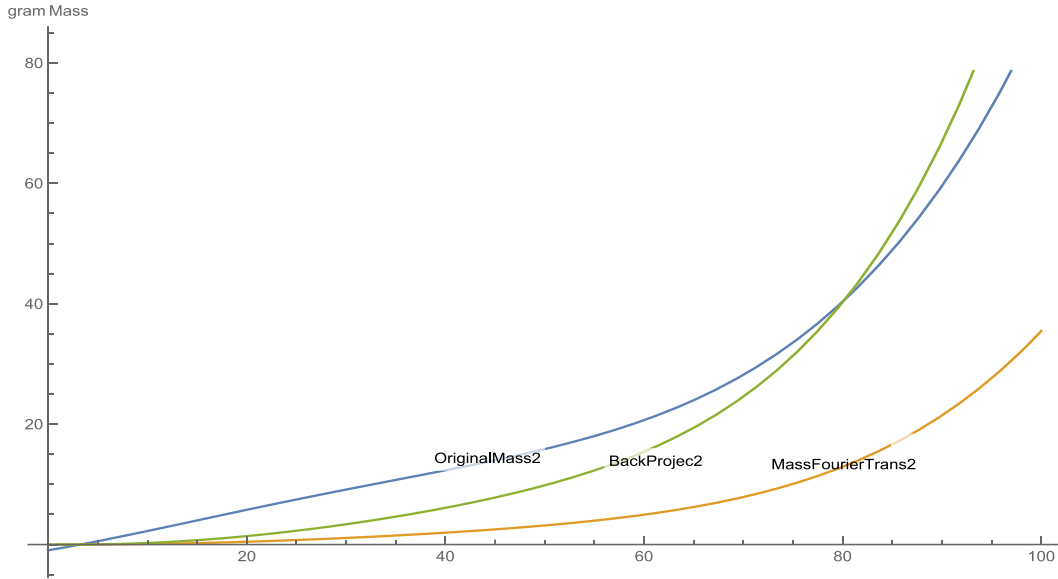


Figure 39: All 3 Plots at $t=14.445$ second

A few conclusions can be drawn from the above data analysis. First, with an appropriate polynomial fit we can predict the mass at any channel and tell which channels recorded more masses during fuel slumping, and their respective percentiles. Second, multiple linear regression coefficients show the dependence of all four rows in the total mass with their weighted coefficients. This help to identify the most significant row. However, there is not any trend with the progression of the transient, so each analysis needs to be done separately at each time interval. Third, FBP technique can be used for any general function and is not limited to a step or a cosine distribution if the function is continuous. Lastly, FBP eliminates the outlier to yield smoother data and removes negative values of the masses which seems more reasonable and physical.

Chapter 6: Hodoscope Data and FBP

A hodoscope provides the capability for recording the fuel motion during the transient. The test specimen placed in the center of the TREAT core is exposed to the high neutron flux and this flux induces fission in the test capsule. These fission neutrons travel through the vehicle's containment wall, through a collimator, and into the detector array. Figure 40 below shows the pixelated view of fuel mass in each collimator slot (Jensen, 2016). This pixelated image was used to illustrate the application of Filtered Back Projection (FBP) for image reconstruction.

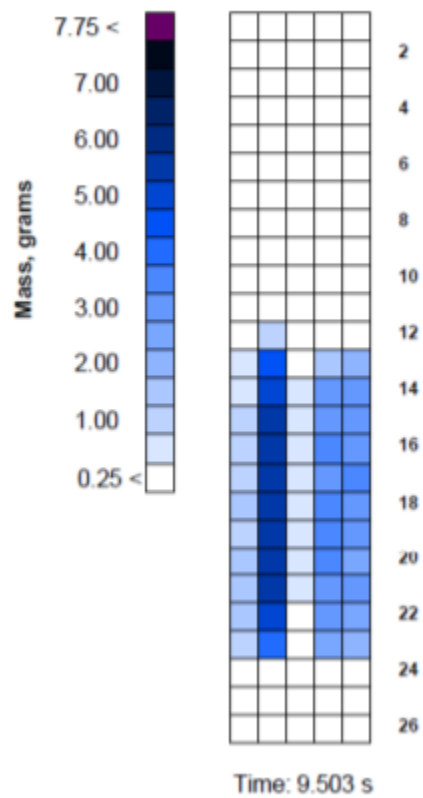


Figure 40: Pixelated Hodogram Plot (Jensen, 2016)

Filtered back projection technique may be applied to the pixelated image with a suitable filter. Figure 41 below shows the reconstruction of the image without using any filter.



Figure 41: Reconstructed Pixelated Hodogram Plot [No Filter]

Figure 42 below shows the reconstruction of the image using the FBP technique with ramp filter. Ramp filter is a high pass filter that filters out the low frequencies and allows the high frequencies. It was found that the ramp filter increased the resolution and quality of the image as noted previously. However, it still magnifies noise coming from the projection data meaning it was not the ideal filter. This filter may work reasonably well for images with less complex frequency distribution but is not a good filter to be used for reconstruction of hodoscope pixelated image.

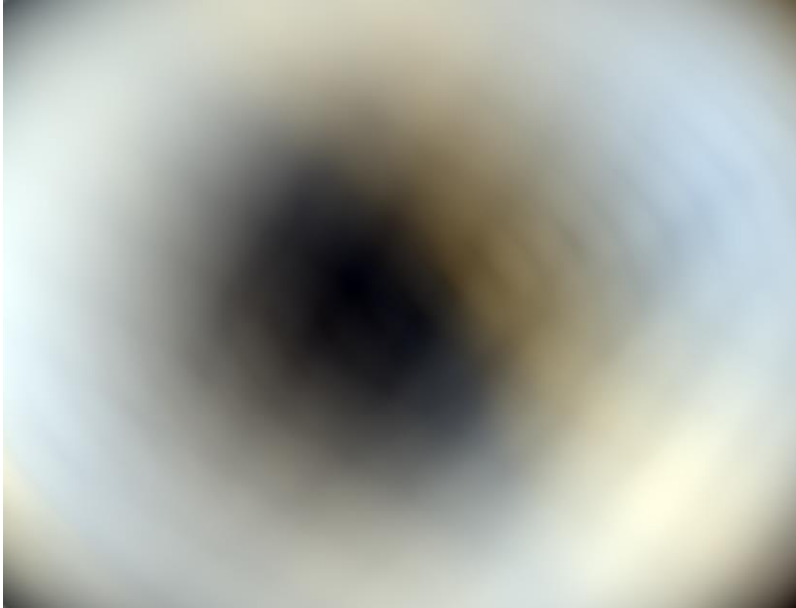


Figure 42: Reconstructed Pixelated Hodogram Plot [Ramp Filter]

Figure 43 below shows the reconstruction of the image using the FBP technique with Hanning filter (Hann filter). The Hann filter is a low pass filter (smoothing filter) that filters out the high frequencies and allows the low frequencies. It was found that the Hann filter increased the resolution and quality of the image. FBP technique in conjunction with Hann filter reduces the noise that causes blurring to yield better resolution image as expected. However, it does not preserve edges and a suitable cut off frequency need to be selected which will be discussed in the following section.

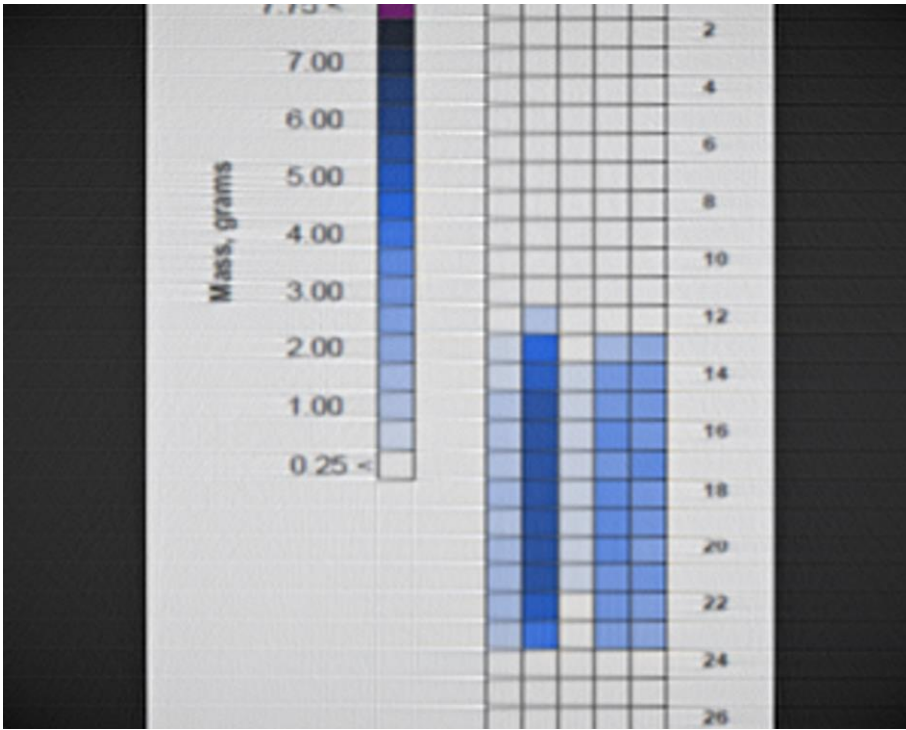


Figure 43: Reconstructed Pixelated Hodogram Plot [Hann]

As seen from the previous plots, we may conclude that the Hann filter works best for reconstruction of the pixelated image and is consistent to what we found while reconstructing TREAT image. Next step is to see the effect of cut-off frequency. Figures 44, 45 and 46 below show the reconstruction image using the Hann filter with varying cut-off frequencies as 0.1, 0.3 and 1 cycles/cm respectively.

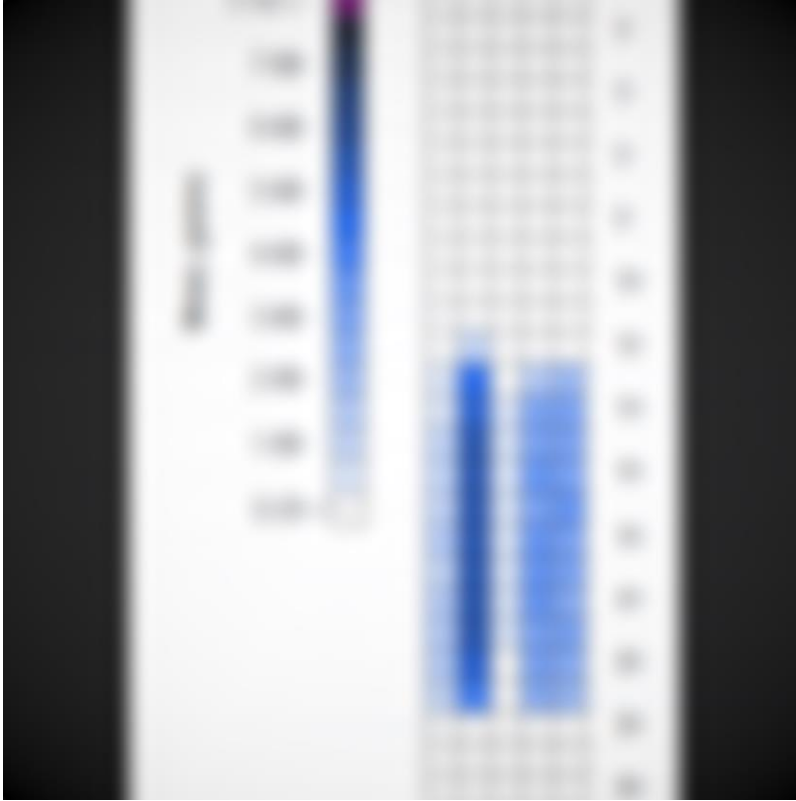


Figure 44: Reconstructed Pixelated Hodogram Plot [Hann Filter] $w=0.1$

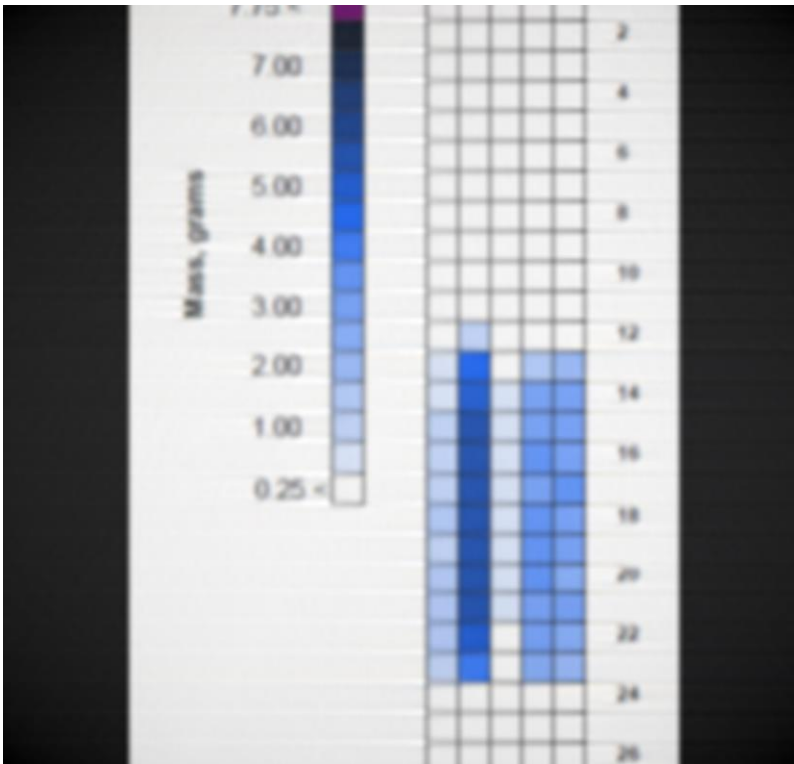


Figure 45: Reconstructed Pixelated Hodogram Plot [Hann Filter] $w=0.3$

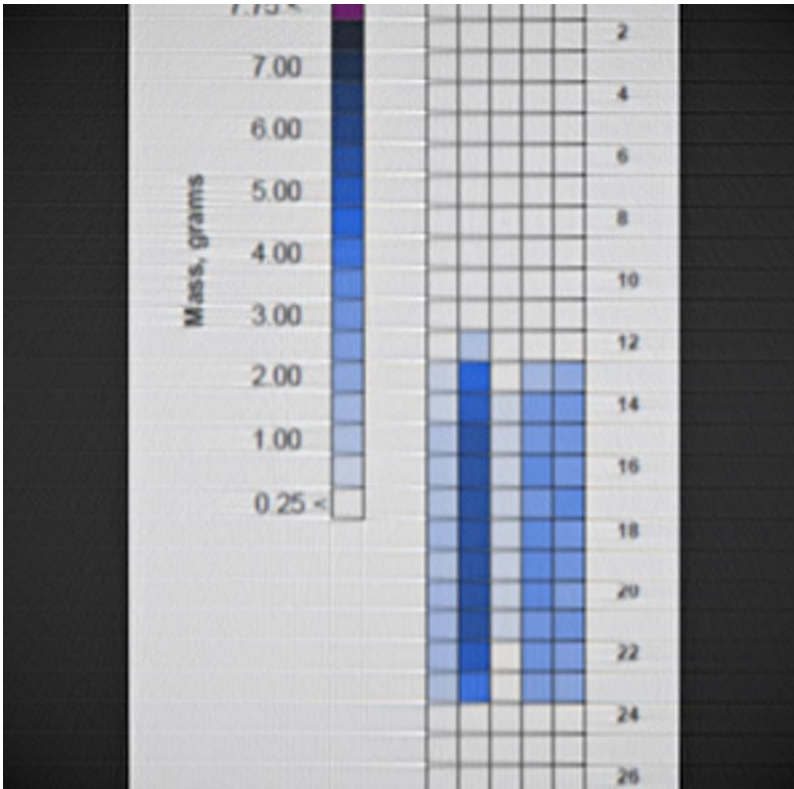


Figure 46: Reconstructed Pixelated Hodogram Plot [Hann Filter] $w=1$

It can be observed from the figures above that the value of cut-off frequency determines how the filter will affect both image noise and resolution. In other words, the higher the cut-off frequency, the better is the spatial resolution and therefore a more detailed image can be obtained. In conclusion, the Hann filter with cut-off frequency close to 1 cycle/cm would be recommended for the final image reconstruction which was as expected and seen from that in TREAT image reconstruction.

Chapter 7: Conclusions and Recommendations

This dissertation presents an alternative method of supporting real time imaging of fuel pins and other structures during transient testing through the study of fuel motion during accident scenarios. Feasibility of portable cloud chamber was studied first. Although in much of the early neutron studies, the neutrons were detected in cloud chambers, this method of detection is not a good choice for TREAT reactor. The cloud trails obtained were so faint and the evaluation of their tracks is very tedious. The difficulties are particularly great when long range particles have to be observed as proton recoils from energetic neutrons (Creutz, 2012). Moreover, cloud chambers have a much larger size compared to other detectors. However, it could be used to measure low energy end of energy spectrum of neutrons produced in fission. Another recent example of its use is in the study of elastic and inelastic scattering of 14 MeV neutrons by oxygen (Creutz, 2012). If a cloud chamber is to be used, a diffusion type cloud chamber is preferred over the pulsed one since in diffusion chamber there is continuous generation of ions and there is no time lag for resetting for pressure build up between ionizations. Moreover, diffusion chambers require less air current and are independent of the gas expansion. Even in a diffusion type, a mechanical system is recommended over the pneumatic as a mechanical type can be more easily controlled manually. Another recommendation is to use higher resolution cameras with greater frame rate that may be capable to capture faint trails. However, it was not obvious even with these improvements that the cloud chamber would provide a viable alternative to a collimated hodoscope. Therefore, we moved forward with the simulation and analytical approach.

This research is focused both on the MCNP simulation (stochastic model) and analytical method (deterministic) to support transient testing. A TREAT MCNP model with central fuel element replaced by dummy slotted fuel with sample was added to get flux information and was previously discussed in section 4.3.

Another avenue of this dissertation is to support imaging of the test specimen during transient and quantify the mass based on hodogram data. An analytical approach of Filtered Back Projection (FBP) can be used to understand imaging and with the right choice of filter, we can improve the resolution. Most of the imaging tools use numerical computations, but analytical analysis helps to build insight and this dissertation provides multiple analytical illustrations on using Fourier transform and filtering. FBP can be used for any general function. Suitable selection of filter is necessary in imaging and Hann filter works best as shown by multiple examples. In addition to the right choice of filter, appropriate choice of cut off frequency removes noises that causes blurring as seen in the previous chapters. Moreover, FBP improves data analysis (removes outliers/ negative masses etc.) to quantify mass during slumping and improves the imaging.

The techniques described in this dissertation can be used in nuclear medicine for developing diagnostic and therapeutic modalities. For instance, to treat tumor cells a radioactive drug is typically administered in targeted organs along with gamma cameras to acquire two-dimensional projections of the activity. These projections data are then filtered and back projected to get the image of the targeted organ. Proper selection of filter and cut-off frequencies are crucial in imaging as discussed in previous sections of the dissertation.

There were a few challenges in completing this dissertation. Some of the shortcomings were: lack of the most recent TREAT hodoscope data, slight mass discrepancies in Loss of Flow (L7) data, and the fact that the integrations in analytical solutions were not straight forward in some cases. In those cases, Taylor series expansion was used to find the first 10 coefficients that gives convergence in solution. Some possible reasons for mass discrepancies might be due to self-shielding, data error or unknown errors. Mass discrepancy might be more prominent in three pins that that in a single pin test fuel due to greater chances of self-shielding. Had there been a single pin test data available, it would be better if we can relate the trend or better explain the behavior. Overall, FBP has several applications in medical imaging and future transient testing.

REFERENCES

1. Gupta, N.N. Das and Ghosh, S.K. A Report on the Wilson Cloud Chamber and its Applications in Physics. Calcutta, 1946.
2. Womack, Cody. The Construction and Characterization of a Large Volume Wilson Cloud Chamber Utilizing Orthogonal Cameras for Image Capture” [Thesis]
3. Wilson, J.G. The Principles of Cloud Chamber Technique, 1951.
4. Roth, J. and Hobbie, Russel K. Intermediate Physics for Medicine and Biology. Textbook. 5th edition, 2015.
5. Xu, Dan. Filtered Back-Projection in 4-Pi Compton Imaging with a Single 3D Position Sensitive CdZnTe Detector. IEEE 2006.
6. Nyathi, Mpumelelo. Utilization of an optimum low-pass filter during filtered back projection in the reconstruction of single photon emission computed tomography images of small structures. Department of Medical Physics, Faculty of Health Sciences, SefakoMakgatho Health Sciences University, Ga-Rankuwa, South Africa 2018.
7. De Volpi and Freese, C.H. Experimental Results and Improvements in the Fast Neutron Hodoscope
8. E. Dickerman. High Power Level Transient Reactor Test (TREAT) Facility Sodium Loop Meltdown Experiment on an Unbonded EBR-II Marl I Fuel Pin.
9. De Volpi, A. Fast Neutron Hodoscope at TREAT: Methods for Quantitative Determination of Fuel Dispersal” by A. De. Volpi et al.; “Fuel-Motion Diagnostics and Cineradiography.

10. Abramowitz, M. and Stegun, I.A. Handbook of Mathematical Functions with Formulas, Graphs and Mathematical Tables. National Bureau of Standards Applied Mathematics Series – 55, 10th Printing, 1972.
11. Pope, Chad. A detailed model of TREAT reactor was built in MCNP. 2016.
12. Lyra, Maria and Ploussi, Agapi. Filtering in SPECT Image Reconstruction. Volume 2011, Article ID 693795, Published 2011.
13. Jensen, Colby. Experiment Instrumentation for Transient Testing. Advanced Sensors and Instrumentation. 2016.
14. James J. Duderstadt, Louis J. Hamilton. Nuclear Reactor Analysis. s.l. : John Wiley & Sons, inc., 1976.
15. Hetrick, David L. Dynamics of Nuclear Reactors. La Grange Park, Illinois : American Nuclear Society, 1993.
16. Kreyszig, Erwin. Advanced Engineering Mathematics. Hoboken, New Jersey : John Wiley & Sons Inc, 2006. ISBN 0471728977.
17. Jackson, John David. Classical Electrodynamics.: John Wiley & Sons, inc., 2007.
18. Lamarsh, John, and Anthony Baratta. Introduction to Nuclear Engineering. 3rd Edition. Upper Saddle River: Prentice Hall, 2001. 1-759. Print.
19. Baum, Edward, Harold Knox, and Thomas Miller. *Chart of the Nuclides: Nuclides and Isotopes*. 16th Edition. 1. Schenectady: Lockheed Martin Corporation, 2002. 1-88 Print.
20. Wolfram Research, Inc., Mathematica, Version 9.0.1, Champaign, IL, 2013.
21. MCNP , Los Alamos National Laboratory (LANL), 1957. Retrived April 2nd, 2017.

23. Creutz, Edward. *Nuclear instrumentation II* = Instrumentelle Hilfsmittel der Kernphysik
24. Robert Mowshyong Wu, *Shelf- shielding corrections for the TREAT hodoscope interpretation*, 1982
25. C.H Bowers, AM Tentner and H.U. Wider, Analysis of TREAT L7 and L8 with SAS3D, LEVITATE and PLUTO2
26. C. N Kelber, et al, *Safety Problems of Liquid Metal Cooled Fast Breeder Reactors*, Argonne National Lab, Feb 1970 Annual Report.
27. A. De Volpi et al. *Fast- neutron Hodoscope at TREAT: Data Processing, Analysis, and Results*, 1976.
28. Wachs, Daniel M. and Bumgardner. John D. *Restarting the Transient Test (TREAT) Facility Reactor for Nuclear Transient Testing Science: A Special Issue of Nuclear Technology*. Nuclear Technology, 205:10, iv-v. 2019
29. Welch, Alex. *Diffusion Cloud Chamber*. Applied Science Research class spring 2012.
30. Anders Johan Nygren. *Filtered Back Projection*. 1997
<http://www.owl.net.rice.edu/~elec539/Projects97/cult/node2.html>
31. <https://www.trexp.anl.gov/about/>

APPENDIX

Appendix A: Cloud Chamber

Cloud Chamber Operation and Checklist

Before turning on the cloud chamber table power sources:

- Ensure cameras are positioned correctly and connected to computer securely
- Ensure all valves are closed
- Ensure the compressors were previously turned off properly

Then:

- Turn both power sources on (if UPS is not already on)
- Turn compressors on
- Close compressor cabinet doors securely
- If needed, add 50 to 200mL of ethyl alcohol/water mixture through the liquid fill valve

Operation

1. Turn on computer (if not already powered on)
2. If proper procedure was previously followed, the pistons should be in the “in” position
3. Start camera/data recording
4. Open ***Air Relief Valve #2*** on the right- hand side manifold
5. Open the ***Pull*** valve on the left -hand side manifold
6. Pistons should move to the “out” position
7. Close the ***Pull*** valve

When the total chamber volume reaches the correct level, cloud trails should form.

When data has been gathered and cloud trails have dissipated, begin next steps.

8. Stop data recording (if not set to automatically stop recording)
9. Open ***Air Relief Valve #1*** on the left-hand side manifold
10. Allow the vacuum of the chamber to pull the pistons most of the way back
11. Close ***Air Relief Valve #2***
12. **Slightly** open the ***Push*** valve on the right-hand side manifold
13. Pistons should **slowly** move to the “in” position
14. Once pistons are in the “in” position, close the ***Push*** valve and ***Air Relief Valve #1***

15. Repeat steps 3-14 for as many data collecting runs as desired, allowing the compressors to refill, as needed.

Lacking all else, please note when using the *PUSH* or *PULL* valves, the *Air Relief Valve* on the OPPOSITE manifold must be opened.

When finished collecting data:

- Ensure the pistons are in the “in” position
- Close all valves
- Carefully open compressor cabinet doors
- Turn compressors off
- Turn power off
- Close compressor cabinet doors securely
- Open chamber air and drain valves, if runs are not planned in the near future
- Empty drain container as needed
- Empty Compressors

To empty the compressors:

1. Repeat Operation steps 4-6
2. Open *Air Relief Valve #1* until the pressure has subsided
3. Close all valves
4. Repeat Operation steps 9 & 12
5. Fully open the *PUSH* valve
6. Open *Air Relief Valve #2* until the pressure has subsided
7. Close all valves

Weekly Checklist

- Check the power cables for any frays or other damage
- Check the compressor and fan power cables any frays or other damage and are plugged tightly into the power supply
- Check the computer and monitor power cables any frays or other damage and are plugged tightly into the power supply
- Check to ensure all hose fittings are tight
- Empty condensation out of compressors*
 - Leave between 1-3 pounds of pressure in each compressor when during the emptying procedure
 - Locate drain valve on bottom of compressor
 - Place paper towels under drain valve, hold securely

- Open drain valve, the remaining pressure will force water out of the drain
- Tip compressor toward drain to ensure all condensation has been drained
- Repeat for another compressor

*This may need to be done more than once a week, if the compressors have been running frequently.

Appendix B: TREAT MCNP

```

TREAT Reactor
c Cell Cards
c
c Standard Fuel Element
c
100 1000 -1.7248 -1 2 -3 4 5 -6 -7 8 u=1
imp:n=1 $ fuel
110 2000 -9.93e-4 -10 11 -12 13 14 -15 -16 17
(1:-2:3:-4:-5:6:7:-8) u=1
imp:n=1 $ gap between fuel and clad
120 3000 -6.53 -20 21 -22 23 24 -25 -26 27
(10:-11:12:-13:-14:15:16:-17) u=1
imp:n=1 $ clad
130 2000 -9.93e-4 20:-21:22:-23:-24:25:26:-27 u=1
imp:n=1 $ gap between fuel elements
c
c Control Rod Element (Rod Inserted)
c
200 5000 -1.6 -55 u=2
imp:n=1 $ control rod B4C meat
201 6000 -7.86 55 -56 u=2
imp:n=1 $ carbon steel tube
202 2000 -9.93e-4 56 -50 u=2
imp:n=1 $ air gap between control rod and guide tube
210 3000 -6.53 50 -51 u=2
imp:n=1 $ control rod guide tube
220 2000 -9.93e-4 51 -52 u=2
imp:n=1 $ control rod guide tube outer gap
230 1000 -1.7248 -1 2 -3 4 5 -6 -7 8 52 u=2
imp:n=1 $ fuel
240 2000 -9.93e-4 -10 11 -12 13 14 -15 -16 17
(1:-2:3:-4:-5:6:7:-8) u=2
imp:n=1 $ gap between fuel and clad
250 3000 -6.53 -20 21 -22 23 24 -25 -26 27
(10:-11:12:-13:-14:15:16:-17) u=2
imp:n=1 $ clad
260 2000 -9.93e-4 20:-21:22:-23:-24:25:26:-27 u=2
imp:n=1 $ gap between fuel elements
c
c Dummy Element
c
600 4000 -1.67 -1 2 -3 4 5 -6 -7 8 u=4
imp:n=1 $ graphite
610 2000 -9.93e-4 -10 11 -12 13 14 -15 -16 17
(1:-2:3:-4:-5:6:7:-8) u=4
imp:n=1 $ gap between graphite and clad
620 3000 -6.53 -20 21 -22 23 24 -25 -26 27
(10:-11:12:-13:-14:15:16:-17) u=4
imp:n=1 $ clad
630 2000 -9.93e-4 20:-21:22:-23:-24:25:26:-27 u=4
imp:n=1 $ gap between fuel elements

```

```

c
c
c 19 x 19 Reactor Assembly (with Graphite Reflection)
c
300 2000 -9.93e-4 -30 31 -32 33 -72 73 lat=1 u=3
imp:n=1 $ core
fill=-9:9 -9:9 0:0
  4 4 1 1 1 1 1 1 1 1 1 1 1 1 1 1 1 4 4
  4 1 1 1 1 1 1 1 1 1 1 1 1 1 1 1 1 1 4
  1 1 1 1 1 1 1 2 1 1 1 2 1 1 1 1 1 1 1
  1 1 1 1 1 2 1 1 1 1 1 1 1 2 1 1 1 1 1
  1 1 1 1 1 1 1 1 1 1 1 1 1 1 1 1 1 1 1
  1 1 1 2 1 1 1 1 1 1 1 1 1 1 1 2 1 1 1
  1 1 1 1 1 1 1 1 1 1 1 1 1 1 1 1 1 1 1
  1 1 2 1 1 4 1 1 1 1 1 1 1 4 1 1 2 1 1
  1 1 1 1 1 1 1 1 1 1 1 1 1 1 1 1 1 1 1
  1 1 1 1 1 1 1 1 1 3 1 1 1 1 1 1 1 1 1
  1 1 1 1 1 1 1 1 1 4 1 1 1 1 1 1 1 1 1
  1 1 2 1 1 4 1 1 1 4 1 1 1 4 1 1 2 1 1
  1 1 1 1 1 1 1 1 1 4 1 1 1 1 1 1 1 1 1
  1 1 1 2 1 1 1 1 1 4 1 1 1 1 1 2 1 1 1
  1 1 1 1 1 1 1 1 1 4 1 1 1 1 1 1 1 1 1
  1 1 1 1 2 1 1 1 1 4 1 1 1 2 1 1 1 1 1
  1 1 1 1 1 1 2 1 1 4 1 2 1 1 1 1 1 1 1
  4 1 1 1 1 1 1 1 1 4 1 1 1 1 1 1 1 1 4
  4 4 1 1 1 1 1 1 1 4 1 1 1 1 1 1 1 4 4

c
400 0 -40 41 -42 43 -70 71 fill=3
imp:n=1
410 4000 -1.67 -60 61 -62 63 -72 73
(40:-41:42:-43:70:-71)
imp:n=1 $ reflector
500 0 60:-61:62:-63:72:-73
imp:n=0

c Surface Cards
1 px 4.83870 $ slug right x surface
2 px -4.83870 $ slug left x surface
3 py 4.83870 $ slug upper y surface
4 py -4.83870 $ slug lower y surface
5 p 1 1 0 -8.57822 $ slug lower left corner
6 p -1 1 0 8.57822 $ slug upper left corner
7 p 1 1 0 8.57822 $ slug upper right corner
8 p -1 1 0 -8.57822 $ slug lower right corner

c
10 px 4.96570 $ clad right x inner surface
11 px -4.95670 $ clad left x inner surface
12 py 4.96570 $ clad upper y inner surface
13 py -4.95670 $ clad lower y inner surface
14 p 1 1 0 -8.82747 $ clad lower left inner corner
15 p -1 1 0 8.82747 $ clad upper left inner corner
16 p 1 1 0 8.82747 $ clad upper right inner corner
17 p -1 1 0 -8.82747 $ clad lower right inner corner

c

```

```

20 px    5.0292      $ clad right x outer surface
21 px   -5.0292      $ clad left  x outer surface
22 py    5.0292      $ clad upper y outer surface
23 py   -5.0292      $ clad lower y x outer surface
24 p     1  1  0    -8.93587 $ clad lower left inner corner
25 p    -1  1  0     8.93587 $ clad upper left inner corner
26 p     1  1  0     8.93587 $ clad upper right inner corner
27 p    -1  1  0   -8.93587 $ clad lower right inner corner
c
30 px    5.0800      $ fuel element right surface
31 px   -5.0800      $ fuel element left surface
32 py    5.0800      $ fuel element upper y surface
33 py   -5.0800      $ fuel element lower y surface
c
40 px   96.5190      $ core right surface
41 px  -96.5190      $ core left surface
42 py   96.5190      $ core top y surface
43 py  -96.5190      $ core bottom y surface
c
50 cz    2.5400      $ guide tube inner
51 cz    2.8575      $ guide tube outer
52 cz    2.9591      $ gap
c
55 cz    1.9050      $ control rod meat radius / clad inner
nom=1.9050
56 cz    2.2225      $ Control rod clad outer
c
60 px   160          $ reflector right side outer surface
61 px  -160          $ reflector left side outer surface
62 py   160          $ reflector upper y side outer surface
63 py  -160          $ reflector lower y side outer surface
c
70 pz   60.4838      $ fuel element upper surface
71 pz  -60.4838      $ fuel element lower surface
72 pz  124.0631      $ reflector upper surface
73 pz -119.9356      $ reflector lower surface

```

c Data Cards

```

kcode 10000 1.0 10 110
ksrc 0 0 0 50 50 0 -50 50 0 -50 -50 0 50 -50 0

```

c mode n

c nps 1000

c sdef pos 0 0 0 erg=d1

c

c energy Spectrum for an Am-Be neutron source

c

```

c sil H      4.14E-07 0.11 0.33 0.54 0.75 0.97 1.18 1.4 1.61 1.82
2.04
c           2.25 2.47 2.68 2.9 3.11 3.32 3.54 3.75 3.97 4.18 4.39
4.61
c           4.82 5.04 5.25 5.47 5.68 5.89 6.11 6.32 6.54 6.75 6.96
7.18
c           7.39 7.61 7.82 8.03 8.25 8.46 8.68 8.89 9.11 9.32 9.53
9.75

```

```

c          9.96 10.18 10.39 10.6 10.82 11.03
c
c sp1 D      0 0.0144 0.0334 0.0313 0.0281 0.025 0.0214 0.0198
0.0175
c          0.0192 0.0222 0.0215 0.0225 0.0228 0.0295 0.0356 0.0368
c          0.0346 0.0307 0.03 0.0269 0.0286 0.0318 0.0307 0.0333
0.0304
c          0.0274 0.0233 0.0206 0.0181 0.0177 0.0204 0.0183 0.0163
c          0.0168 0.0168 0.0188 0.0184 0.0169 0.0143 0.0097 0.0065
c          0.0043 0.0037 0.0038 0.0051 0.0062 0.0055 0.0047 0.0037
c          0.0028 0.0015 0.0004
c
c cut:n J J 0 0 J
c
c Tally
c
f15:n 0 0 0 1
f25:n 0 0 -10 0.5
f35:n 0 0 -20 0.5
f45:n 0 0 -30 0.5
f55:n 0 0 -40 0.5
f65:n 0 0 -50 0.5
f75:n 0 0 -60 0.5
f85:n 0 0 -70 0.5
f95:n 0 0 -80 0.5
f105:n 0 0 -90 0.5
f115:n 0 0 -110 0.5
c
c Meshes
c
FMESH4:N      ORIGIN= -100 -0.5 -100
              IMESH= 100      iints= 200
              JMESH= 0.5      jints= 1
              KMESH= 100      kints= 200      out=col
c
c
FMESH14:N     ORIGIN= -100 -100 0
              IMESH= 100      iints= 200
              JMESH= 100      jints= 200
              KMESH= 1        kints= 1      out=col
c
c
FMESH24:N     ORIGIN= -100 -100 -110
              IMESH= 100      iints= 200
              JMESH= 100      jints= 200
              KMESH= -109     kints= 1      out=col
c
m1000  92235.70c 8.6849e18  92238.70c 6.2967e17  8016.70c 1.8623e19
        6000.70c 8.6227e22  5010.70c 1.3802e17  5011.70c 5.9224e17
        26056.70c 1.1160e19
$ fuel
mt1000  grph.10t
m2000  7014.70c 8.399e19  8016.70c 1.2678e19  18040.70c 2.5122e17
$ air

```

```

m3000  40090.70c 2.2054e22  40091.70c 4.83089e21  40092.70c
7.35992e21
      40094.70c 7.4280e21  40096.70c 1.19165e21  50120.70c
9.2780e19
      26056.70c 1.9930e20  24052.70c 2.2691e18  28058.70c
3.3494e17      $ zircalloy 3
m4000  6000.70c 8.3655e22  26056.70c 1.8010e19  5010.70c 3.5167e16
      5011.70c 1.5090e17
$ graphite
mt4000  grph.10t
m5000  5010.70c 0.796 5011.70c 3.204 6000.70c 1
$ B4C poison
m6000  26056.70c -99 6000.70c -1
$ Carbon Steel Poison Rod Clad

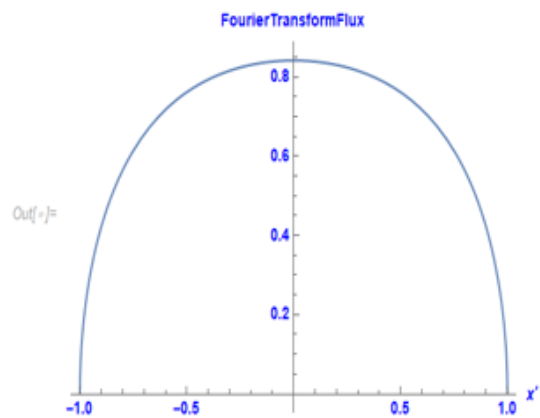
```

Appendix C: Filtered Back Projections Calculation

```
Out[ ]:= a = 1;  
Func = Sin[Sqrt[a^2 - y^2]];
```

```
In[ ]:= TrigToExp[Func];
```

```
In[ ]:= Plot[Func, {y, -1, 1}, AxesLabel -> {x', FourierTransformFlux}, LabelStyle -> Directive[Blue, Bold]]
```

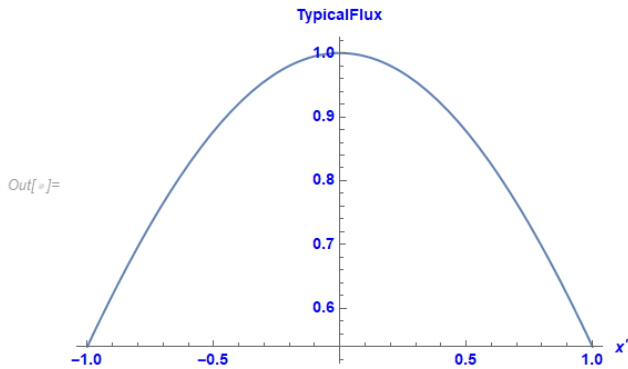


```
In[ ]:= OriginalFun = Cos[x]
```

```
Plot[OriginalFun, {x, -1, 1}, AxesLabel -> {x', TypicalFlux}, LabelStyle -> Directive[Blue, Bold]]
```

```
In[ ]:= OriginalFun = Cos[x]
Plot[OriginalFun, {x, -1, 1}, AxesLabel -> {x', TypicalFlux}, LabelStyle -> Directive[Blue, Bold]]
```

```
Out[ ]:= Cos[x]
```



```
In[ ]:=
FilterFun = Sin[Sqrt[a^2 - y^2] * Cos[k * y]];
```

```
In[ ]:= ExpansionFilter = Normal[%];
```

```
In[ ]:= FT = Integrate[ExpansionFilter, {y, 0, 1}]
```

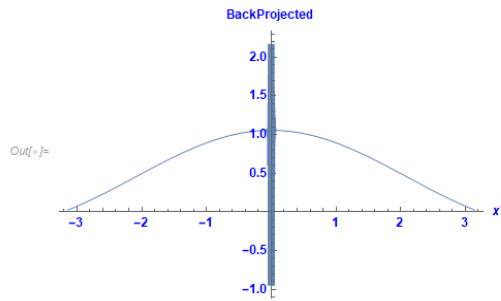
$$\begin{aligned} \text{Out[]:= } & \frac{1}{6} (-1 - k^2) \cos[1] + \sin[1] + \frac{1}{5} \left(\frac{1}{8} \frac{k^2}{4} + \frac{k^4}{24} \right) \cos[1] - \frac{1}{2} \left(\frac{1}{2} \frac{k^2}{2} \right) \sin[1] + \frac{1}{7} \left(\frac{1}{6} \frac{k^2}{2} \right) \cos[1] + \left(\frac{1}{16} \frac{k^2}{16} + \frac{k^4}{48} + \frac{k^6}{720} \right) \cos[1] - \left(\frac{1}{2} \frac{k^2}{2} \right) \left(\frac{1}{8} \frac{k^2}{4} + \frac{k^4}{24} \right) \sin[1] + \\ & \frac{1}{9} \left(\frac{1}{2} \frac{k^2}{2} \right) \left(\frac{1}{8} \frac{k^2}{4} + \frac{k^4}{24} \right) \cos[1] + \left(\frac{5}{128} \frac{k^2}{32} + \frac{k^4}{192} + \frac{k^6}{1440} + \frac{k^8}{40320} \right) \cos[1] + \frac{1}{24} \frac{k^2}{2} \sin[1] - \frac{1}{2} \left(\frac{1}{8} \frac{k^2}{4} + \frac{k^4}{24} \right)^2 + 2 \left(\frac{1}{2} \frac{k^2}{2} \right) \left(\frac{1}{16} \frac{k^2}{16} + \frac{k^4}{48} + \frac{k^6}{720} \right) \sin[1] + \\ & \frac{1}{11} \left(\frac{1}{120} \frac{k^2}{2} \right) \cos[1] + \left(\frac{7}{256} \frac{k^2}{256} + \frac{k^4}{384} + \frac{k^6}{5760} + \frac{k^8}{80640} + \frac{k^{10}}{3628800} \right) \cos[1] - \\ & \frac{1}{6} \left(\frac{1}{2} \frac{k^2}{2} \right) \left(\frac{1}{8} \frac{k^2}{4} + \frac{k^4}{24} \right)^2 + \left(\frac{1}{2} \frac{k^2}{2} \right) \left(\frac{1}{16} \frac{k^2}{16} + \frac{k^4}{48} + \frac{k^6}{720} \right) + \left(\frac{1}{2} \frac{k^2}{2} \right) \left(\frac{1}{8} \frac{k^2}{4} + \frac{k^4}{24} \right)^2 + 2 \left(\frac{1}{2} \frac{k^2}{2} \right) \left(\frac{1}{16} \frac{k^2}{16} + \frac{k^4}{48} + \frac{k^6}{720} \right) \cos[1] + \\ & \frac{1}{6} \left(\frac{1}{2} \frac{k^2}{2} \right)^3 \left(\frac{1}{8} \frac{k^2}{4} + \frac{k^4}{24} \right) \sin[1] - \frac{1}{2} \left(\frac{1}{8} \frac{k^2}{4} + \frac{k^4}{24} \right) \left(\frac{1}{16} \frac{k^2}{16} + \frac{k^4}{48} + \frac{k^6}{720} \right) + 2 \left(\frac{1}{2} \frac{k^2}{2} \right) \left(\frac{5}{128} \frac{k^2}{32} + \frac{k^4}{192} + \frac{k^6}{1440} + \frac{k^8}{40320} \right) \sin[1] \end{aligned}$$

```
In[ ]:= InverseFun = 1/2*Pi + Integrate[FT * Cos[k * y], {k, 0.001, 1}]
```

$$\begin{aligned} \text{Out[]:= } & \frac{1}{2y^{11}} \pi \left(0.15962 y - 0.013443 y^3 + 0.0000134793 y^5 + 5.85988 \times 10^{-6} y^7 + 0.000159558 y^9 \right) \cos\left[\frac{y}{1000}\right] + \\ & (-159.62 y + 40.0463 y^3 - 3.58414 y^5 + 0.140082 y^7 - 0.161801 y^9) \cos[y] - 159.62 \sin\left[\frac{y}{1000}\right] + 13.4431 y^2 \sin\left[\frac{y}{1000}\right] - 0.0134837 y^4 \sin\left[\frac{y}{1000}\right] - 0.00585988 y^6 \sin\left[\frac{y}{1000}\right] - \\ & 0.159558 y^8 \sin\left[\frac{y}{1000}\right] - 0.698658 y^{10} \sin\left[\frac{y}{1000}\right] + 159.62 \sin[y] - 93.2529 y^2 \sin[y] + 13.3858 y^4 \sin[y] - 0.782698 y^6 \sin[y] + 0.179819 y^8 \sin[y] + 0.618728 y^{10} \sin[y] \end{aligned}$$

```
In[ ]:= Plot[%, {y, -Pi, Pi}, AxesLabel -> {x', BackProjected}, LabelStyle -> Directive[Blue, Bold]]
```

```
In[ ]:= Plot[%, {y, -Pi, Pi}, AxesLabel -> {x', BackProjected}, LabelStyle -> Directive[Blue, Bold]]
```



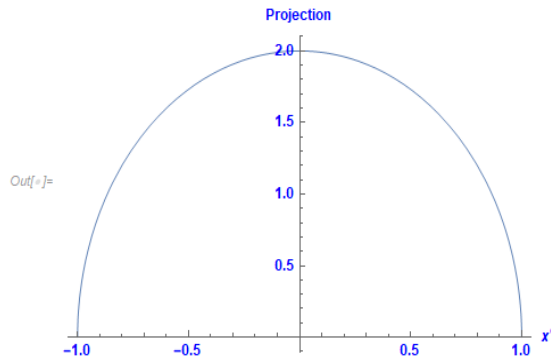
Step Function :

```
In[ ]:= a = 1;
```

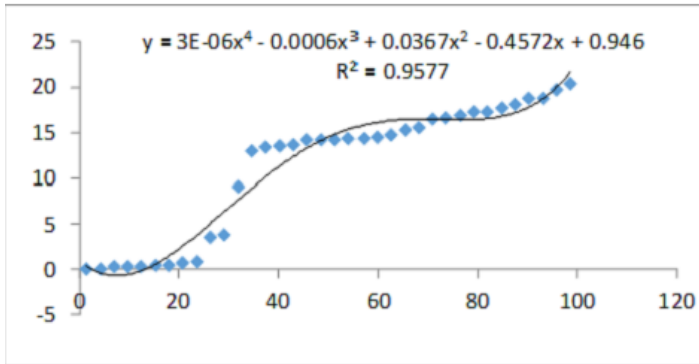
```
ProjectStep = 2 * Sqrt[a^2 - x^2]
```

Out[]:= $2 \sqrt{1 - x^2}$

```
In[ ]:= Plot[ProjectStep, {x, -1, 1}, AxesLabel -> {x', Projection}, LabelStyle -> Directive[Blue, Bold]]
```

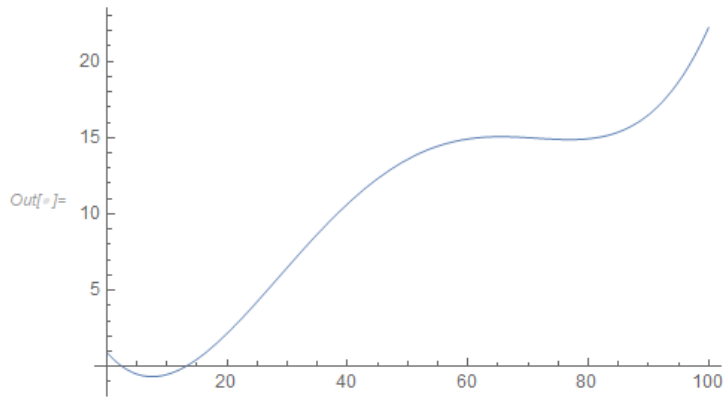


Mass Intensity at t=2.24164s :



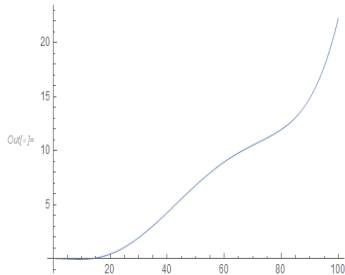
In[]:= **OriginalMass1 = 3 * 10^-6 * x^4 - 0.0006 * x^3 + 0.0367 * x^2 - 0.4572 * x + 0.946;**

In[]:= **p1 = Plot[%, {x, 0, 100}]**



In[]:= **MassFourierTrans = 0.005 * OriginalMass1 + 2 * Sqrt[x^2 - 1];**

In[]:= **p2 = Plot[%, {x, 0, 100}]**



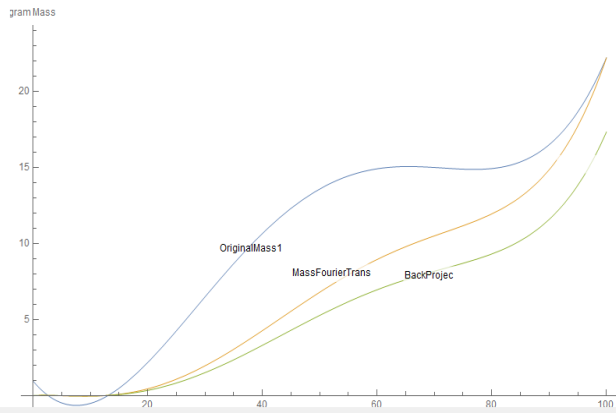
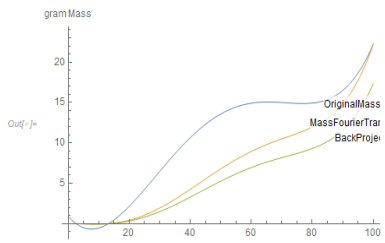
In[]:= **Series[MassFourierTrans, {x, 0, 10}]**

BackProjec = 0.25 * MassFourierTrans + 2 * ArcCos[1/x]

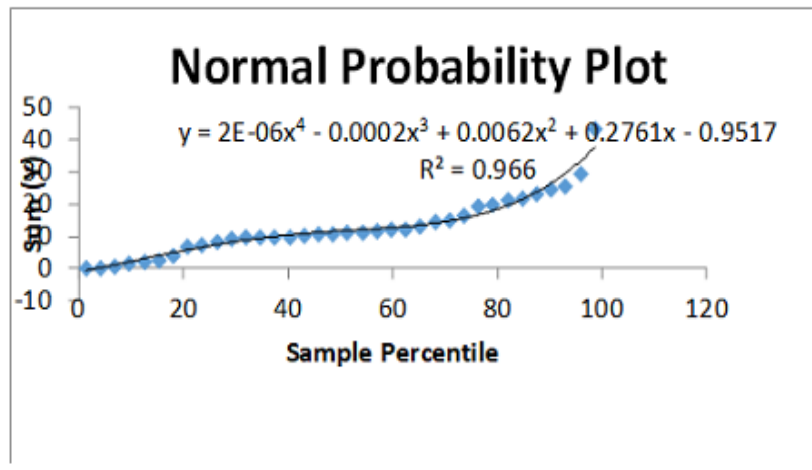
$$\begin{aligned} & \left[\begin{aligned} & -(0. + 0.00946 i) + (0. + 0.004572 i) x + (0. + 0.004363 i) x^2 - (0. + 0.00228 i) x^3 + (0. + 0.00136597 i) x^4 - & \text{Im}[x^2] < 0 \\ & (0. + 0.0005745 i) x^5 + (0. + 0.00063714 i) x^6 - (0. + 0.0002865 i) x^7 + (0. + 0.000392472 i) x^8 - (0. + 0.000178969 i) x^9 + (0. + 0.00027301 i) x^{10} + 0[x]^{11} \end{aligned} \right. \\ & \left. \left[\begin{aligned} & (0. + 0.00946 i) - (0. + 0.004572 i) x - (0. + 0.004363 i) x^2 + (0. + 0.00228 i) x^3 - (0. + 0.00136597 i) x^4 + & \text{True} \\ & (0. + 0.0005745 i) x^5 - (0. + 0.00063714 i) x^6 + (0. + 0.0002865 i) x^7 - (0. + 0.000392472 i) x^8 + (0. + 0.000178969 i) x^9 - (0. + 0.00027301 i) x^{10} + 0[x]^{11} \end{aligned} \right. \right] \end{aligned}$$

$$\text{Out[]:= } 0.005 \sqrt{-1 + x^2} \left(0.946 - 0.4572 x + 0.0367 x^2 - 0.0006 x^3 + \frac{3 x^4}{1000000} \right) \text{ArcCos}\left[\frac{1}{x}\right]$$

```
Plot[{OriginalMass1, MassFourierTrans, BackProjec}, {x, 0, 100}, PlotLabels -> Placed[Automatic, Top], AxesLabel -> Mass (gram) ]
```

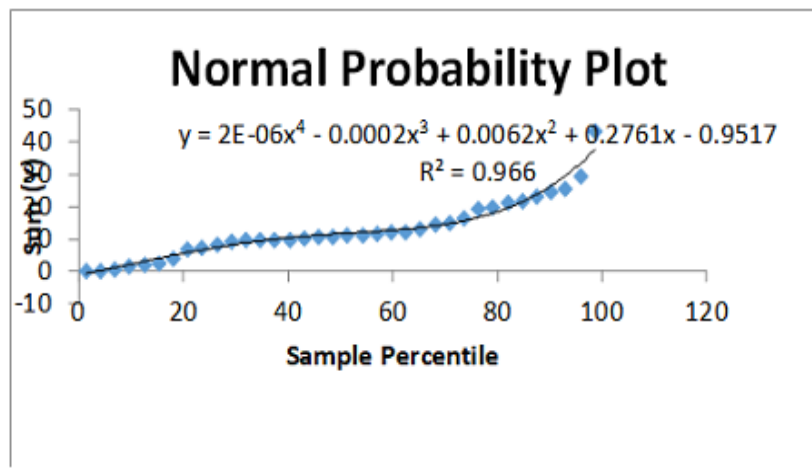


$$Out[] = -0.9517 + 0.2761 x + 0.0062 x^2 - 0.0002 x^3 + \frac{x^4}{500000}$$



Out[] =

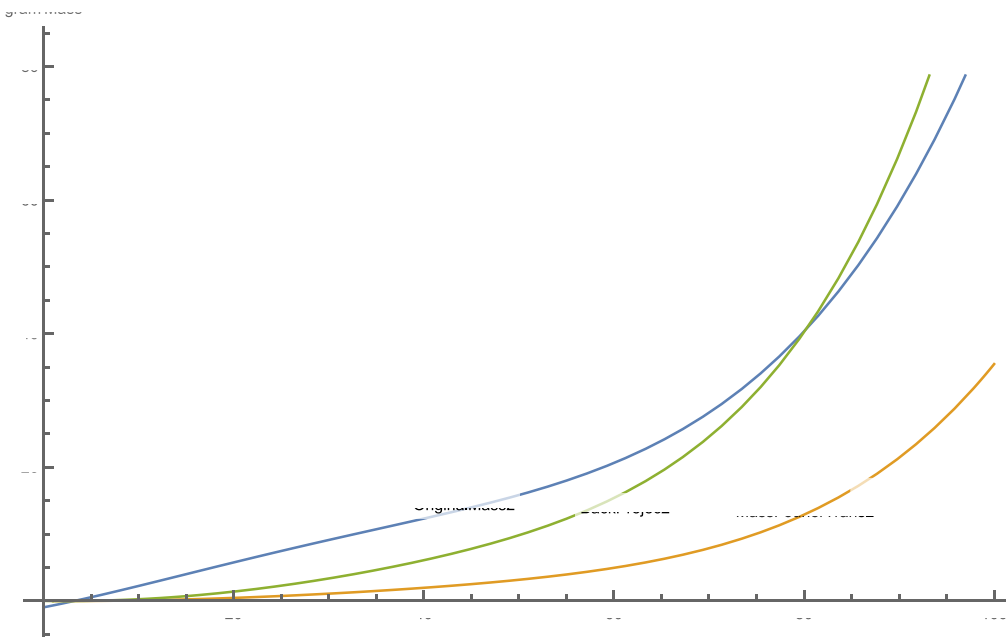
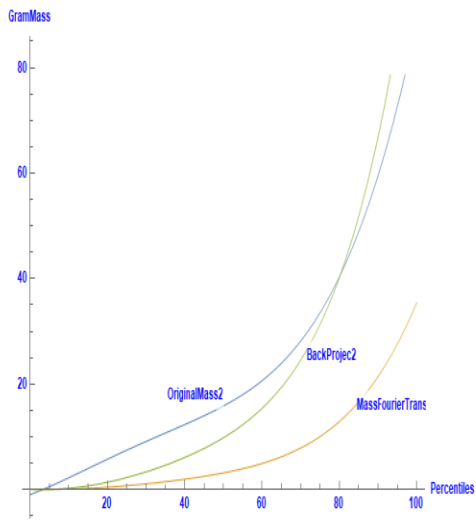
$$Out[] = -0.9517 + 0.2761 x + 0.0062 x^2 - 0.0002 x^3 + \frac{x^4}{500000}$$



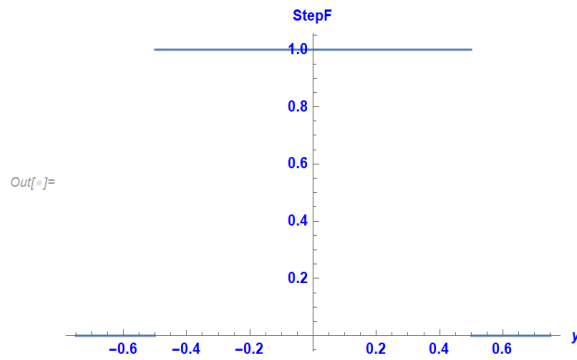
Out[] =

$$Out[] = -0.9517 + 0.2761 x + 0.0062 x^2 - 0.0002 x^3 + \frac{x^4}{500000}$$

```
inj:= Plot[{OriginalMass2, MassFourierTrans2, BackProjec2}, {x, 0, 100}, PlotLabels -> Placed[Automatic, Top], AxesLabel -> {Percentiles, GramMass}, LabelStyle -> Directive[Blue, Bold]]
```



`In[]:= Plot[HeavisidePi[x], {x, -0.75, 0.75}, AxesLabel -> {y, StepF}, LabelStyle -> Directive[Blue, Bold]]`



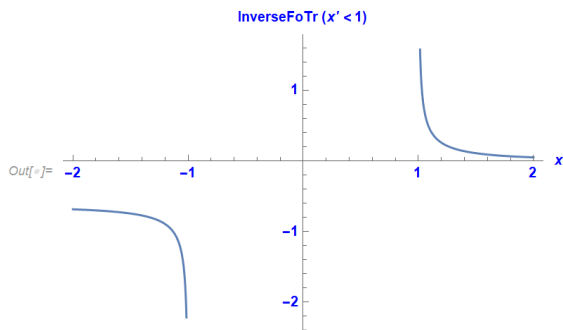
`In[]:=`

`a = 1;`

`InverseFT = (1/Pi) * {1/((Sqrt[(x/a)^2 - 1]) * ((x/a) + Sqrt[(x/a)^2 - 1]))}`

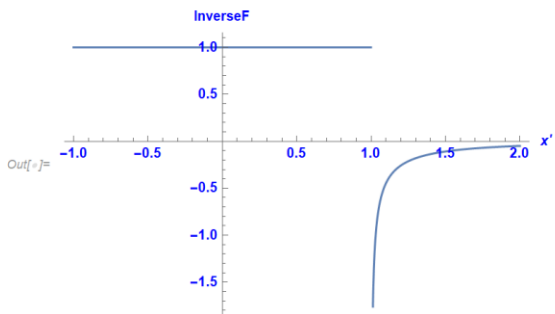
$$\text{Out[]} = \left\{ \frac{1}{\pi \sqrt{-1 + x^2} (x + \sqrt{-1 + x^2})} \right\}$$

`In[]:= Plot[InverseFT, {x, -2, 2}, AxesLabel -> {x', InverseFoTr (x' < a)}, LabelStyle -> Directive[Blue, Bold]]`



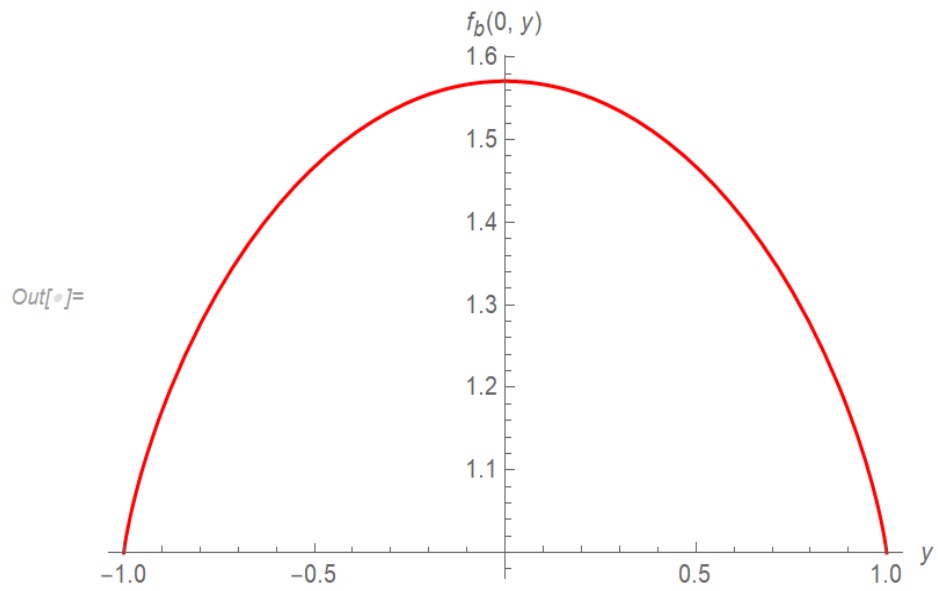
`In[]:= Plot[Piecewise[{{1, x < 1}, {-1/(Pi*Sqrt[-1+x^2]*(x+Sqrt[-1+x^2])), x > 1}}, {x, -1, 2}, AxesLabel -> {x', InverseF},`

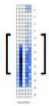
`LabelStyle -> Directive[Blue, Bold]]`



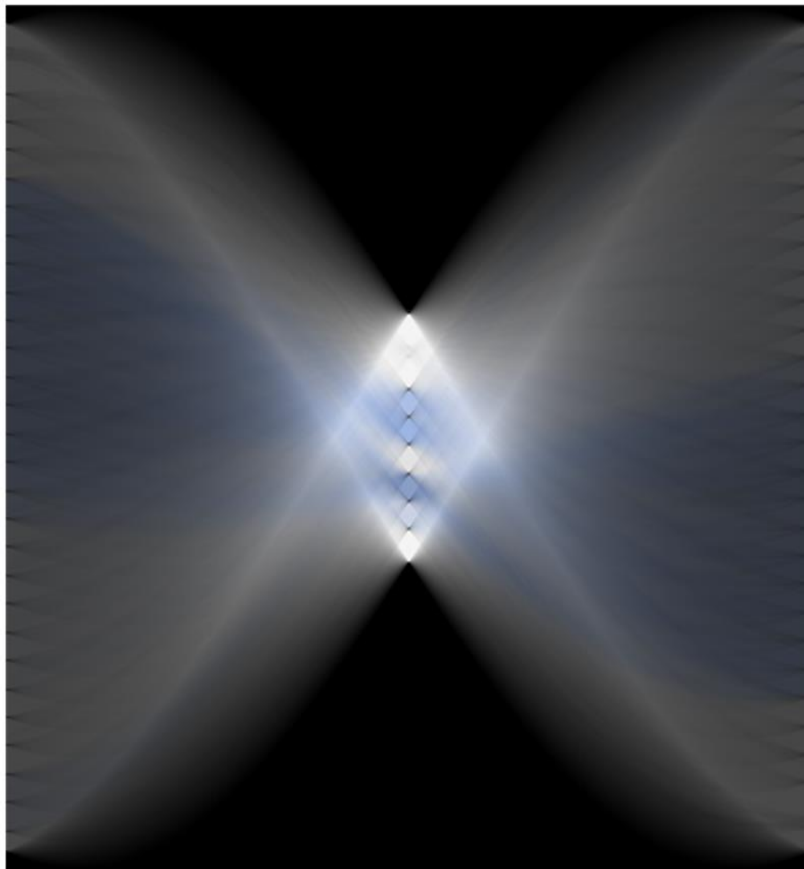
No Filtering:

```
In[*]:= Plot[EllipticE[y^2], {y, -1, 1},  
PlotStyle -> Red,  
AxesLabel -> TraditionalForm /@ {y, f_b(0, y)}]
```



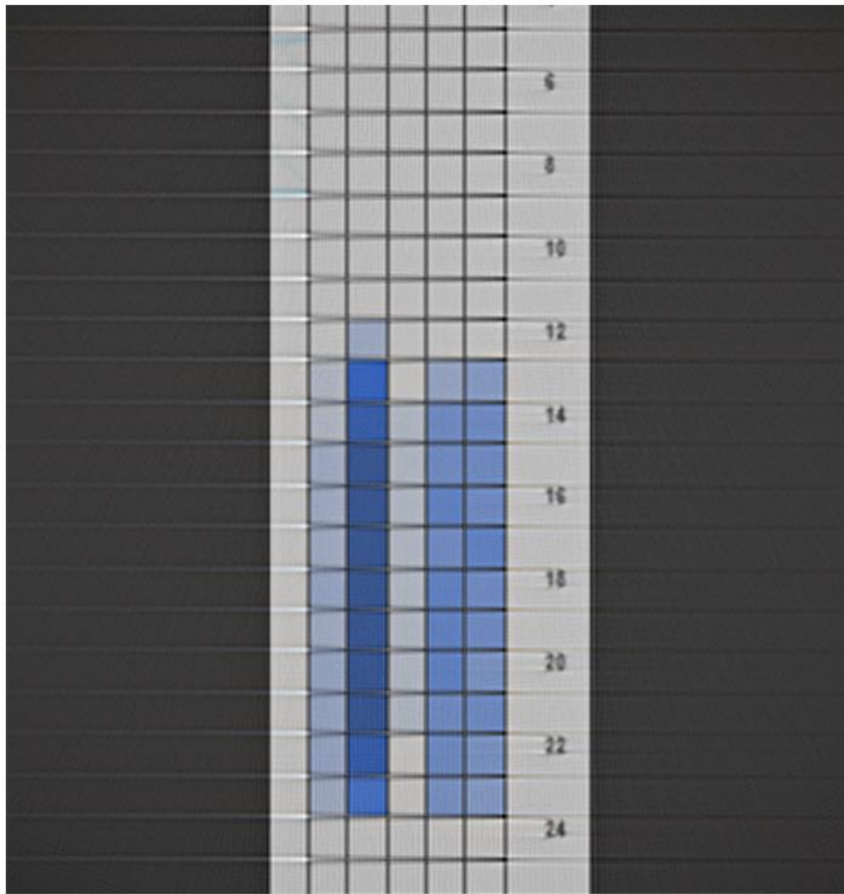
`In[]:= Radon[`  `]`

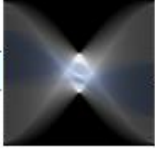
`Out[]:=`

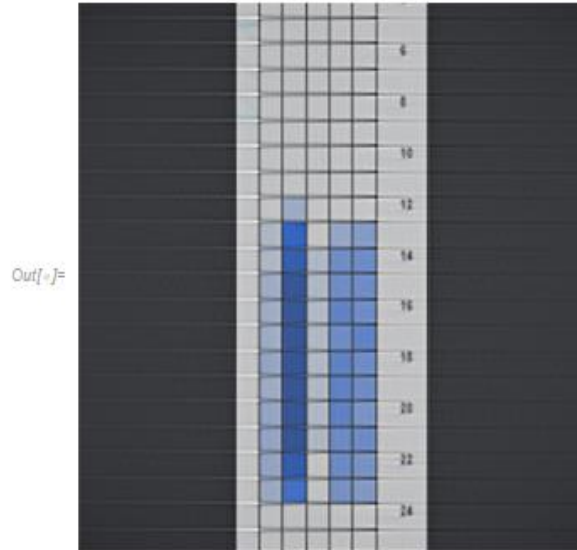


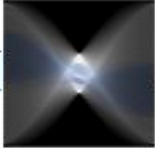
```
In[ ]:= InverseRadon[, Automatic, 1000] // ImageAdjust
```

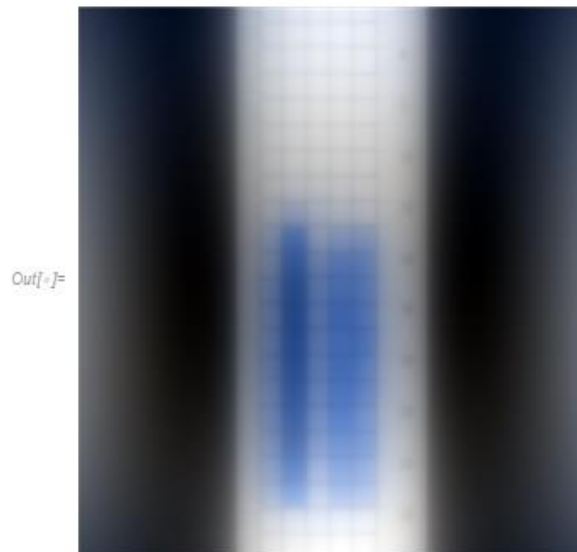
Out[]:=

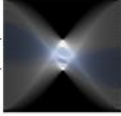


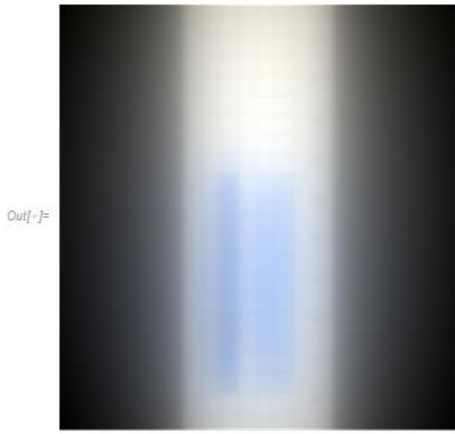
```
In[ ]:= InverseRadon[ , {300, 300}] // ImageAdjust
```

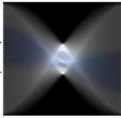


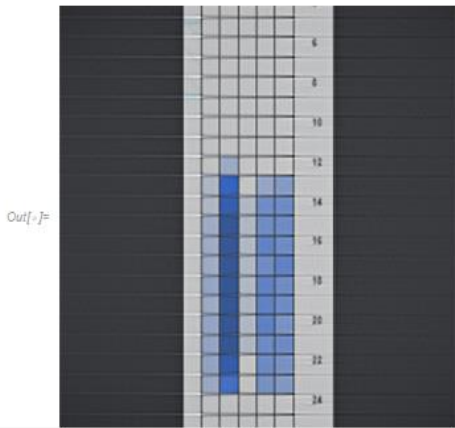
```
In[ ]:= InverseRadon[ , {300, 300}, Method -> {# &} ] // ImageAdjust
```



```
In[ ]:= InverseRadon[, {300, 300}, Method -> None] // ImageAdjust
```



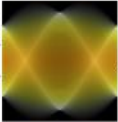
```
In[ ]:= InverseRadon[, {300, 300}, Method -> {Automatic, "CutoffFrequency" -> 1}] // ImageAdjust
```



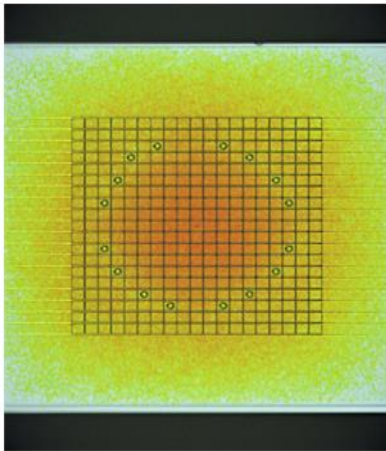
```
In[ ]:= InverseRadon[%, {300, 300}, Method -> None] // ImageAdjust
```

Out[]:=



```
In[ ]:= InverseRadon[, {300, 300}, Method -> {Automatic, "CutoffFrequency" -> 1}] // ImageAdjust
```

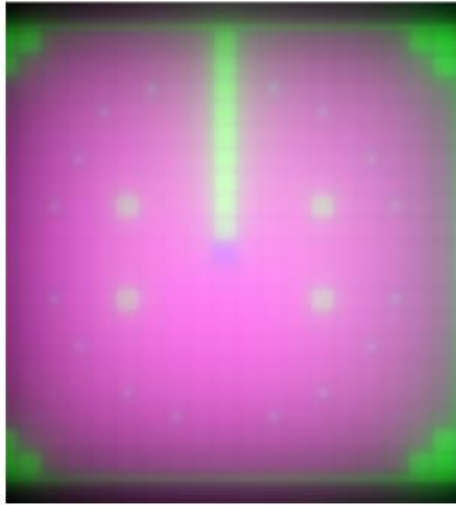
Out[]:=



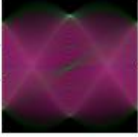
A) With No Filter

```
In[ ]:= InverseRadon[%, {300, 300}, Method -> None] // ImageAdjust
```

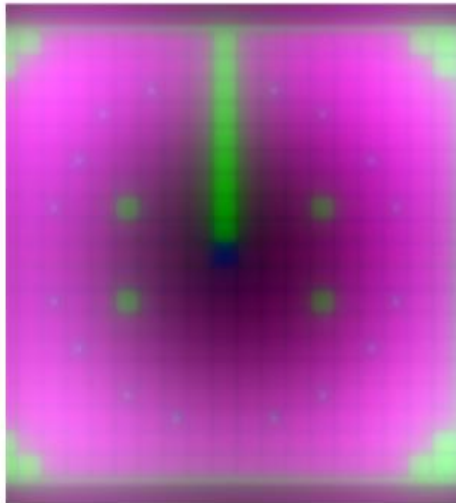
Out[]:=



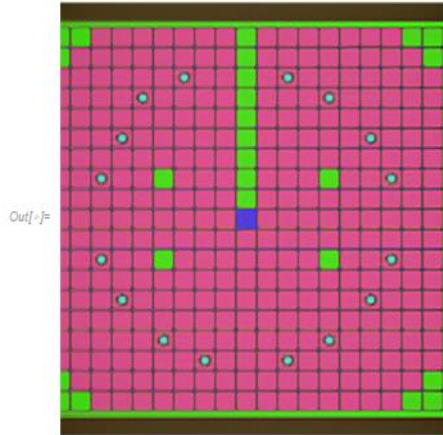
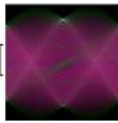
B. With Ramp Filter

```
In[ ]:= InverseRadon[, {300, 300}, Method -> (# &)] // ImageAdjust
```

Out[]:=

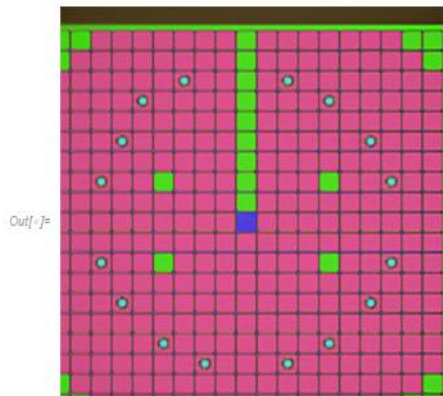
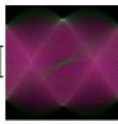


```
In[ ]:= InverseRadon[ , {300, 300}] // ImageAdjust
```



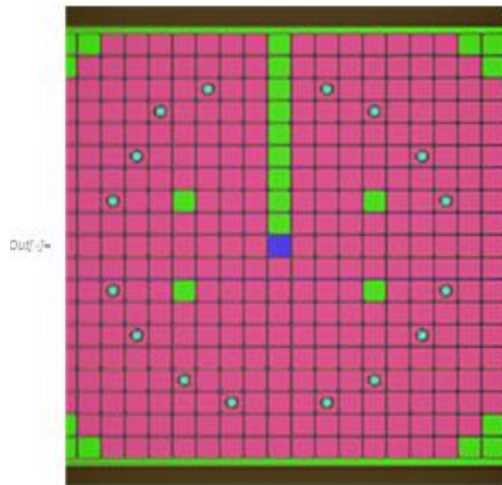
D. with Hann Filter and Cut off 1

```
In[ ]:= InverseRadon[ , {300, 300}, Method -> {Automatic, "CutoffFrequency" -> 1}] // ImageAdjust
```



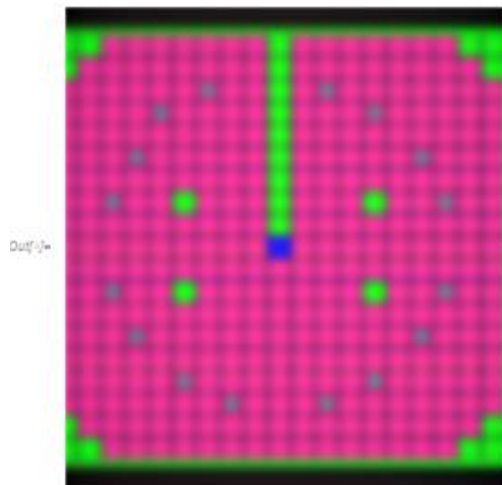
D. with Hann Filter and Cut off 1

```
in[-]> InverseRadon[, {300, 300}, Method->{Automatic, "CutoffFrequency"->1}] // ImageAdjust
```

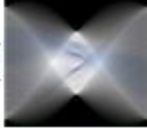


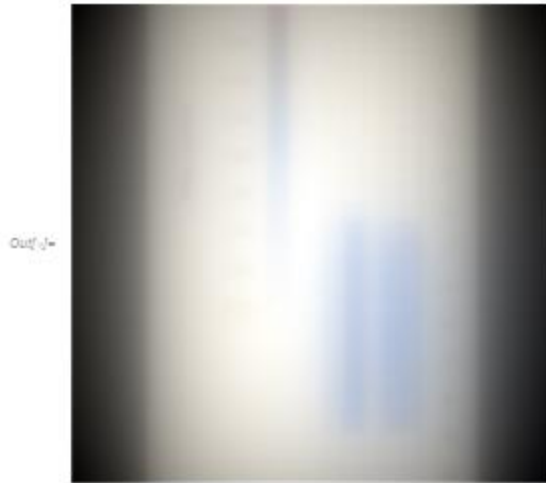
D. with Hann Filter and Cut off 0.1

```
in[-]> InverseRadon[, {300, 300}, Method->{Automatic, "CutoffFrequency"->0.1}] // ImageAdjust
```



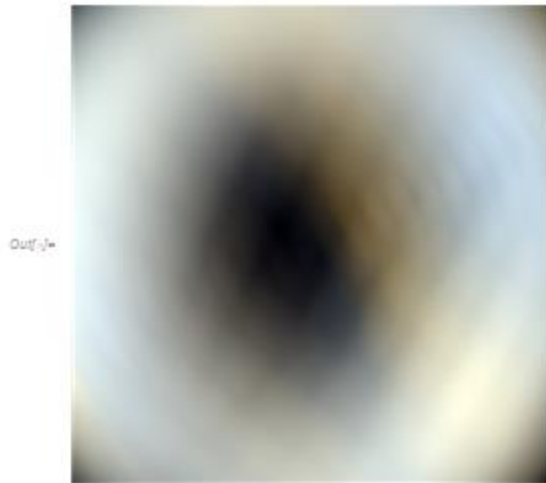
A) No Filter

```
In[ ] := InverseRadon[, {300, 300}, Method -> None] // ImageAdjust
```

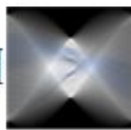


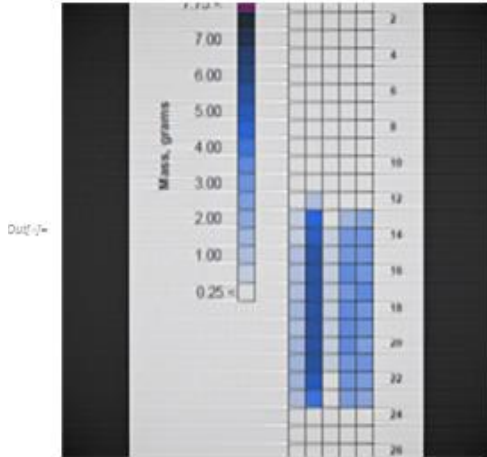
B) With Ramp Filter

```
In[ ] := InverseRadon[, {300, 300}, Method -> (# &)] // ImageAdjust
```

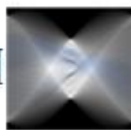


C) Hann Filter

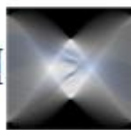
```
In[ ]:= InverseRadon[ , {300, 300}] // ImageAdjust
```

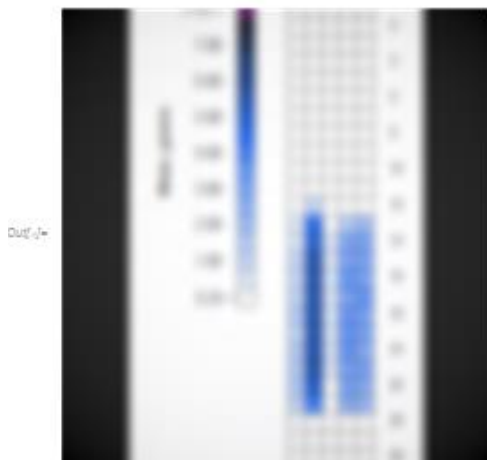


D) Hann Filter and Cut off 1

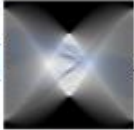
```
In[ ]:= InverseRadon[ , {300, 300}, Method -> {Automatic, "CutoffFrequency" -> 1}] // ImageAdjust
```

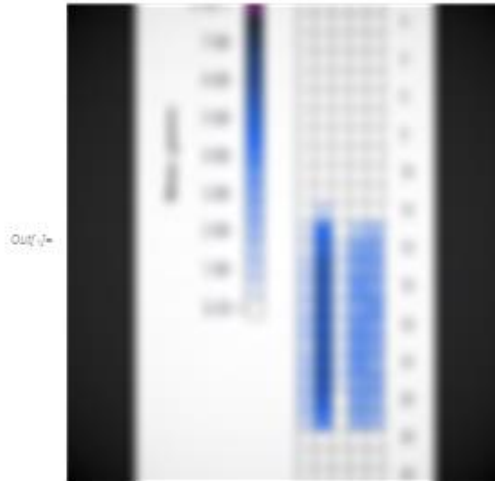
E) Hann Filter with cut of 0.1

```
In[ ]:= InverseRadon[ , {300, 300}, Method -> {Automatic, "CutoffFrequency" -> 0.1}] // ImageAdjust
```



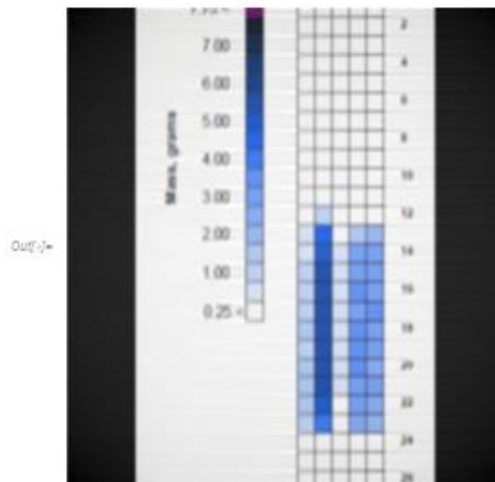
E) Hann Filter with cut of 0.1

```
In[ ]:= InverseRadon[ 
```



F) Hann Filter with Cut off 0.4

```
In[ ]:= InverseRadon[ 
```



Mathematical Equation

$$\begin{aligned}
 J_\nu(z) &= \frac{(\frac{1}{2}z)^\nu}{\pi^{\frac{1}{2}}\Gamma(\nu+\frac{1}{2})} \int_0^\pi \cos(z \cos \theta) \sin^{2\nu} \theta d\theta \\
 &= \frac{2(\frac{1}{2}z)^\nu}{\pi^{\frac{1}{2}}\Gamma(\nu+\frac{1}{2})} \int_0^1 (1-t^2)^{\nu-\frac{1}{2}} \cos(zt) dt \quad (\Re \nu > -\frac{1}{2})
 \end{aligned}$$

$$\begin{aligned}
 \int_0^\infty J_\mu(at) \cos bt dt &= \frac{\cos \left[\mu \arcsin \frac{b}{a} \right]}{(a^2 - b^2)^{\frac{1}{2}}} \quad (0 \leq b < a) \\
 &= \frac{-a^\mu \sin \frac{\pi\mu}{2}}{(b^2 - a^2)^{\frac{1}{2}} [b + (b^2 - a^2)^{\frac{1}{2}}]^\mu} \\
 &\quad (b > a > 0) \quad (\Re \mu > -1)
 \end{aligned}$$

Appendix D: ANL Hodogram Data

TIME = 2.24164 SECONDS

S/P = .08157

ROW	7	6	5	4	SUM	ERR75	ERR65	RULE	%
1	.3	.0	.0	.0	.3	.7	.4	3	100
2	.0	.0	.0	.0	.0	.7	.4	3	100
3	.3	.1	.4	.1	.9	.7	.4	3	100
4	.1	.2	.0	.0	.3	.7	.4	3	100
5	.3	.0	.0	.0	.3	.7	.4	3	100
6	.4	.0	.1	.0	.5	.7	.4	3	100
7	.2	.0	.1	.4	.8	.7	.4	3	100
8	.5	.9	1.6	.8	3.7	.8	.4	3	100
9	2.2	5.7	4.3	1.3	13.6	1.1	.6	3	100
10	.6	5.4	9.6	1.6	17.2	1.4	.8	3	100
11	.0	6.0	7.7	1.6	15.4	1.4	.8	3	100
12	.8	5.3	6.2	1.3	13.6	1.3	.7	3	100
13	.8	7.0	8.3	.8	17.0	1.5	.9	3	100
14	.3	4.5	8.7	.7	14.3	1.3	.7	3	100
15	.6	5.4	7.2	1.0	14.3	1.3	.7	3	100
16	.5	5.7	10.7	1.2	18.2	1.7	1.0	3	100
17	.8	5.9	7.7	1.1	15.5	1.3	.7	3	100
18	.6	7.6	8.7	.7	17.6	1.5	.9	3	100
19	1.0	5.7	6.7	.7	14.1	1.2	.7	3	100
20	.7	5.1	6.0	1.2	13.0	1.3	.7	3	100
21	.6	6.4	5.9	.5	13.3	1.2	.7	3	100
22	.4	6.5	10.7	1.1	18.6	1.8	1.0	3	100
23	.5	6.6	6.3	.9	14.3	1.4	.8	3	100
24	.9	8.7	9.5	.6	19.7	1.7	1.0	3	100
25	.0	11.6	7.7	1.0	20.3	2.0	1.2	3	100
26	.2	8.9	8.9	.9	18.8	1.6	.9	3	100
27	.8	6.8	8.5	1.0	17.1	1.5	.9	3	100
28	.9	5.9	6.7	1.0	14.6	1.3	.7	3	100
29	.3	5.3	7.2	1.5	14.3	1.3	.7	3	100
30	.7	7.2	6.9	1.6	16.4	1.4	.8	3	100
31	.4	6.9	7.5	1.8	16.6	1.4	.8	3	100
32	.9	6.1	6.6	1.1	14.6	1.4	.6	3	100
33	.3	3.6	4.4	.8	9.2	.9	.5	3	100
34	.9	.4	1.7	.5	3.5	.8	.4	3	100
35	.0	.0	.1	.0	.1	.7	.4	3	100
36	.4	.1	.0	.0	.5	.7	.4	3	100
SUM	19.3	161.7	192.5	28.9	402.2	43.5	24.9	(GRAMS)	

CONFIDENCE LEVEL : 75% 65%

TIME = .4.87934 SECONDS

S/P = .07735

ROW	7	6	5	4	SUM	ERR75	ERR65	RULE	%
1	.0	.0	.0	.3	.3	.7	.4	3	100
2	.0	.1	.0	.8	.9	.7	.4	3	100
3	.0	.0	.0	.0	.0	.7	.4	3	100
4	.0	.0	.0	.0	.0	.7	.4	3	100
5	.0	.4	.4	.0	.9	.7	.4	3	100
6	.9	.3	.1	.2	1.5	.7	.4	3	100
7	.0	.0	.0	.0	.0	.7	.4	3	100
8	.4	1.2	1.0	.2	2.8	.7	.4	3	100
9	1.3	5.8	3.8	.9	11.8	1.0	.6	3	100
10	.9	6.9	9.0	1.6	18.4	1.4	.8	3	100
11	.0	5.8	9.1	1.5	16.3	1.4	.8	3	100
12	1.1	5.9	9.3	1.5	17.8	1.4	.8	3	100
13	1.0	6.1	8.2	1.5	16.8	1.5	.8	3	100
14	.6	5.7	8.5	.8	15.5	1.3	.7	3	100
15	.8	6.4	8.7	1.3	17.2	1.4	.8	3	100
16	.8	6.2	9.0	1.3	17.2	1.4	.8	3	100
17	1.0	5.7	8.4	1.2	16.3	1.3	.7	3	100
18	1.0	6.5	8.5	1.3	17.2	1.4	.8	3	100
19	.6	6.9	7.2	.9	15.7	1.3	.8	3	100
20	.5	5.6	7.1	.9	14.3	1.2	.7	3	100
21	.9	7.0	6.9	1.4	16.2	1.3	.8	3	100
22	.5	7.3	9.0	.9	17.7	1.4	.8	3	100
23	.9	7.7	6.4	.9	15.8	1.3	.8	3	100
24	1.0	7.2	9.0	.6	17.8	1.4	.8	3	100
25	.5	6.8	8.2	1.2	16.6	1.4	.8	3	100
26	.7	7.1	9.4	1.1	18.3	1.5	.9	3	100
27	.8	7.5	8.9	1.2	18.5	1.5	.8	3	100
28	.7	7.3	6.4	1.4	15.5	1.3	.8	3	100
29	.5	6.5	7.4	1.1	15.6	1.4	.8	3	100
30	.4	6.1	7.5	1.2	15.2	1.4	.8	3	100
31	.5	5.6	7.5	1.6	15.2	1.2	.7	3	100
32	.9	6.7	7.2	1.2	15.9	1.4	.8	3	100
33	.2	3.7	3.9	.9	8.6	.8	.5	3	100
34	1.3	1.0	.7	.0	3.1	.7	.4	3	100
35	.0	.0	.0	.0	.0	.7	.4	3	100
36	.0	.0	.0	.0	.0	.7	.4	3	100
SUM	20.9	162.7	196.6	30.8	411.0	41.3	23.6	(GRAMS)	

CONFIDENCE LEVEL : 75% 65%

TIME = 14.44543 SECONDS

S/P = .13715

ROW	7	6	5	4	SUM	ERR75	ERR65	RULE	%
1	.0	.3	.3	.0	.6	1.0	.6	3	100
2	.0	.1	2.2	.4	2.8	2.4	1.4	1	84
3	.0	.3	.1	.0	.5	1.0	.6	3	100
4	.0	2.1	.1	.0	2.3	1.1	.6	2	91
5	.0	.1	.2	.0	.4	.8	.5	4	78
6	.2	.0	1.3	.3	1.8	.8	.5	4	83
7	.1	.6	2.9	.5	4.1	.7	.4	5	87
8	1.5	4.8	9.9	5.3	21.5	1.6	.9	5	86
9	3.3	4.8	10.2	7.1	25.4	2.0	1.2	5	86
10	4.8	6.0	10.6	7.8	29.2	2.3	1.3	5	86
11	1.7	5.6	8.1	6.3	21.7	1.6	.9	5	86
12	1.2	4.5	6.3	3.1	15.1	1.2	.7	5	91
13	.7	3.7	4.6	2.1	11.1	.9	.5	5	92
14	.7	4.9	5.3	3.6	14.6	1.5	.8	3	100
15	.5	3.2	7.3	5.4	16.3	1.6	.9	4	92
16	1.0	3.8	13.0	5.6	23.4	2.4	1.4	4	90
17	1.5	4.7	12.1	25.0	43.3	14.0	11.2	4	91
18	1.3	5.1	12.3	5.9	24.6	2.6	1.5	4	91
19	.7	3.1	5.3	1.8	10.9	1.2	.7	4	92
20	.7	4.6	5.3	1.4	12.0	1.2	.7	4	92
21	1.1	2.5	4.9	1.5	10.0	1.0	.6	4	92
22	1.0	2.5	3.7	2.4	9.6	1.0	.6	4	92
23	.8	2.5	3.3	1.0	7.6	1.0	.6	4	92
24	1.3	3.8	3.9	1.9	11.0	1.4	.8	2	91
25	.6	3.0	5.0	1.3	9.8	1.0	.6	4	90
26	.5	3.2	3.9	.8	8.3	1.0	.6	4	90
27	.0	3.3	5.7	1.1	10.1	1.2	.7	4	89
28	.6	4.3	4.2	.8	9.8	1.1	.7	4	88
29	.7	7.1	4.7	.5	13.0	1.6	.9	3	100
30	.4	2.3	3.5	.9	7.1	1.0	.5	4	90
31	.5	5.3	4.7	.7	11.2	1.2	.7	4	92
32	.8	4.2	5.3	1.4	11.6	1.2	.7	4	91
33	.3	3.1	4.6	1.4	9.4	1.1	.6	4	91
34	.1	3.4	14.9	1.6	20.0	2.4	1.4	5	91
35	.1	4.0	6.5	1.8	12.5	1.1	.6	5	90
36	1.2	4.4	10.3	3.3	19.2	3.2	1.8	1	91
SUM	30.0	121.2	206.4	104.1	461.7	63.4	39.4	(GRAMS)	

CONFIDENCE LEVEL : 75% 65%